A Study of the Erosion Suppression Mechanisms of Nanofilled Silicone Rubber Composites for HVDC Outdoor Insulation Applications

by

Alhaytham Yousef ALQUDSI

MANUSCRIPT-BASED THESIS PRESENTED TO ÉCOLE DE TECHNOLOGIE SUPÉRIEURE IN PARTIAL FULFILLMENT FOR THE DEGREE OF DOCTOR OF PHILOSOPHY
Ph.D.

MONTREAL, JANUARY 20, 2022

ÉCOLE DE TECHNOLOGIE SUPÉRIEURE
UNIVERSITÉ DU QUÉBEC

BOARD OF EXAMINERS

THIS THESIS HAS BEEN EVALUATED

BY THE FOLLOWING BOARD OF EXAMINERS

Mr. Éric David, Thesis Supervisor
Department of Mechanical Engineering, École de Technologie Supérieure

Mr. Refat Ghunem, Thesis Co-supervisor
Metrology Research Center, National Research Council Canada

Mr. Handy Fortin Blanchette, Chair, Board of Examiners
Department of Electrical Engineering, École de technologie supérieure

Mrs. Nicole Raymonde Demarquette, Member of the jury
Department of Mechanical Engineering, École de Technologie Supérieure

Mrs. Mona Ghassemi, External member of the jury
Department of Electrical and Computer Engineering
Virginia Polytechnic Institute and State University

THIS THESIS WAS PRENSENTED AND DEFENDED

IN THE PRESENCE OF A BOARD OF EXAMINERS AND THE PUBLIC

ON

AT ÉCOLE DE TECHNOLOGIE SUPÉRIEURE

DEDICATION

To my mother and father. I wish I gave you more. If God wills, I will give you more.

To my wife Dana. You are the gift that no one will ever have alike.

To my daughters Mariam and Lujain. You define your excellence and not others.

ACKNOWLEDGMENT

"My lord, I am in dire need of whatever good you might send down to me." (Quran 28:24). I thank the All-merciful Almighty Allah for placing the good people, bad people, great opportunities and unfortunate events in the path that led me to this point.

Foremost, I would like to thank my research directors Dr. Ghunem and Professor David for giving me this opportunity. I thank them for their support, guidance and motivation in this doctoral study. I also would like to thank Professor Fortin Blanchette, Professor Demarquette and Professor Ghassemi for their valuable comments on improving the thesis. I would also acknowledge the efforts of many from the ÉTS community including Mr. Simon Laflamme, Dr. Mohammad Saadati, Mr. Joel Grignon and Professor Souheil-Antoine Tahan for providing the necessary help, permission and assistance with various parts of this work. I also thank Dr. Yazid Hadjadj, Dr. Amr Said and Dr. Harold Parks from the NRC on their advice and assistance which was provided during the course of this PhD. A special thanks to Mr. Yuksum Tam for his help and advice in the electronic circuitry parts of the work. I would also thank my teacher and friend Dr. Ayman El-Hag for connecting me to Dr. Ghunem during the search for a PhD opportunity.

For my spectacular family. My beautiful mother Sajidah, wise father Yousef, beacon of hope and wife Dana, fashion icon sister Leen and brother Spoktash Hamoodeh. You are the reason I started this chapter in life.

For my beautiful daughters Marium and LuLu who made it very difficult for me to finish this work and were not by any means helpful. You are my greatest accomplishment. You are the reason for me to finish this chapter in life and start the next. I love you.

For my many friends who gave me the joyful part of this PhD (the name order reflects no preference): Abu ElYoush Elhaj, Abu Steif Harbaji, Adeily Ahmad Dalaq, Hesham Gamal, Protein Shake K. Hindawi, El-Akh Dr Diab Abu Eida, El-Akh Dr Issam Qamhieyeh, El-Rafeeq Omar JadaAllah, Ghassan El-Dadah, Dr. Enad Chigurh Mahmoud and Alaa Elkhatib. I thank Alaa Elkhatib for his reappearance again after 5 year absence.

Étude des mécanismes de la suppression de l'érosion des nano-composites caoutchouc silicone pour des applications externes CC haute tension

Alhaytham Yousef ALQUDSI

RÉSUMÉ

Cette thèse présente une étude des mécanismes de suppression de l'érosion pour des composites caoutchouc silicone chargés de de particules inorganiques de dimension nanométrique et ce, dans l'optique d'applications comme isolant externe pour la haute tension CC. Le test d'érosion CC du plan incliné ainsi que le test de résistance à l'arc électrique ont été employés afin d'évaluer la performance des composites dans des situations d'érosion. De plus, des analyses thermiques et morphologiques ont été utilisées pour investiguer l'effet des nano-renforts sur la résistance à l'érosion sous CC du caoutchouc silicone. Cette nouvelle approche utilisant un ensemble de techniques est définie comme approche basée sur les mécanismes pour l'investigation des effets de suppression de l'érosion des nano-renforts, ce qui représente un critère critique pour la conception des isolants externes en caoutchouc silicone pour les applications en CC.

L'étude commence par l'investigation du rôle de l'interface renfort/caoutchouc silicone sur la suppression de l'érosion en CC. Cette influence est analysée de façon comparative avec l'influence de l'augmentation de la conductivité thermique procurée par des renforts ayant une conductivité thermique élevée. La silice en fumée, l'alumine nanométrique tri-hydratée et le nitrure de bore hexagonal submicronique ont été utilisés comme renforts dans le caoutchouc silicone pour cette partie de l'étude. Il a été observé que la silice en fumée a une plus grande influence sur l'amélioration de la résistance à l'érosion que les autres types de renforts, malgré le fait qu'elle confère aux composites une conductivité thermique semblable aux autres renforts. En effet, l'interaction favorable entre la silice en fumée et le caoutchouc silicone empêche la dépolymérisation du silicone et entraine la réticulation du matériau durant l'érosion sous CC. De plus, les mesures de courant de fuite indiquèrent l'initiation la plus lente pour l'établissement d'un arc stable pour le composite renforcé par de la silice en fumée. Ceci met en lumière l'importance de l'interface entre la nanoparticule et le polymère dans la suppression de l'érosion, mécanisme qui est plus important que l'amélioration de la conductivité thermique du composite.

Cette étude analyse également la corrélation entre le rôle de l'interface silice-silicone et l'écran résiduel du composite formé durant la présence d'arcs de bandes sèches en utilisant à la fois de la silice en fumée et de la silice broyée. Des analyses thermiques indiquèrent une plus grande quantité de résidus réticulés avec davantage d'interactions avec le renfort dans le cas de la silice en fumée par rapport à la silice broyée. La morphologie de la surface des résidus érodés des composites ayant subis le test du plan incliné a indiqué l'importance du rôle de la silice en fumée sur l'amélioration de l'intégrité et la cohérence du résidu menant à un effet barrière protégeant le caoutchouc silicone du volume contre l'érosion progressive. Cette conclusion a été supportée par les essais de résistance à l'arc montrant des caractéristiques de résidu semblables à celles obtenues durant les essais de plan incliné.

Les résultats mentionnés ci-dessus ont été vérifiés pour des cas plus pratiques en utilisant des nano-renforts comme additifs pour des composites caoutchouc silicone pour isolation externe

afin d'améliorer leur résistance à l'érosion. Dans ce contexte, la silice en fumée et la nano-alumine tri-hydratée ont été utilisés comme additifs, à un taux inférieur à 5% sur une base massique, en conjonction avec des micro renforts de silice broyée et d'alumine tri-hydratée présents en plus grande quantité. L'efficacité de l'effet de barrière des renforts a été synergétiquement obtenue en ajoutant de la silice en fumée au renfort principal, soit de silice broyée, soit de l'alumine tri-hydratée, en maintenant l'intégrité des résidus obtenant ainsi une résistance supérieure à l'érosion sous tension CC par rapport aux autres échantillons testés. Ce résultat est important puisqu'il confirme l'effet barrière comme un mécanisme important dans la suppression de l'érosion sous tension CC des nano-renforts qui renforcent l'effet de volume des micro additifs remplaçant le caoutchouc silicone dépolymérisable.

Afin d'étudier d'avantage le rôle de l'effet écran dans la suppression des arcs stables sur bandes sèches, la résistance à arc a été proposée comme méthode de test rapide. Des composites renforcés par différentes concentrations et tailles d'alumine tri-hydratée ont été testés avec le test de résistance à l'arc ainsi que le test du plan incliné. Le classement des différents composites en fonction de la quantité de matière érodée s'est avéré être le même pour les deux tests. Ce classement a également aussi été en accord avec les résultats de l'analyse thermique. Ce bon accord dans les différents résultats indique la possibilité d'utiliser le test d'arc électrique comme une méthode rapide pour l'analyse de la résistance à l'érosion du caoutchouc silicone.

Mots clefs: arc sec, érosion, mécanisme de suppression d'érosion, Isolation externe haute tension, nano-renforts, composites de caoutchouc silicone.

A Study of the Erosion Suppression Mechanisms of Nanofilled Silicone Rubber Composites for HVDC Outdoor Insulation Applications

Alhaytham Yousef ALQUDSI

ABSTRACT

This thesis presents a study on the erosion suppression mechanisms of nano-sized inorganic fillers in silicone rubber composites for high-voltage-direct-current outdoor insulation applications. The DC inclined plane tracking-erosion test and the dry-arc resistance test are employed to evaluate the erosion performance of the composites in the study. Thermal and surface morphology analyses are utilized to investigate the effect of nano fillers on the DC erosion resistance of silicone rubber. This novel approach in using these techniques collectively is defined as the mechanistic-based framework for investigating the erosion suppression effects of nano fillers as critical material design aspects of DC silicone rubber outdoor insulators.

The study begins by investigating the role of the filler-silicone interface on suppressing the DC erosion of silicone rubber. The influence of the interface on suppressing erosion is comparatively analyzed against the influence of enhancing the composite thermal conductivity with the inclusion of thermally conductive fillers. Fumed silica, nano alumina tri-hydrate and thermally conductive sub-micron hexagonal boron nitride are filled in silicone rubber as part of the study. Fumed silica in silicone rubber is found to have a more influential effect on improving its DC erosion resistance as opposed to incorporating the other fillers, despite the composites having comparable thermal conductivities. Fumed silica's favorable interaction with silicone rubber suppressed silicone depolymerization and promoted crosslinking during DC erosion. Moreover, leakage current data indicates the slowest inception for the stable eroding arc for the fumed silica composite. This highlights the significance of the nano filler's interface in suppressing the erosion of silicone rubber, which is more important than improving the composite thermal conductivity with thermally conductive fillers.

The study investigates the correlation between the role of silica-silicone interaction and the residue shield of the composites during the DC dry-band arcing using fumed silica and ground silica fillers as part of the study. Thermal analyses indicating higher additional crosslinked residue with more filler polymer interactions with the fumed silica composite as compared to ground silica. Surface morphology of the eroded residue of composites tested under the inclined plane test indicate a vital role for fumed silica on improving the residue's integrity and coherency, which is the residue barrier effect shielding the bulk silicone against progressive erosion. A conclusion which is supported by the dry-arc resistance test showing similar residue characteristics to those obtained under the DC inclined plane test.

The aforementioned findings are verified for a more practical application of using nano fillers in silicone rubber outdoor insulation composites as additives to improve the DC erosion resistance. In this approach, fumed silica and nano alumina trihydrate are added as additives, of less than five percent by weight, to base micro fillers of either ground silica or alumina trihydrate which are of much higher weight fractions. The viability of the filler barrier effect is synergistically achieved by adding fumed silica to the main ground silica filler, thereby maintaining the residue integrity and achieving a superior DC erosion resistance as compared

to the other tested composites. This is an important finding which confirms the barrier effect as an important DC erosion suppression mechanism of nano filler additives aiding the volume effect of micro fillers replacing the depolymerizable silicone rubber content.

To further investigate the role of the shield effect in the suppression of stable dry-band arcing, the dry-arc resistance is introduced as a quick testing method. Alumina trihydrate filled composites of different filler levels and sizes are examined with the dry-arc resistance test and the inclined plane test. The ranking order of the composites in terms of the eroded quantities coincide under both tests. This ranking order is also consistent with the levels of silicone rubber combustion found under thermal analysis. The consistency in the outcomes indicate the possibility of using the dry-arc test as quick testing method for analyzing the erosion resistance of silicone rubber and investigating erosion produced outcomes such as the shielding effects of inorganic fillers.

Keywords: eroding dry-band arcing, erosion resistance, erosion suppression mechanisms, high voltage direct current outdoor insulation, nano fillers, silicone rubber composites.

TABLE OF CONTENTS

Page

LIST OF TABLES

Page

LIST OF FIGURES

Page

LIST OF ABREVIATIONS AND ACRONYMS

+DC	Positive polarity of direct current voltage
-DC	Negative polarity of direct current voltage
A25a5	Hybrid SiR composite containing nano alumina trihydrate and micro alumina trihydrate
A25s5	Hybrid SiR composite containing nano alumina trihydrate and fumed silica
AC	Alternating current
AC DBA	Dry-band arcing under alternating current voltage
AC IPT	Inclined plane tracking-erosion test under alternating current voltage
Al_2O_3	Alumina/Aluminum Oxide
ATH/ $Al_2O_3.3H_2O$	Alumina trihydrate
ATH05/ATH30/ ATH50/ATH60/ A30	Alumina trihydrate filled SiR composite
BN	Boron Nitride
CS	Current step of the dry-arc resistance test
DBA	Dry-band arcing
DC	Direct current
DC DBA	Dry-band arcing under direct current voltage
DC IPT	Inclined plane tracking-erosion test under direct current voltage
DTA	Differential thermal analysis
DTGA	Differential thermogravimetric analysis
EPDM	Ehtylene propylene diene monomer

EPR	Ethylene propylene rubber
EVA	Ethylene vinyl acetate
GS10	Ground silica filler
GCMS	Gas chromatography-mass spectroscopy
h-BN / BN137	Hexagonal boron nitride filler
HTV	High temperature vulcanized
HVDC	High voltage direct current
IPT	Inclined plane tracking-erosion test
LC	Leakage current
MDH	Magnesium hydroxide
MTPS	Modified transient plane source
N_2	Nitrogen
NA10	Alumina trihydrate filler
NS07/FS07	Fumed silica filler
O_2	Oxygen/air
PDMS	Polydimethylsiloxane
RMS	Root-Mean-Square
RTV	Room temperature vulcanized
S30	Ground silica filled SiR composite.

LIST OF SYMBOLS

wt%	Percentage by weight
k	Thermal conductivity
N_{fp}	Number of filler particles per unit volume of the filler
R_a	Average surface roughness
R_{add} / W_{add}	Additional residue formed during TGA testing
R_{asm} / W_{TGAasu}	Final assumed residue under TGA testing
r_{fp}	Average filler particle radius size
ρ_f	Filler density
R_{TGA}/ W_{TGA}	Final wt% of TGA remnant residue
SA_f	Total surface area of the filler interfacial layer available
sa_{fp}	Surface area per spherical filler particle
v_{fp}	Volume per spherical filler particle
W_{ATH}	Weight fraction of the ATH filler in the composite
W_{dep}	Weight of depolymerized SiR content during TGA
W_{filler}	Weight fraction of the filler in the composite
W_{silica}	Weight fraction of the silica filler in the composite
W_{SiR}	Weight fraction of SiR in the composite.

CHAPTER 1

INTRODUCTION

1.1 Overview

In the conventional overhead power transmission and distribution systems, outdoor insulators play a vital role in mechanically supporting the high voltage line conductors. Polymeric outdoor insulators have been introduced as replacements to the conventional porcelain and glass insulators mainly due to the substantial reduction in the weight of the insulator associated with their use and the superior pollution performance of polymer insulators. The reliability of the polymeric insulator is essential to safeguard the continuous operation of the power system with minimal interruption. Maintaining the insulator reliability is subjected to the performance of the insulator's polymer material under outdoor contaminated conditions. Under rigorous weather conditions, contaminant films could adhere on the insulator surface leading to the formation of leakage currents which evolve into sustained dry-band arcing (DBA). The severity of the DBA is reflected in terms of the amount of heat it releases on the insulator surface. Silicone rubber (SiR) is one of elastomeric materials used in polymeric outdoor insulators due to their excellent pollution performance and characteristic hydrophobic surface properties. The hydrophobicity of SiR hinders the formation of conductive films across its surface, thus making it highly desirable for outdoor insulation applications. The intrinsic hydrophobicity of SiR is dynamic which makes it capable of transferring hydrophobic properties to its surface upon the adherence of outdoor pollutants under severe weathering conditions. A property which is highly desirable for recovering the surface hydrophobicity after temporary loss during sustained DBA.

Through thorough research, SiR is found to be a track-resistant material. However during the temporary loss of hydrophobicity, SiR is prone to erosion under sustained DBA in heavily polluted conditions. Progressive erosion of the SiR material could eventually expose the fiber glass core of the insulator to outdoor contamination leading to its complete fracture and subsequent interruption of power supply. The erosion resistance, or erosion performance, of

SiR was researched for high voltage alternating current (HVAC) outdoor insulation. The primary conclusions highlight a significant role for inorganic fillers in enhancing the erosion resistance of the SiR material. As an early practice alumina tri-hydrate (ATH), for example, was filled in SiR due to its intrinsic water of hydration which is released at high temperatures during DBA. The released water of hydration diluted the gaseous phase of SiR arc to subsequently suppress the combustion of the material during arcing. Later on, the improvement in the erosion performance of SiR was found to be influenced by the role of the filler in relatively increasing the thermal conductivity of SiR in its composite form as compared to that of its unfilled form. Higher composite thermal conductivity aids in dissipating the impinged heat from the insulator surface during DBA.

Developing the research for enhancing the erosion resistance of SiR for HVAC outdoor insulators has been done through decades of experimentation and accumulated field experience on the application of the silicone polymer in the field service of AC lines. Using the same experience-based approach for high voltage direct current (HVDC) outdoor insulators is impractical given the lack of knowledge and field experience on the ageing of such insulators as a result of the relatively lower DC lines that existed globally. Thus reliable SiR housing material designs have to be developed for HVDC outdoor insulation applications using a mechanistic-based framework. Within the context of this thesis, the mechanistic-based framework is defined as the collective application of standard material screening tests, material characterization tools and analysis to investigate the erosion suppression effects of nano fillers as critical material design aspects of DC SiR insulators.

1.2 Motivation

The application of HVDC transmission systems has been gaining attention in the light of increased interest in integrating distributed renewable energy resources into the power grid. HVDC transmission has superior advantages over HVAC transmission in terms of enabling efficient power transmission over long distances (General Electric 2016). One key advantage is the capability for supplying power from remote renewable energy based sources, such as solar farms, to distant load centers. A significant benefit which will reinforce the ongoing efforts to mitigate the climate crisis by gradually transitioning into renewable based energy

generation as replacements for fossil-fuel based electric power generation. Moreover, the application of DC transmission facilitates interconnecting different AC power networks and enabling the exchange of electric power across these networks as needed. Collectively, these advantages signal an ongoing gradual evolution from the conventional AC transmission system to that of DC to meet the ever-changing field demands of cleaner power generation with reduced carbon footprint. Accordingly, this dictates the use of reliable outdoor insulators that will be installed as backbone components in the HVDC grid. The reliability of these insulators is defined in terms of their ability to sustain the continuous operation while being exposed to polluted environmental conditions.

With the understanding that erosion is the critical ageing mechanism involved with SiR outdoor insulators as a result of DBA, a careful consideration should be given to the voltage stress under which the insulator is operating. Employing the same research findings of SiR AC based outdoor insulators to those of DC is unfeasible given the higher severity of the DBA exhibited by the insulators under DC voltage. Recent review on the field experiences of the pollution performance of composite SiR insulators on DC lines indicate higher failure rates as compared to AC stressed lines (Akbar, Mehmood 2020). The relatively higher leakage current magnitudes and longer discharge periods with DC DBA, as compared to AC DBA, dictates a greater influx of heat energy being transmitted to the insulator surface thereby causing more severe damage to the insulator material. Improvements on the DC outdoor insulator design were centered on changes in the physical geometry, rather than the actual SiR material design. Developments on the material design would require a study to comprehend the role of inorganic fillers and their attributes of size, type and loading level, on the erosion suppression mechanisms introduced during DC DBA. Such a study could expand the common understanding of the role of inorganic fillers on suppressing DC erosion of SiR. A development which transitions from relying on general experience of common perceptions, to a more thorough understanding of the mechanisms of the filler in suppressing erosion during DC DBA.

Recent research on developing the SiR material design for DC outdoor insulation using micro sized fillers concluded the presence of a number of erosion suppression mechanisms governing the improvements in the erosion resistance. For instance, the filler volume fraction in the SiR composites was found to be an influential factor in suppressing erosion as it replaces the depolymerizable SiR content fueling progressive erosion during DC DBA. Exploring the effect of incorporating nano-sized fillers in SiR composites could potentially shed the light on a number of additional erosion mechanisms that would reinforce the DC erosion resistance in the composites. Particularly, investigating the application nano sized fillers in SiR composites could emphasize the role of the filler interface on suppressing erosion under DC DBA. Though the application of nano-sized fillers in SiR was extensively researched for the AC outdoor insulation applications, it has been merely investigated for DC outdoor insulation applications.

Developing the mechanistic-based framework to analyze and test the SiR composite material design would essentially require the use of several testing tools. One of the main tools is the inclined-plane tracking erosion test (IPT) which has been utilized in industry and laboratories as the standard testing method for qualifying materials for AC outdoor insulation. The equivalent DC IPT testing guideline has just recently been published after thorough research given the increasing interest to improve the material design for use in the field. Aiding this recently developed standard in (IEEE 2021) with additional accelerated-ageing testing tools that mimic actual DBA in materials like SiR could further expand the analysis in understanding the role of the inorganic fillers in improving the DC erosion resistance of SiR. The dry-arc resistance test, for example, which is conventionally used as an accelerated ageing testing method for determining the tracking resistance of polymers, could also be employed towards supporting the DC IPT outcomes for ranking the erosion resistance of SiR composites for outdoor insulation applications. Unlike the DC IPT, the dry-arc test allows for more controllability of the arcing scintillations in the in terms of discharge duration and magnitude. Accordingly, this could make the dry-arc test a quick testing method that could be used for investigating certain erosion suppression mechanisms in SiR such as the shielding effect introduced by the fillers to suppress stable dry-band arcing in the composites.

1.3 Objectives

This thesis presents a mechanistic-based framework for analyzing the role of nano sized inorganic fillers in the enhancing the DC erosion resistance of SiR composites. The incorporation of nano sized fillers in SiR is investigated as means to develop the SiR material design for use in HVDC outdoor insulation applications. Thus, the objectives of the research presented in this thesis are sequentially described as follows:

1. To establish a study for investigating the effect of the nano filler's interface with silicone on suppressing the DC erosion of SiR nanocomposites. The influence of the favorable interaction at the interface on suppressing erosion is comparatively analyzed against the influence of enhancing the composite thermal conductivity with the inclusion of thermally conductive fillers. This approach essentially highlights the erosion suppression mechanisms the fillers introduce and compares the relative influence of these mechanisms.
2. If the interface of particular nano filler is found in the earlier study to be significantly influential on suppressing DC erosion as compared to the others, the next step will be to examine the effect of that filler when used in the nanometric size as opposed to micrometric size. The essentially investigates the correlation between the role of filler-silicone interaction and the erosion suppression mechanisms involved with the inclusion of the nano filler in SiR as compared to the micro-filler.
3. To employ nano fillers as additives in SiR composite formulations containing micro fillers at high loading levels and investigate the synergism of nano-micro fillers towards suppressing DC erosion of SiR.
4. To investigate the feasibility of introducing the dry-arc resistance test as a supplementary testing method aiding the outcomes of the DC IPT. The arcing scintillations produced during the dry-arc resistance test are repeatable and controllable, which makes the test capable of mimicking the DBA dynamics exhibited by composites in the DC IPT under a more controlled testing environment. The eroded surfaces on the SiR composites could be produced through only minutes of testing time.

This would essentially allow further exploration of the factors governing DC erosion suppression against stable dry-band arcing using a quick testing method like the dry-arc test.

1.4 Methodology

1.4.1 The Overall Mechanistic-based Framework

To achieve the objectives of this thesis, a mechanistic-based framework is followed which involves the preparation and testing of different SiR composite materials. Accordingly, the mechanistic-based framework in this thesis is set to include the input parameters and the material analysis response parameters as shown in Figure 1.1. The input parameters are the inorganic filler attributes of the type, size and loading level. The type and preparation method of the SiR polymer is consistent with all the prepared composites. This would facilitate an attentive analysis for the impact of the filler rather than the type of polymer used. A two-part room temperature vulcanized (RTV) SiR is used to prepare the composites using a high shear mixer. Several filler types are used in this research as the filler type parameter which include silica (SiO_2), alumina tri-hydrate ($Al_2O_3.3H_2O$) and hexagonal boron nitride (h-BN). The particle sizes used in this research range from the nano to the micron range.

The response parameters in this framework are defined in terms of the observed outcomes from three main analytical methods. Those are the electrical, thermal analyses along with the morphology observation. The DC IPT outcome from electrical analysis is considered as the primary parameter in defining the DC erosion resistance of SiR composites. Outcomes from the DC IPT include measurements of the leakage current (LC) during the test, and measurements for the erosion depth of the samples post-testing. The response outcomes from dry-arc resistance test are also employed in this thesis as part of the electrical analysis in different parts of the research. The thermal analyses are used for the thermal characterization of the prepared material. These analyses include the thermogravimetric-differential (TGA-DTA) thermal analysis and the thermal conductivity measurements. Scanning electron microscopy (SEM) is used for two purposes which include observing the filler particle dispersion within the SiR polymer, and to study the morphology characteristics of the eroded

SiR residue from the IPT and the dry-arc resistance test. In summary, the framework adapts the strategy of observing the material analysis response parameters with respect to the change in a given input parameter. The outcomes of the different material analysis parameters will be analyzed and correlated to essentially give a conclusion on the effectiveness of a particular filler and its associated erosion suppression mechanisms on the DC erosion resistance of SiR.

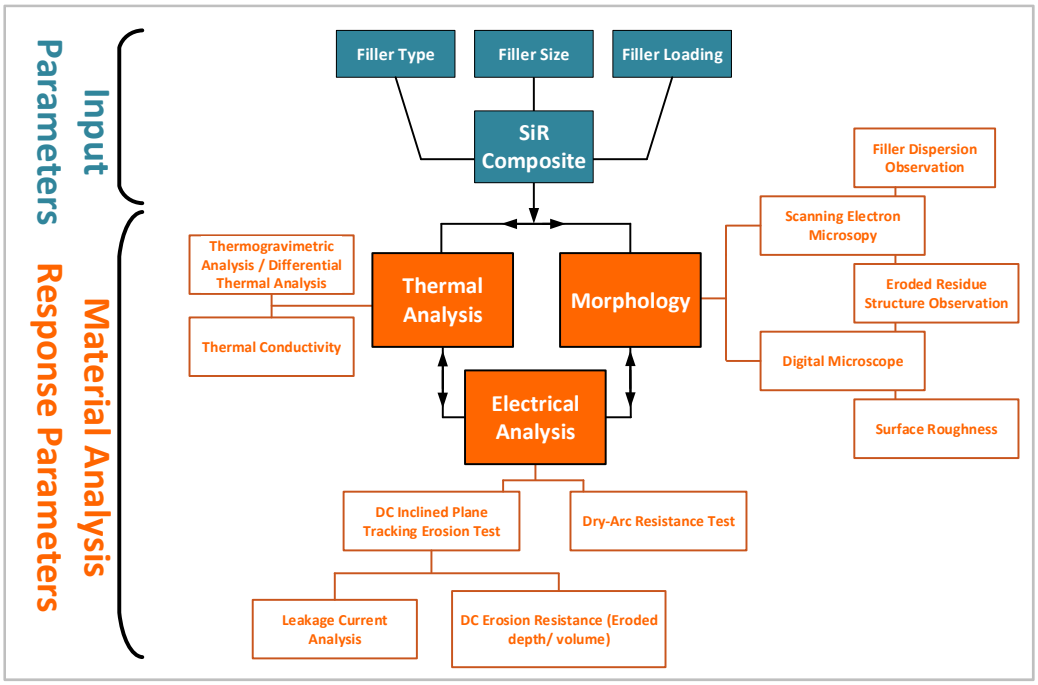

Figure 1.1 Methodology employed in this study based on the mechanistic-based framework

1.4.2 The Inclined Plane Tracking-Erosion Test

The specifics of each of the methods and tools shown in Figure 1.1 including the preparation of the composites will be explained in the forthcoming article chapters of this thesis. With the IPT being one of the main tools for assessing the tracking and erosion resistance of insulating materials, it is essential to elaborate on the basics of the test in this introductory chapter of the thesis for better understanding of the literature findings.

The IPT, shown in Figure 1.2, is set as per the ASTM D2303 (ASTM 2013) or IEC 60585 (IEC 2007) standards to rank the tracking and erosion performance of insulating materials under AC voltage. The test produces accelerated ageing conditions for insulation materials with the aid of a liquid contaminant. As per Figure 1.2, the samples under test are fixed at a 45° inclination with respect to the horizontal plane, and are connected to the setup via the electrode pair assembly. A total of 5 testing specimens of the same composite material are tested simultaneously during a test run. A liquid contaminant is poured into the test material surface through a pneumatic tube which is fed from a peristaltic pump. To ensure the smooth flow of the contaminant, the tube pours the liquid into a filter paper pad which is attached to the upper electrode which is in turn connected, via screws, to the testing circuit. When the test is energized, the contaminant film flowing across the insulator surface connects the top and bottom electrodes, thereby forming a conductive channel connecting the electrodes. The film conducts leakage current (LC) across its surface leading towards the formation of dry-bands and subsequent DBA. The test standard sets the contaminant conductivity, contaminant flow rate, voltage level and ballast resistance (for stabilizing the DBA discharge) for assessing the AC tracking and erosion performance of the material under test. The test is altered for DC testing, +DC or –DC, by rectifying the power source and following the modified testing parameters outlined in IEEE guidelines recently published in IEEE std.2652-2021.

As per ASTM D2303 and IEC 60587, the constant voltage method and stepwise voltage method, or initial tracking method, could be applied during the test. The initial tracking method follows a stepwise procedure of incrementing the voltage level by 0.25kV through three voltage steps of predetermined starting/ending voltage levels to determine the initial voltage that would cause tracking in the material tested. Moreover, both test standards utilize a constant voltage method which stresses the test sample under a fixed voltage level for a long number of hours with a fixed contaminant flow rate and electrical conductivity. Both standards define failure through the initiation of tracking at lengths exceeding 1 inch from the bottom electrode. IEC 60587 includes additional failure criteria for LC exceeding 60mA and deep erosion penetrating the tested sample. Under both standards, the erosion depth is measured at the end of the IPT as means to asses the erosion resistance of the tested material. For the study presented throughout this thesis, the constant voltage method is used to assess the erosion

resistance of the composites. The erosion resistance is determined on the basis of eroded depth or mass at the end of the IPT.

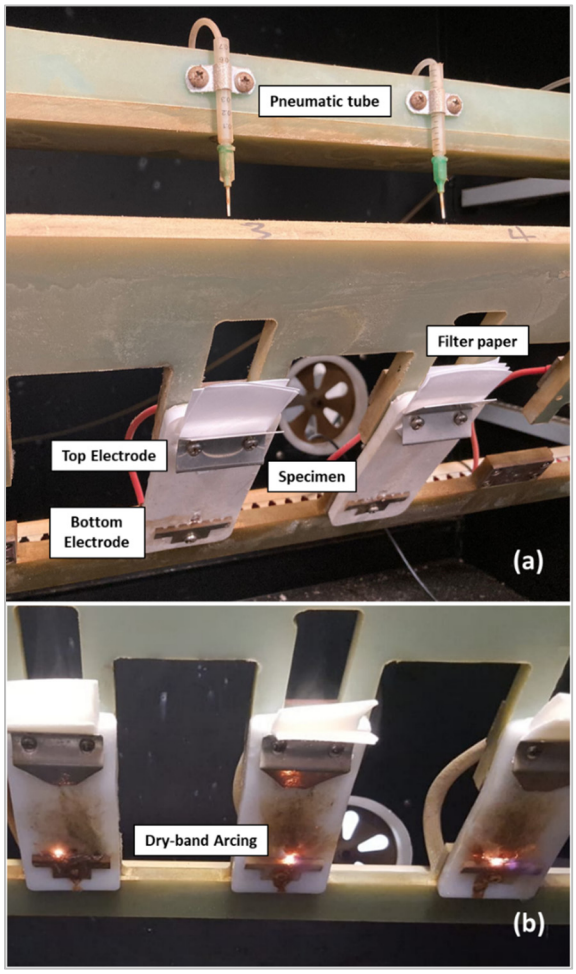

Figure 1.2 (a) The IPT setup showing the testing components
(b) An IPT test run for SiR material under test showing DBA

1.5 Thesis Organization

This thesis is structured to include this introductory chapter followed by eight consecutive chapters. The contents of these subsequent chapters are summarized as follows:

1. Chapter 2: This chapter provides the necessary background and literature review for understanding the subject of this research. The chapter will briefly present the concepts

and background concerned with the field of polymeric high voltage outdoor insulators and the use of SiR in outdoor insulation. The chapter will then illustrate the state-of-the-art work that has been achieved at this point in developing nanofilled SiR outdoor insulators for outdoor insulation applications. The chapter goes on with illustrating the literature findings explaining the key differences of testing SiR under AC and DC voltages. The chapter concludes with the explaining the work done on understanding the role of inorganic fillers, nano and micro sized, on the DC erosion suppression of SiR.

2. Chapter 3: This chapter presents the contents of the first research article which has been published in the IEEE Transactions on Dielectrics and Electrical Insulation journal. The study in this article investigates the role of filler interface on suppressing the DC erosion of RTV SiR composites filled with nano-sized fumed silica, nano ATH and sub-micron hexagonal BN fillers. The study primarily investigates the influence of the nano-filler type and its interfacial properties on suppressing the depolymerization and DC erosion of SiR using the methodology followed in this thesis.
3. Chapter 4: This chapter presents the contents of the second research article which has been published in the Energies journal under the special issue titled “Outdoor Insulation and Gas Insulated Switchgears”. The study investigates the effect of ground (micro-sized) and fumed silica (nano-sized) fillers on suppressing DC erosion in SiR. Fumed silica and ground silica fillers are incorporated in SiR at different loading levels and comparatively analyzed in this study. The objective of this study is to understand the main influential difference between micro and nano fillers on the erosion resistance during DC DBA. This includes investigating the coherency and roughness of the formed residue which could suppress erosion by shielding the unaffected material underneath the damaged surface during DBA, thereby preventing progressive erosion.
4. Chapter 5: This chapter presents the contents of the third research article which has been submitted to the IEEE Transactions on Dielectrics and Electrical Insulation journal. The study in this article investigates the filler barrier effect on suppressing the erosion of SiR composites during the DC dry-band arcing, by supplementing main micro fillers in silicon rubber, ground silica and micro-sized ATH, with fumed silica

and nano-sized ATH fillers. This study integrates the conclusions drawn in the first and second article to employ nano fillers and their interfacial properties towards practical SiR composite formulations of high micro filler loading levels. This essentially examines the synergism between the base fillers and the supplemented nano fillers in creating the barrier effect which acts as an erosion suppressant during DC DBA.

5. Chapter 6: This chapter introduces a study on investigating the use of the dry-arc resistance test for ranking the DC erosion resistance of SiR composites. The study aims to use the dry-arc resistance test as an accelerated testing method towards supplementing the outcomes of the DC IPT in qualifying outdoor insulation materials. The study uses different ATH fillers to prepare different SiR composites at different loading levels to test these composites under the DC IPT and dry-arc resistance test. The study then comparatively ranks the erosion depth and eroded volume outcomes for both tests. The high controllability of the dry-arc test combined with its relatively short testing time makes it suitable for studies investigating the role of inorganic fillers in the DC erosion performance of SiR composites and possibly other material composites.
6. Conclusion and Recommendations: These two chapters summarize the studies presented in this research in accordance with the objectives highlighted earlier. The Recommendations chapter closes the thesis with recommendations on future work that can further solidify the outcomes of this study towards developing SiR materials for HVDC outdoor insulation.

CHAPTER 2

BACKGROUND AND LITERATURE REVIEW

2.1 Polymeric outdoor insulators

Electric power systems heavily rely on outdoor insulators for their transmission and distribution systems. The primary function of the insulator is to mechanically support the live conductors whilst being electrically isolated from the supporting overhead grounded structure like the transmission tower. The typical type of insulator used is that of ceramic material which includes porcelain and toughened glass. Porcelain and glass insulators are known to be highly resistant to degradation under outdoor service conditions and can withstand heating from arc discharges (Gorur et al. 1999). However, these insulators are heavy and highly brittle making them easily vulnerable to fracture under forcible stress, vandalism or poor handling. Polymeric outdoor insulators have superior advantages in terms of their resilience to vandalism, significantly lower weight, and having hydrophobic surfaces as compared to ceramic insulators. Polymeric outdoor insulators could be of either the post or suspension type depending on where its being used in the power system. Figure 2-1 shows a schematic of the suspension-type polymeric outdoor insulator used in transmission tower.

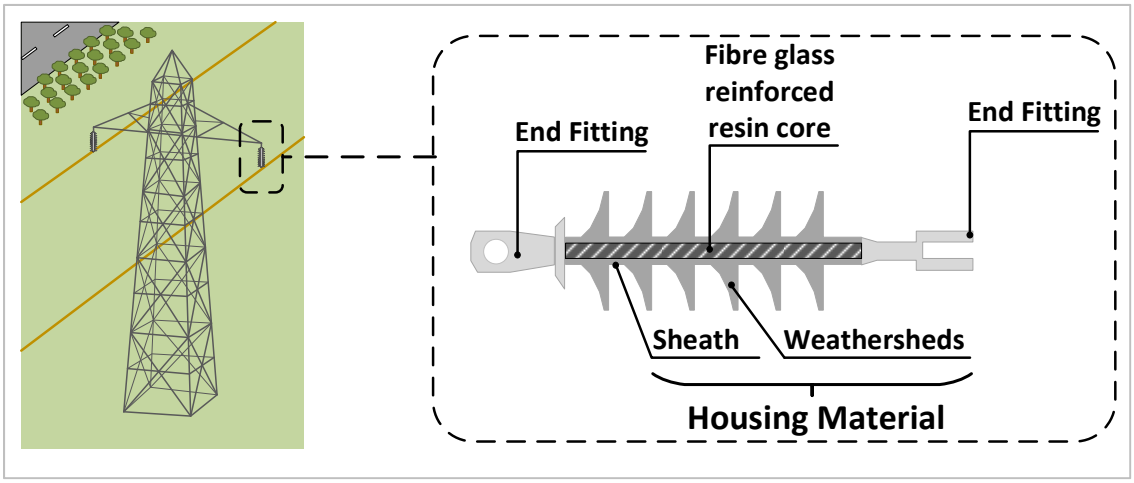

Figure 2.1 Schematic of the polymeric outdoor insulator as used in the transmission system

The insulator comprises of a fiber glass core which provides the mechanical strength of the insulator to withstand the weight of the conductor. The polymer housing material consists of the weathersheds and sheath which serve to encapsulate the core and prevents its exposure to outdoor contamination. Exposure of the core to outdoor contamination combined with the existing voltage gradient during operation could effectively degrade the core. The gradual degradation of the core occurs as it exhibits tracking along its length during outdoor weathering conditions. Eventually, the core undergoes brittle fracture failure which subsequently results into a line drop and electric service interruption (Gorur et al. 1999). Thus, maintaining the reliability of the outdoor insulator is subject of improving the pollution performance of the housing material under weathering conditions. Some of the polymers used in the housing material of outdoor insulators include ethylene propylene rubber (EPR), ethylene propylene diene monomer (EPDM), ethylene vinyl acetate (EVA) and SiR (Hackam 1999).

2.1.1 Development of Dry-Band Arcing

Depending on the area in which the insulator is installed, different types of contaminants and weathering conditions could be encountered during service which effectively degrades the insulator surface. This includes exposure to moisture particles in coastal areas, salt environments, fog and mist. Other contamination could be in the form of airborne dust particles or oil particles (Mathes, Sieffert et al. 1949; Gorur et al. 1999; Butt et al. 2020). Furthermore, exposure of organic polymers to ultraviolet irradiance from sunlight could degrade the material surface by undergoing chemical reactions that could result in breaking chemical bonds or crosslinking (Gorur et al. 1999). The adherence of surface pollutants on the polymer insulator surface hinders the intrinsic hydrophobic properties of the polymer making it hydrophilic. As a result, wet contaminant films from moisture particles begin to form across the insulator surface which, when combined with the voltage stress, would result in the conduction of LC across the insulator surface. This current would essentially cause localized surface heating which boils off parts of the wet contaminant, and results in the formation of discontinuities, or dry-bands, in the contaminant film. The voltage across the dry-bands would result in the ionization and subsequent formation of DBA across the air-channel above the dry-band.

Depending on the LC magnitude and discharge duration, heat is released from the DBA which transmits through the air and impinges on the insulation surface leading to the formation of hot spots. Moreover the transmitted heat from the DBA would result in formation of further dry-bands in neighbouring wet films, which results in multiplying the DBA and creating in sustained scintillations leading to tracking and erosion (Mathes, McGowan 1962).

Progressive tracking and erosion of the insulation material could eventually lead to the failure of the material in outdoor insulation. A surface tracking failure refers to the formation of partially conductive paths across the insulator surface as a result of the formation of carbonaceous residue products from thermal decomposition of the insulation material. Meanwhile, erosion refers to the progressive wearing away of the insulation material as a result of sustained DBA. Substantial improvements have been made towards improving the tracking and erosion performance of the polymers in outdoor insulators to the performance levels obtained with ceramic insulators (Kuffel, Zaengl et al. 2000). The application of polymeric outdoor insulators in high voltage AC service lines can go to voltages as high as 735 kV (Vaillancourt et al. 1998), and ±800kV DC voltage levels in DC lines (Zhang et al. 2013). Figure 2-2 visually illustrates the stages through which DBA occur across the insulator surface leading to tracking and erosion.

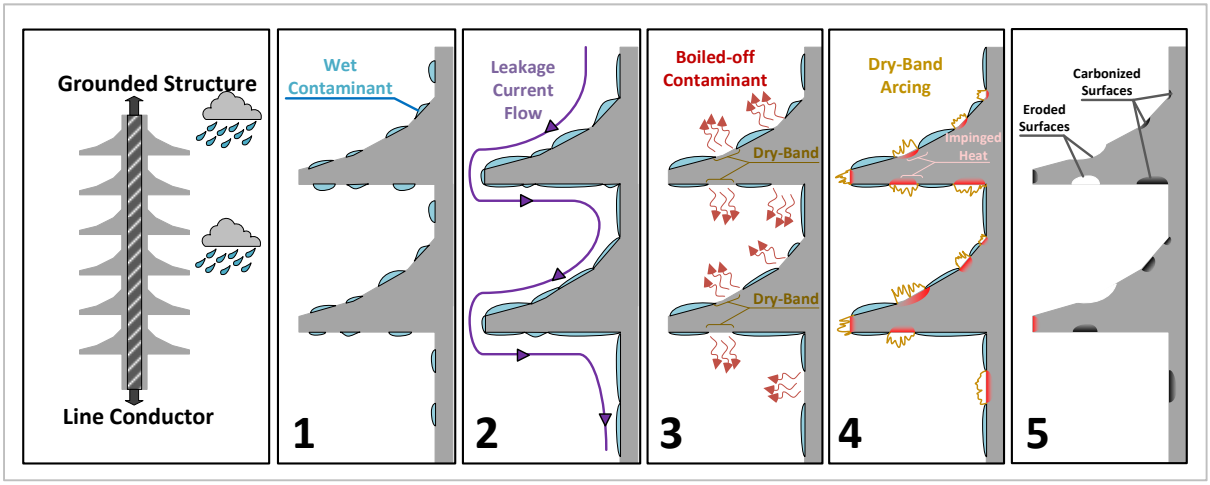

Figure 2.2 Illustration of the stages leading towards the failure of the outdoor insulators under polluted conditions

2.1.2 SiR in Polymeric Outdoor Insulators

SiR was introduced as the candidate material for polymeric outdoor insulators having superior electrical performance to that of ceramic outdoor insulators under polluted conditions (Gorur, Karady et al. 1992). SiR is an elastomeric polymer with alternating silicone and oxygen atoms in their backbone chain, or the siloxane chain.

The typical molecular structure and repeat unit of SiR is shown in Figure 2-3. The side groups attached to the siloxane chains, R and R', determine the properties of the silicone polymer such as its viscosity and crosslinking density. The basic silicone, or polydimethylsiloxane (PDMS), comprises of methyl (CH_3) side groups in their molecular structure. SiR with vinyl groups (CH_2=CH_3), or VMQ SiR which contains both vinyl and methyl substituent groups (ASTM 2005), are typically used for outdoor insulation as they have excellent electrical properties and withstand harsh weathering conditions such as ultraviolet exposure, ozone cracking and oxidation (Callister, Rethwisch 2007).

The silicone material could vulcanize at high temperatures as well as at room temperature depending on the application used. RTV SiR has been utilized for coatings on ceramic insulators, surge arrestors and other power components that are impractical to replace due to economic constraints (CIGRE 2011). High temperature vulcanized (HTV) SiR is mainly used in the weathersheds of newly constructed polymeric outdoor insulators. Both types of SiR are ideally chosen as the candidate material for outdoor insulation due to their characteristic hydrophobicity.

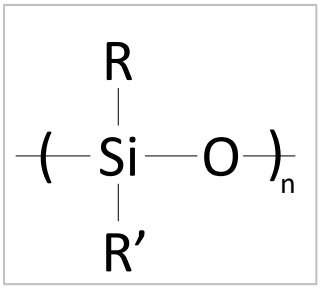

Figure 2.3 Repeat unit structure of SiR with radical side groups
Taken from Callister et al. (2007,)

The hydrophobicity of SiR combined with its electrical insulating property makes it highly desirable for use in outdoor insulation. This is especially important to repel the formation of water-based wet contaminant films across the insulator surface which would otherwise lead to the conduction of LC. Continuous exposure to weathering conditions such as rainfall, dust and other environmental elements would result in the temporary loss of hydrophobicity thereby gradually making the SiR surface hydrophobic. Furthermore, adherence of dry contaminants and oil pollutants on the silicone surface could also lead to altering the hydrophobicity on the surface. However, this temporary loss of hydrophobicity is recovered back within hours of the inception of normal dry conditions which is a key advantage of using SiR for these insulators. The diffusion of the low molecular weight (LMW) silicones fluid component to the SiR surface and the reorientation of the hydrophobic side groups of the polymer on the surface (Kumagai, Yoshimura, 2003) lead to this recovery hydrophobicity.

2.1.3 Thermal Decomposition of SiR in Outdoor Insulation

Compared to organic polymers, the carbon-deficient content in the backbone chain of SiR makes its relatively more resistant to carbonization or tracking as compared to other used polymers in outdoor insulation (Meyer 2005). The carbon content of SiR is mainly found in organic side groups attached to the silicone atoms. The analysis of the residue formed as a result of DBA in RTV SiR was found to contain 1 wt% of elemental carbon in the form hydrocarbon, amorphous carbon and graphite, which was considered insignificant to promote tracking failure (Kumagai, Wang et al. 1998). Moreover, the thermal degradation of silicone composites would result in the release of gaseous methane and carbon dioxide by-products which reduces the amount of carbonaceous residue on the surface that could cause tracking (Kumagai, Yoshimura 2001). Rather, SiR degrades by erosion under the effect of the generated heat during DBA when used for outdoor insulation. Accordingly, all the silicone insulating materials have to be verified for their tracking and erosion performance in the IEC 60587 or ASTM D2303 for outdoor high voltage insulation applications (IEC 2007; ASTM 2013).

Ozone reactions and UV light exposure are considered as secondary aging mechanisms for degrading SiR (Meyer, Jayaram et al. 2005) but are not as severely degradative as eroding DBA.

The thermal degradation mechanisms of SiR were investigated in literature. It was concluded that silicones thermally depolymerize through three mechanisms which are namely the 'unzipping', 'random scission', and 'externally catalyzed' mechanisms (Dvornic 2000). The unzipping mechanism is mainly influenced in silicones containing silanol end groups. Under heating, the silanol groups promote intramolecular redistribution reactions to produce cyclic trimers and tetramer oligomers. This volatilization results in shortening the siloxane chains and degrading the silicone polymer (Hamadani, Longuet et al. 2009).

Random scission is the primary mechanism governing depolymerization in all silicones. This mechanism involves the thermal depolymerization of the siloxane chains through the scission the Si-O bonds to generate cyclic oligomers, hexamethylcyclotrisiloxane, and shorter siloxane chains. The depolymerization rate in this mechanism is governed by the flexibility of the siloxane chains and the high polarity of the siloxane bonds (Camino, Lomakin et al. 2001). The produced cyclic oligomer undergoes thermal oxidation to produce an inert silica ash residue on the degraded surface. The random scission mechanism could progress anywhere throughout the siloxane chain (the middle, end, etc.) further shortening the chain length until no more oligomers could be produced.

The final mechanism which could degrade silicones is through externally catalyzed reactions. These involve the presence of polar impurities and additives that could trigger the Si-O bond scission to degrade the SiR. An example of this would be the hydrolysis of the Si-O bond by the introducing a hydroxyl anion (Hamadani, Longuet et al. 2009). Figure 2-4 shows the thermal degradation mechanisms of SiR as illustrated in by (Hamadani, Longuet et al. 2009).

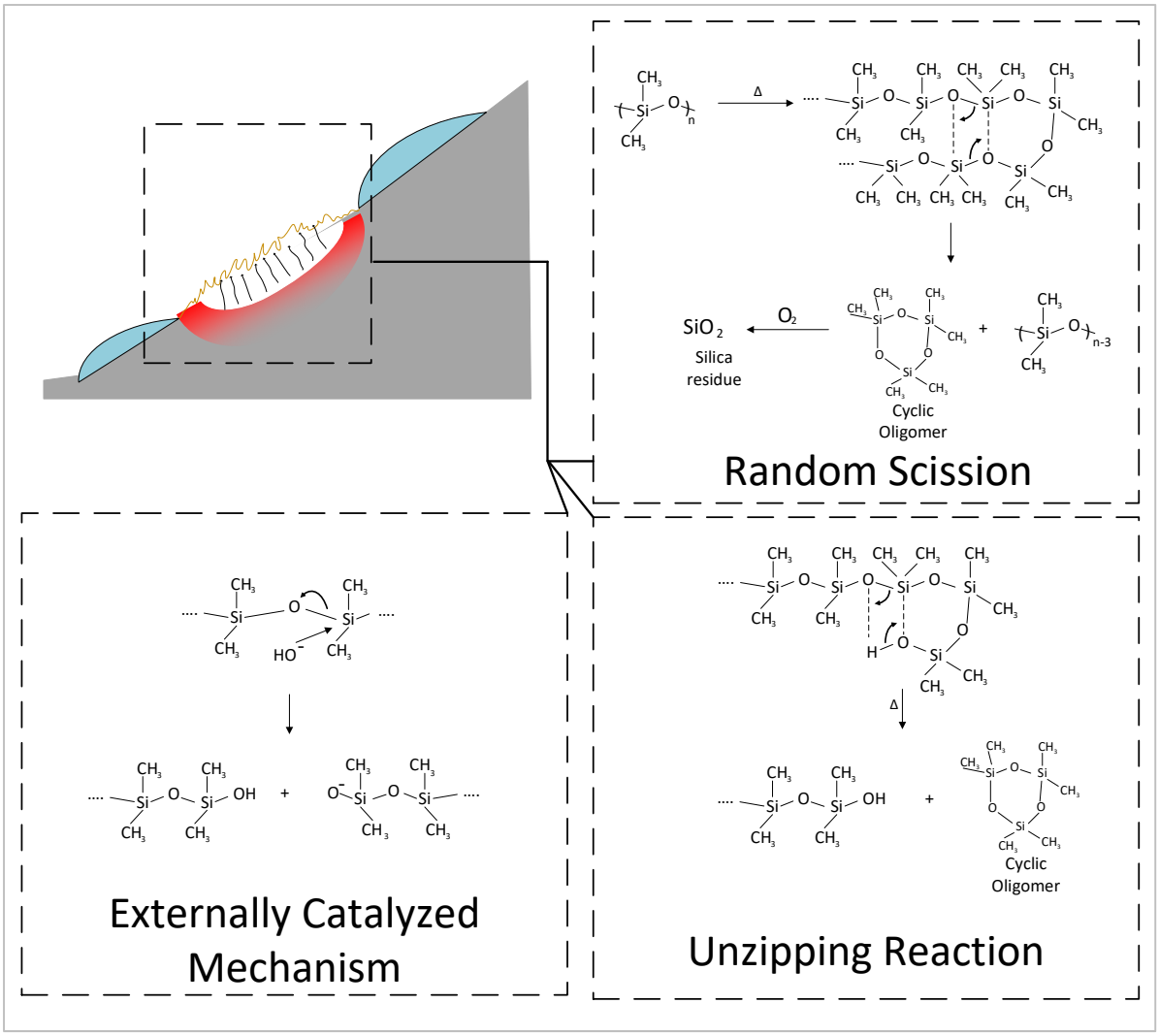

Figure 2.4 Thermal degradation of SiR through random scission, unzipping reaction and externally catalyzed mechanisms
As illustrated by Hamadani el al. (2009, p. 466-467)

2.2 Inorganic Fillers in SiR Composites and Nanocomposites for Outdoor Insulation

Inorganic fillers are incorporated in polymers to create composites of these polymers of enhanced mechanical, thermal or electrical properties. In the case of outdoor insulators, inorganic fillers are filled in polymers to primarily reduce their processing cost by replacing a

significant amount of the silicone content by the inorganic filler. Moreover, research indicates that the addition of certain fillers to SiR would essentially improve the material's tracking and erosion resistance. As such, incorporating inorganic fillers in SiR and other polymers has been researched thoroughly with respect to the different filler types, mixing methods, and curing methods that could enhance the tracking and erosion resistance of the composites for outdoor insulation applications. Fillers are incorporated in SiR in the industry at loading levels of more than 60wt%. Higher loading levels than that would impact the mechanical properties of the composite, making them impractical for fabrication for outdoor insulators.

Introducing certain mineral inorganic fillers, such as ATH, could initiate a number of flame retardant effects that would help improve the thermal decomposition properties of the polymer. First, the filler's endothermic decomposition at temperatures below that of the polymer decomposition could significantly improve the heat capacity of the composite. Secondly, decomposing fillers could produce inter diluent gases which reduce the concentration of combustible volatiles that could self-sustain the flammability of the polymer. An example for this would be the release of water vapor with ATH or carbon dioxide with calcium carbonate fillers. The third flame retardant mechanism would be the formation of an inert layer residue shielding the bulk composite from the influx of heat and obstructing the diffusion of oxygen into the composite (Rothon 2003; Hull, Witkowski et al. 2011).

Adding inorganic fillers to SiR to formulate composites for outdoor insulators has been the subject of immense research to improve the tracking and erosion resistance of the material. Silica and ATH are the most commonly used fillers for SiR composites in industry (Meyer, Omranipour et al. 2002). Using silica comes from its high electrical resistivity and low dielectric constant which makes it a suitable filler for dielectric polymer composites used in insulating materials (Huang, Jiang et al. 2011). Incorporating ATH fillers in SiR for outdoor insulators was used as a common practice in the outdoor insulation industry given its flame retardant properties and its lower decomposition temperature of ATH (180-220 °C) compared to the silicone polymer (400 °C) (Hackam 1998). The addition of silica and ATH in SiR composites was found to improve the thermal conductivity of the overall composite as compared to unfilled SiR (Meyer, Cherney et al. 2004). Using other fillers that could

substantially increase the thermal conductivity of SiR such as silicon carbide or zinc oxide is unfeasible given the high permittivity of these fillers for use in dielectric materials and for high voltage insulation applications (Cherney 2013; Huang, Jiang et al. 2011). Unlike silica, zinc oxide filled SiR could become highly conductive under high electric fields when the filler concentration surpasses the percolation threshold as was shown in (Gao et al. 2016).

2.2.1 Introduction to Nano Fillers and Nanofilled composites in High Voltage Insulation

Introducing nano-sized fillers in polymer materials has gained a wide interest for numerous applications in industry including high voltage insulation. Nanofilled composites or nanocomposites are defined as polymers that are filled with homogenously dispersed nano-sized fillers which are in the 1-100 nm size range with low weight content ranging from 1 to 10wt% (Tanaka, Montanari et al. 2004). If the nano fillers, or nano filler, are well dispersed, the inter-filler spacing between these particles are in the nanometric range which is much smaller than that of micron-sized filler particles spacing in polymer composites. Thus for the same volume fraction of the filler, the number of particles would be numerously larger for nano fillers as compared to micro fillers. This could result in formulated composites having significant improvements in their electrical, thermal and physical properties.

Reducing the inorganic filler particle size to the nanometric range would result in a substantial increase in the interfacial area available to interact with the matrix polymer (Lewis 2004). This is not similarly observed with micro-sized fillers in which the increase in the interfacial area, or interaction zone, is marginal with a massive increase in the filler volume fraction (Nelson 2010). In the interaction zone, the polymer chains interact with the filler particles through either physical or chemical forces of attraction. These forces could be in the form of ionic, covalent, hydrogen bonding and Van der Waals forces of attraction (Tanaka 2010). Depending on the surface groups on the filler surface, the polymer matrix chains could strongly or favorably interact with the filler particles to become immobile at the bound layer (the second layer). Thus, the flexibility of the polymer matrix chains is highly the subject of the amount of

surface area available in the filler to interact with the polymer matrix. This observation is the prime advantage for using nano fillers as means of improving the thermal and mechanical properties of the material.

Incorporating nano filler in nanocomposites for electrical insulation applications was primarily investigated as means to improve the dielectric breakdown strength and the voltage endurance of these materials (Tanaka, Montanari et al. 2004; David, Fréchette 2013). This would essentially improve the insulating properties of the composites against high electrical stresses caused by defects and voids in the insulating materials. Some of the tested nanocomposites included polyefin polymers such as polyethylene and polypropylene, and elastomers like SiR and EPDM, with silica, alumina and other metallic oxides, and layered silicate fillers (David, Fréchette 2013). Supplementing nano fillers to conventionally filled micro-composites was explained as being greatly advantageous in terms of obtaining high voltage insulating materials of superior electrotechnical performance as compared to microcomposites (Fréchette, Reed 2006). For outdoor insulation applications, the use of nano fillers in SiR materials shows promising outcomes in high voltage insulating materials as indicated in literature. The primary disadvantage of using using nano fillers in the outdoor insulation industry, however, are their associated high costs which limits the use of nanocomposites in outdoor insulation. Rather, supplementing SiR composites containing micro fillers with nano fillers introduces practical low-cost SiR formulations with improved pollution performance as compared to conventional microcomposites (Cherney 2013).

2.2.2 SiR Nanocomposites for Outdoor Insulation

Fumed silica is one of the nano-sized fillers that have been widely used to reinforce SiR composites through low filler loading levels by wt%. The current industry practice incorporates approximately 2wt% fumed silica in silicone compounds used in surge arresters housings and bushings (Cherney 2013). Incorporating fumed silica (nano-sized) in SiR for outdoor insulation applications was investigated by El-hag et al. and analyzed against micron-sized silica in SiR composites (El-Hag, Simon el al. 2006). In their research, fumed silica filled by

10wt% in SiR had a better erosion resistance as compared to 50wt% micro silica filled SiR as indicated by the outcomes of the IPT. Through TGA, El-Hag explained the role of the interactive bonding between fumed silica and SiR in increasing the final residual weight and improving the thermal stability of the SiR nanocomposite. This was evident with the higher calculated additional residual weight obtained at the end of the TGA run as compared to unfilled SiR. The effect of nano silica on improving the erosion resistance of SiR was further explored by Muniraj et al. on virgin and thermally aged SiR composites (Loganathan, Muniraj et al. 2014). Using the IPT, it was observed that increasing the nano silica filler loading improved the erosion resistance of aged SiR composites as compared to micro silica filled SiR aged composites at the same loading level. This was attributed to the role of the hydroxyl groups attached to the nano silica surface interacting with SiR which improved the thermal stability of the SiR composite even after accelerated thermal ageing.

Ramirez et al. studied the application of surfactants and the effect of calcination on the erosion resistance of fumed silica and micro silica filled SiR composites (Ramirez, Jarayam et al. 2009). It was illustrated that the concentration of silanol groups on the silica surface is an important factor that defines the filler-silicone bonding and, subsequently, the thermal stability of the composite against DBA. Using the IPT, salt-fog test and the laser ablation tests, it was found the SiR composites containing the combination of surface treated fumed silica and micro silica fillers, at 20wt% and 2.5wt% respectively, had the lowest recorded eroded masses amongst all composites. According to Ramirez, the surfactant weakens the surface energy of the filler particles and lowers their interfacial tension leading to better dispersion in the silicone matrix and reduced agglomeration. Calcinating the fillers proved to have adverse effects on the silanol group concentration on the silica surface, thus worsening the erosion resistance of these composites under all tests. Application of high concentrations of the surfactant were shown to have a negative impact on the hydrophobicity of the SiR composites, leading towards being hydrophilic. In other research concerning the dispersion methods of the filler particles in SiR, it was concluded that the application of hydrophobic surface treatment on nano silica fillers resulted in a poorer dispersion of silica with higher agglomerates as compared to untreated nano silica (Kozako, Higashikoji et al. 2012). The cause of this was due to the silanol

groups on the silica surface being attracted to the surface treatment agent which could have otherwise been bonded to the SiR siloxane chains via hydrogen bonding as is the case with untreated silica. The treated silica had weak and loose interactions with SiR through Van der Waals forces at the interphase. This outcome highlighted the role of the filler surface groups on the dispersion and filler-polymer interactions in silica filled SiR nanocomposites.

Application of thermally conductive nano sized fillers to create SiR nanocomposites of enhanced thermal conductivity has been a subject of research in recent years. An example of such fillers is nano-sized alumina (Al_2O_3) which was studied as a candidate filler for use in outdoor insulation applications in SiR nanocomposites. In a recent study by Nazir et al., nano alumina was found to have substantial effects on improving the tracking and erosion resistance of SiR nanocomposites (Butt, Nazir et al. 2020). The thermal conductivity of SiR was significantly improved with the addition of alumina which evidently enhanced the erosion performance of the composites under the IPT. This was attributed to the network of interaction zones formed by the alumina particles, providing thermally conductive chains for the dissipation of heat from the insulator surface. Another assumption was the increase in phonon transport through alumina particles which facilitated the heat flow. Nano alumina was also investigated as part of a co-filled combination of fillers in SiR composites containing silicone nitride (Si_3N_4) (Zha, Dang et al. 2014). An improvement in the thermal conductivity was observed with the increasing volume fraction of nano alumina in the SiR composite which was attributed to the role of the nano filler in filling the gaps between the micron-sized Si_3N_4 particles in the composite and thereby facilitating more pathways for the conduction of heat. However, the agglomeration of nano alumina at higher volume fractions was a decisive factor in reducing the impact of the nano filler on thermal conductivity enhancement. Using the IPT, Venkatesulu et al. illustrated a comparable erosion resistance of 4wt% nano alumina filled SiR to 30wt% micro ATH filled SiR (Venkatesulu, Thomas et al. 2010). This was attributed to the role of the nano filler in interactively bonding with SiR to immobilize its siloxane chains, and in turn improve its thermal stability and erosion resistance under the IPT. In a research conducted by Ramirez et al. 2008 for analyzing the heat ablation performance of SiR nanocomposites under laser ablation tests, surface treated nano alumina filled at 2.5wt% had higher eroded masses compared to surface treated fumed silica filled SiR of the same loading

level (Ramirez, Cherney et al. 2008). Ramirez explained that the fumed silica SiR nanocomposite could have introduced an additional residue barrier mechanism that protected the underlying silicone from further erosion, which was not similarly introduced with nano alumina. However, no additional evidence was presented to support this conclusion.

Despite nano alumina being a relatively cheap filler with a high electrical resistivity, it has a drawback of having a high dielectric constant (9 at 1 MHz) which, according to Huang et al (Huang, Jiang et al. 2011), limits its use for insulation applications. Boron nitride is one of the fillers of exceptional thermal conductivity that has a high electrical resistivity. The application of hexagonal boron nitride (h-BN) to enhance the thermal conductivity and maintain excellent dielectric properties of polymers for high voltage insulation applications was shown to be successful (Wang, Lizuka et al. 2011; Heid, Fréchette et al. 2015). Accordingly, h-BN in the nanometric size range was investigated as a filler in SiR nanocomposites (Kemaloglu, Ozkoc et al. 2010; Khanum, Jayaram 2019). Kemaloglu et al. observed that for a given filler loading level, the thermal conductivity of SiR is increased to higher levels with micron-sized BN as compared to BN nano filler which was attributed to the higher aspect ratio of the micro filler (Kemaloglu, Ozkoc et al. 2010). A drawback was found with increased filler loading of nano and micro BN which is the weakening of the mechanical properties of the SiR composite and adversely impacting its tensile strength. The deterioration of the tensile strength was a result of the absence of strong interactions between the silicone polymer and the filler particles. Still, however, the BN filled SiR composites had better tensile strength and modulus as compared to the micron-BN filled composites. Khanum et al. explored the use of nano BN in micro silica filled SiR of high filler loading for outdoor insulation (Khanum, Jayaram 2019). In the study it was found that increasing the BN loading to 5wt%, with 55wt% micro silica, had an evident effect on improving the erosion resistance of the composites under the IPT as compared to 60wt% silica filled SiR. This was obtained despite the slight improvement in the composite thermal conductivity between the two composites. The outcomes of this study were useful in depicting the effect of supplementing a nano filler of high thermal conductivity to a base filler that favorably interacts with SiR.

Hydrated nano fillers such as nano-ATH and nano-magnesium hydroxide (MDH) have been investigated for use in SiR as flame retardant fillers of high specific surface area. Venkatesulu et al. filled MDH nano filler by 5wt% in SiR and compared its erosion resistance to unfilled SiR and 5wt% silane treated micro ATH filled SiR under the IPT (Venkatesulu, Thomas 2008). Both fillers endothermically decompose in SiR to release water vapor at different temperatures, leaving behind an inert alumina and magnesium oxide residue respectively. It was concluded that the MDH filler had a slightly better role in suppressing erosion as compared to micron-ATH, and both had a much-pronounced erosion resistance as compared to unfilled SiR. The high specific area of the MDH filler and the improved thermal stability of the composite were used to explain the marginal improvement in the erosion resistance. However, no clear explanation on difference between the erosion suppression mechanisms between the fillers was presented. Jeon et al. examined the tracking resistance of nano-ATH filled SiR composites with loading levels ranging from 1 to 20wt% (Jeon, Hong et al. 2019). Their preliminary outcomes indicate a superior tracking resistance in terms of the time-to-track for the 5wt% nano-ATH as compared to 20wt% micro silica filled SiR attributing to the high specific surface area of nano-ATH. However, the nano-ATH particles agglomerated to sub-micron size aggregates with just 5wt% loading level as was shown using transmission electron microscopy (TEM) images which possibly dismisses the high specific surface area of the filler as a governing factor to suppress tracking in their study. Moreover, not much attention was given to the erosion resistance of the composites as part of the conducted study with more emphasis being on tracking which is not the governing ageing mechanism of SiR.

2.3 SiR Composites and Nanocomposites for HVDC Outdoor Insulation

The aforementioned literature is mainly concerned with investigating SiR nanocomposites for use in HVAC outdoor insulation applications, which has been an issue of wide interest given the high number of existing AC lines globally at the time. Investigating the application of nano fillers in SiR for HVDC outdoor insulation is gaining momentum in recent years given the rising interest in HVDC power transmission. The assumption of using the same experience and knowledge developed for SiR composites for AC outdoor insulation towards DC outdoor

insulators is feasible if the same erosion performance levels can be obtained under both modes of voltages. Accordingly, studies on this issue have been rigorously investigated in literature.

2.3.1 Erosion Performance of SiR under AC and DC Voltages

Investigating the tracking and erosion performance of polymers under polluted environments was compulsory given the thermal degradation of these materials under sustained DBA. This was not the issue with ceramic insulators where DBA does not age the insulator material, but rather promotes flashovers under polluted environments. Examining the impact of DBA on polymeric materials such as SiR and EPDM on the basis of the type of voltage stress, AC or DC, was examined in 1988 under the salt-fog test (Gorur, Cherney et al. 1988). The test involved cylindrical rods of HTV SiR composites, containing ATH and silica fillers, which were sprayed with a vapor contaminant and stressed under high voltage through end fitted carbon electrodes. Under the test it was observed the SiR had a much lower resistance to tracking and erosion under the negative DC (-DC) voltage as compared to AC and positive DC (+DC) voltages. Under -DC, the samples demonstrated a faster transition into hydrophilic surfaces with higher LC magnitudes across the insulator surface.

Later research conducted for investigating the pollution performance of ATH filled SiR composites under the IPT showed an inferior tracking and erosion performance for the composites under the +DC voltage as compared to AC (Moreno, Gorur 1999). The samples were artificially polluted by immersion in a slurry non-soluble contaminant prior testing under the IPT. The test outcomes were analyzed with respect to the parameters of the adhered pollutant density concentration and the wet contaminant electrical conductivity of the IPT. It was found that the samples subjected to +DC stress failed, either by high tracking lengths or deep erosion, at equivalent and lower pollution and conductivity levels compared to those stressed under AC, with higher DBA LC current magnitudes and longer discharge durations.

Gustavsson et al. examined the ageing of SiR composites containing ATH and silicone oil in a coastal field substation in Sweden under AC and -DC voltages with different voltage stress levels (Gustavsson, Gubanski et al. 2001). In their findings, it was observed that DC stressed

samples exhibited inferior erosion levels with higher LC magnitudes than those stressed under AC voltage. Analyzing the eroded surfaces of the insulators using X-ray photoelectron spectroscopy (XPS) lead to the conclusion that SiR oxidative crosslinking, typically resulting from corona discharge, was not the governing ageing mechanism for the tested samples. Rather, outcomes of gas chromatography-mass spectroscopy (GCMS) indicated high levels of low molar mass siloxane tetramers (D_3-D_6) found in the eroded surfaces indicating depolymerization initiated by DBA. Lower concentrations of the low molar mass siloxanes were found in on the surfaces DC tested samples which was assumed to be the result of the higher discharge activity and, subsequently, higher amount of volatiles released during depolymerization.

Heger et al. investigated the severity of erosion and hydrophobicity retention properties of ATH filled RTV and HTV SiR composites, along with EPDM samples tested under the IPT using AC, +DC, and -DC voltages (Heger, Vermeulen et al. 2010). In their findings, RTV SiR experienced the highest erosion depths under -DC while HTV SiR exhibited deep erosion under +DC. EPDM, however, had the worst erosion performance under AC. All materials experienced the fastest loss of hydrophobicity during the IPT under -DC voltage, which was recovered within a 24 hour period for the SiR samples only. The average root-mean-square leakage (RMS) LC during the IPT for the HTV SiR samples was comparable under all stresses, which was not similarly observed with the RTV SiR exhibiting highest LC under +DC testing. Thus the authors explained that the LC magnitudes and the average dissipated energy over the test run are not necessarily indicators of the erosion severity of HTV SiR under the IPT.

The pollution performance of SiR stressed under different voltage modes whilst being exposed to severe industrial conditions was also investigated in literature. Rajini et al. (Rajini, Udayakumar 2009) studied the impact of the voltage type on the tracking and erosion resistance of SiR exposed to radiation environments such as those in nuclear power plants. SiR was exposed to different dose rates of gamma radiation, and were later tested using the IPT. In their findings it was concluded that AC IPT tested samples neither tracked nor eroded after exposure to the gamma radiation with all different gamma dosage levels used. With DC voltages, however, erosion exceeding 2 mm in depth was observed for all the tested samples

after radiation exposure under all the tested radiation doses. The -DC voltage polarity was noted as the most severe voltage leading to the highest erosion depths and shortest tracking time. Verma et al. tested RTV and HTV SiR composites under the IPT with a nitric acid component being added to the standard solution contaminant to mimic the effect of acid rain on the insulator surface (Verma, Reddy 2018). The LC under AC and +DC testing was intensified in terms of magnitude with the addition of the acidic contaminant as compared to the regular contaminant of the same electrical conductivity. Still, the +DC voltage had more adverse effects on the erosion of RTV SiR as compared to AC under acidic contamination.

Using commercial SiR composites that were used in HVAC outdoor insulation, Bruce et al. illustrated through the DC IPT the impact of the voltage polarity on the erosion performance of the composites (Bruce, Rowland et al. 2010). The positive voltage polarity was indicated as being the most severe voltage leading to deep erosion of SiR under the IPT. In their experiments, they indicated that the positive electrode (upper electrode) undergoes electrolysis during the IPT which results in the liberation of metallic ions into the contaminant and thus increasing their electrical conductivity. The effects of electrolysis are demonstrated in terms of the higher arcing power exhibited by the composites during the DC IPT. Electrolysis of the upper electrode was also explained to be a contributing factor in high leakage currents of +DC tested samples by Vas et al. (Vas, Venkatesulu et al. 2012) and Verma et al. (Verma, Reddy 2018). The effect of the DC electric field on the attraction of airborne contaminants to the electrodes was cited as a potential cause of the increased severity of the LC (CIGRE 2015). In the case of AC stressed insulators, the net effect of the electric field is nil which does not result in the drift of contaminants to the electrodes. Another contributing factor was related to the electro-hydrodynamic effects of the voltage stress on the contaminant which could impact the LC magnitude across the insulator surface (Bruce, Rowland et al. 2010).

Ghunem et al. explained the impact of electrowetting on the contaminant conductance during the IPT as a function of the type of voltage mode applied on SiR composites (Ghunem, Jayaram et al. 2013). Based on observations of the initial tracking voltage and LC measurements, it was suggested that the lowest expulsion of droplets from contaminant rivulet in the IPT was during

+DC testing. This consequently leads to a relatively higher conductance of the contaminant, as compared to AC or -DC, and the higher LC. Moreover, Ghunem et al. illustrated that the relatively shorter arc lengths observed under +DC leads to a more localized heating over smaller areas in the sample to which the DBA power is dissipated causing higher erosion severity as compared to other voltages.

2.3.2 Role of Inorganic Fillers in the Erosion Performance of SiR DC Voltage

The role of inorganic fillers in suppressing erosion in SiR composites was thoroughly researched for AC outdoor insulation applications. Through many works such as (Meyer, Jayaram et al. 2005), it was concluded that enhancements in the thermal conductivity of SiR through the incorporation of fillers could significantly improve the erosion resistance of the material. For DC outdoor insulation applications various types of inorganic fillers have been experimented for developing the reliable use of SiR material under DC voltages.

Du et al. employed nano BN in RTV SiR composites through different loading levels ranging from 1wt% to 7wt% (Du, Xu 2014). The thermal conductivity of the SiR composite significantly enhanced with the increasing weight fraction of BN as indicated through several measurements in their work. Accordingly, the DC IPT outcomes showed an improved erosion resistance with low erosion depths and eroded material masses as the loading level of BN increased. Through measurements of LC, it was concluded that the total discharge quantity, in coulombs, of DBA was significantly decreased at high loading levels of BN. This was mainly attributed to the role of BN in improving the heat dissipation of the composites against the influx of heat, resulting with lower localization of hot spots and subsequent formation of dry-bands and DBA. This improvement in heat dissipation was further illustrated through thermal imaging of the samples during the IPT.

Vas et al. in (Vas, Venkatesulu et al. 2012) investigated the role of micron-sized ATH and nano alumina in enhancing the erosion resistance of SiR composites under DC voltage. The composites were tested under both voltage polarities, +DC and –DC, and analyzed on the basis of eroded mass, LC and surface morphology. In their findings, -DC testing did not show the impact of the different filler sizes in suppressing erosion under the IPT which was indicated in

the comparable erosion resistance outcomes. With +DC, however, 4wt% nano alumina had a clear impact on improving the erosion resistance of SiR which was comparable in the performance of 30wt% micro ATH filled SiR. Through SEM, Vas et al. illustrated the impact of both fillers in improving the surface morphology of the eroded pit showing a more coherent residue as compared to unfilled SiR. The crack-density and residue coherency was improved with the inclusion of nano alumina as compared to micro ATH. This residue was highlighted as a protective mechanism which could shield SiR from progressive erosion under DC voltage.

Micron-sized ATH and silica fillers in SiR were investigated for HVDC outdoor insulation in the work of Ghunem et al. (Ghunem, Jayaram et al. 2015). It was highlighted that 30wt% ATH and silica filled SiR composites had a slower inception for stable DBA as compared to unfilled SiR. It was explained that the volume effect of the fillers replacing the depolymerizable SiR content had a clear effect on delaying the stable DBA inception and lowering its magnitude compared to unfilled SiR in the DC IPT as indicated by the 3rd detail wavelet component of the measured LC. Using differential thermal analysis (DTA), lower exotherms were observed for 30wt% silica filled SiR as compared to unfilled SiR. This was attributed to the role of the filler in suppressing SiR depolymerisation which subsequently reduces the amount depolymerized combustible SiR volatiles. With 30wt% ATH, the inception of the 3rd detail component was relatively slower compared to 30wt% silica which indicated the secondary role of the enthalpy of dehydration of ATH in suppressing erosion by diluting the gaseous phase of volatile SiR.

In a recent research conducted by Kone et al. using micron-sized silica fillers in SiR, a number of observations were noted regarding the erosion suppression mechanisms introduced by fillers in SiR under the DC IPT (Koné, Ghunem et al. 2019). In addition to the primary role of the filler volume in replacing the SiR content in the composite, the characteristics of the residue formed during the erosion of SiR played a secondary role in hindering progressive erosion. The thermo-oxidation of SiR volatiles during DBA yields a silica-based residue which adheres on the eroded pit. The residue was observed to be more coherent with a higher integrity with

smaller filler particle sizes, which resulted in significant enhancements in the DC erosion resistance of SiR.

The significance of the residue characteristics in impeding progressive erosion was also highlighted in SiR composites filled with hydrated fillers (Ghunem, Koné et al. 2020). ATH and MDH filled SiR composites, at equivalent loading levels, were tested under AC and DC voltages in the IPT and analyzed using TGA-DTA. A comparable erosion performance was observed amongst all the composites under the AC IPT which did not highlight the role of the filler type on supressing erosion. With the DC IPT, however, MDH filled SiR had inferior erosion performance as compared to ATH filled SiR under +DC. Through SEM, the ATH filled composites appeared to have more coherent residue with lower porosity as compared to that of MDH filled SiR residue. Using TGA-DTA, a difference in filler dehydration mechanisms was observed with the different fillers. Specifically, the outcomes indicate that MDH dehydrates during the depolymerization of SiR while ATH dehydrates prior SiR depolymerization which results in a more porous incoherent residue with the former. Thus the hydrated filler type clearly has an influence on the residue characteristics and, in turn, the erosion resistance of SiR under DC.

Limited work was conducted on investigating the role of nano fillers to enhance the DC erosion resistance of SiR. Rather, most of the recent contributions were related to the impact of micron-sized fillers on the DC erosion resistance of SiR composites and investigation the filler's associated erosion suppression mechanisms. The key difference exhibited by a given SiR composite under DC and AC testing is the increased stability of the arc under DC as compared to AC voltages (particularly +DC). Since promising outcomes have been found with using nano fillers in SiR for AC outdoor insulation, it would be plausible to assume that significant findings could be observed with the application of nano fillers in SiR for DC outdoor insulation since the ageing mechanism of SiR is a thermal erosion problem under both AC and DC voltages. Thus, this thesis presents a framework for highlighting the role of nano-sized inorganic fillers in suppressing DC erosion under DBA and identifying the erosion suppression mechanisms associated with the use of such fillers in SiR composites.

CHAPTER 3

ANALYZING THE ROLE OF FILLER INTERFACE ON THE EROSION PERFORMANCE OF FILLED RTV SILICONE RUBBER UNDER DC DRY-BAND ARCING

Alhaytham Y. Alqudsi[a], Refat A. Ghunem[b] and Éric David[a]

[1]Department of Mechanical Engineering, École de technologie supérieure,
1100 Notre-Dame West, Montreal, Quebec, Canada H3C 1K3
[2]Metrology Research Center, National Research Council Canada,
1200 Montreal Road, Ontario, Ottawa, Canada K1A 0R6

Paper published in *IEEE Transactions on Dielectrics and Electrical Insulation,* June 2021

Abstract

This study investigates the role of filler interface on suppressing the erosion of room temperature vulcanized silicone rubber composites filled with fumed silica, nano alumina trihydrate and sub-micron hexagonal boron nitride fillers during DC dry-band arcing. Simultaneous thermogravimetric-differential thermal analyses indicate a superior effect for fumed silica in suppressing the depolymerization of silicone rubber and promoting radical based crosslinking. This could be attributed to favorable interactions at the fumed silica-silicone interface tethering the siloxane chains. At low filler loading of alumina trihydrate, water of hydration had insignificant effects on suppressing depolymerization compared to that influenced by fumed silica's interface at equal filler loading. Similarly, incorporating thermally conductive boron nitride filler in silicone rubber did not show improvement in the depolymerization rate compared to that influenced by fumed silica. These findings correlate with the +DC inclined plane tracking and erosion test outcomes indicating superior erosion performance for the fumed silica filled composite. This accordingly supports the influential role of the filler interface over the water of hydration and thermal conductivity enhancement in suppressing the DC erosion of silicone rubber composites under the test conditions of this study. A statistical boxplot analysis technique is introduced to elucidate the inception of the

stable dry-band arc in terms of the change in leakage current randomness during the +DC inclined plane tracking and erosion test. The boxplots reveal a slow inception of the stable dry-band arc with the fumed silica filled composite delaying the erosion of silicone rubber during the test. This finding confirms the influence of the filler interface over composite thermal conductivity in suppressing erosion of silicone rubber under DC dry-band arcing.

Keywords: Silicone rubber, DC inclined-plane test, erosion, inorganic filler, filler interface, thermal conductivity.

3.1 Introduction

Silicone rubber (SiR) is commonly utilized as a housing material for polymeric outdoor high voltage insulators. Using inorganic fillers, developing the SiR insulator housing material requires improving its erosion performance against heat ablation caused by the dry-band arc (DBA) impinging the insulator surface in outdoor polluted conditions. Research indicates that SiR composites inferiorly perform under the DC voltage compared to AC as a result of the increased severity of the DBA (Cherney, Gorur et al. 2015; Bruce, Rowland et al. 2010; Vas, Venkatesulu et al. 2012). This essentially raised an awareness on improving the SiR composite material design to develop reliable high voltage DC (HVDC) outdoor insulators. Such insulators could be crucial when integrated in the HVDC infrastructure serving the future renewable-energy based electric grid.

Meyer et al. illustrated a correlation between the overall composite thermal conductivity and erosion performance of SiR composites tested in the AC inclined plane tracking and erosion test, IPT (Meyer, Cherney et al. 2004). Research on improving the erosion performance of SiR under DC voltage was similarly approached with enhancing the overall thermal conductivity. Through the DC IPT, Du et al. in demonstrated the role of thermally conductive hexagonal boron nitride (h-BN) fillers in suppressing the erosion of SiR (Du, Xu 2014). Du reported the h-BN effect on improving the SiR composite thermal conductivity with increased filler loading. In addition to improving the composite thermal conductivity, inorganic fillers could introduce a number of erosion suppression mechanisms during DC DBA as suggested by Ghunem (Ghunem, Jayaram

at al. 2015; Ghunem, Koné et al. 2020). It was illustrated that hydrated fillers such as ATH could improve the heat capacity of SiR through the endothermic dehydration mechanism of the filler initiated at temperatures beyond 200 °C. The water of hydration released from hydrated fillers such as ATH could suppress erosion by diluting the DC DBA plasma during the depolymerization of SiR (Ghunem, Jayaram at al. 2015; Ghunem, Koné et al. 2020). This could accordingly redefine the common understanding of the mechanisms by which inorganic fillers can suppress erosion under DC voltage and expand the role of inorganic fillers from merely improving the thermal conductivity of the SiR composites.

The effect of the filler properties such as that of size and interface characteristics on the erosion performance of SiR composites under was thoroughly investigated with fillers such as fumed silica and nano alumina (Ramirez, Jayaram et al. 2009; Khanum, Sharma et al. 2020). As illustrated by Lewis (Lewis 2004), reducing the inorganic filler particle size to the nanometric range would result in having prominent effects for the interfacial area of the filler. Limited research was found to address the erosion suppression effects that are attributed to the filler-polymer interface characteristics during DC DBA. Asad et al. employed silica-coated TiO_2 nano filler in SiR and illustrated a significant improvement in the erosion performance in comparison with unfilled SiR under the DC IPT (Asad, Amin et al. 2020). Still, the influence of filler interface could have been further investigated in comparison with a higher particle size filler. Such comparison was observed in the work of Vas et al. (Vas, Venkatesulu et al. 2012), in which nano alumina and micro ATH fillers were filled in SiR and tested under the DC IPT at both voltage polarities. A notable difference was observed in the erosion performance under the +DC IPT, with nano alumina superiorly performing at much lower loading of 4% by weight (4 wt%) compared to micro ATH which was primarily ought to the interfacial role of the lower particle size.

To develop reliable HVDC SiR outdoor insulators, a thorough understanding is required for the mechanisms by which inorganic fillers can suppress erosion under DC voltage. Though several of such mechanisms have been outlined in literature for micro fillers, additional analysis is required to investigate the suppression effects associated with nano and sub-micron fillers particularly when it comes to the higher interfacial area provided at such lower particle

sizes. Comparing the erosion suppression effects of the filler interface with those effects influenced by mechanisms such thermal conductivity enhancement or endothermic dehydration was not examined which undermines the true role of the filler interface. Analyzing room temperature vulcanized (RTV) SiR composites filled with fumed silica, nano ATH and sub-micron h-BN could fulfil the aforementioned objective. Therefore this paper comparatively analyzes the erosion suppression effects influenced by fumed silica's favorably interactive interface against those effects associated with nano ATH and sub-micron h-BN fillers.

3.2 Materials and Methods

3.2.1 Material Specimen

A two part RTV SiR, RTV 615, from Momentive was used as the base polymer for the composites in the study. Fumed silica, nano ATH and sub-micron two-dimensional h-BN, whose properties and loading levels are shown in Table 3.1, were denoted in this study as NS07, NA10, and BN137 respectively. NS07 was obtained from Sigma Aldrich, while NA10 was obtained from US Research Nanomaterials, and BN137 was obtained from Nanostructured and Amorphous Materials, Inc. The aforementioned fillers are the only ones used in the composites of this study. All fillers have been filled at the loading level of 5wt%. Given its high intrinsic thermal conductivity, BN137 was additionally filled at 10 wt% to effectively increase the composite thermal conductivity and in turn examine the impact on the erosion performance of the prepared composite. Depending on the composite formulation, weighed proportions of the filler were gradually mixed with the base silicone using a high shear mixer. Once all the filler has been added to the base silicone, a crosslinking agent is added to the mixture whilst maintaining a 10:1 weight ratio between the base silicone and the crosslinking agent. The mixture is then degassed under vacuum and poured into the sample molds. The poured composites are left to be vulcanized at room temperature for 24 hours and post-cured at 87 °C for 4 hours. Specimen samples from each composite formulation have been prepared for the IPT, along with testing samples dedicated for thermal analysis and thermal conductivity measurements.

Table 3.1 Fillers and SiR composite samples used in the study

Filler Type	Filler Code	Average Particle Size (nm)	Specific Surface Area (m^2/g)	Filler Density ρ_f (g/cm^3)	Filler wt%	Composite Code
Fumed Silica	NS07	7.0	390±40	2.3	5.0	SiR+5wt% NS07
Alumina Trihydrate	NA10	10.0	650.0	2.40	5.0	SiR+5wt% NA10
Hexagonal-Boron Nitride	BN137	137.0	19.4	2.25	5.0	SiR+5wt%BN137
				2.25	10.0	SiR+10wt%BN137

Scanning electron microscopy (SEM) was used in this study to observe the dispersion of the filler particles within the polymer matrix. The samples were prepared by cryogenic blade cutting using microtome, followed by sputter coating with platinum. Figure 3.1 shows the SEM images obtained for this study for 5wt% filled NS07, NA10, and BN137 SiR composites. Compared to the NS07 filled composite SEM image, the NA10 and BN137 particles are poorly dispersed with agglomerates visibly evident in the corresponding SEM images. This could be attributed to the silica surface silanol groups interactively bonding with the base silicone (Vondráček, Schätz et al. 1977), which in turn effectively disperses the filler particles and reduces agglomeration during high shear mixing.

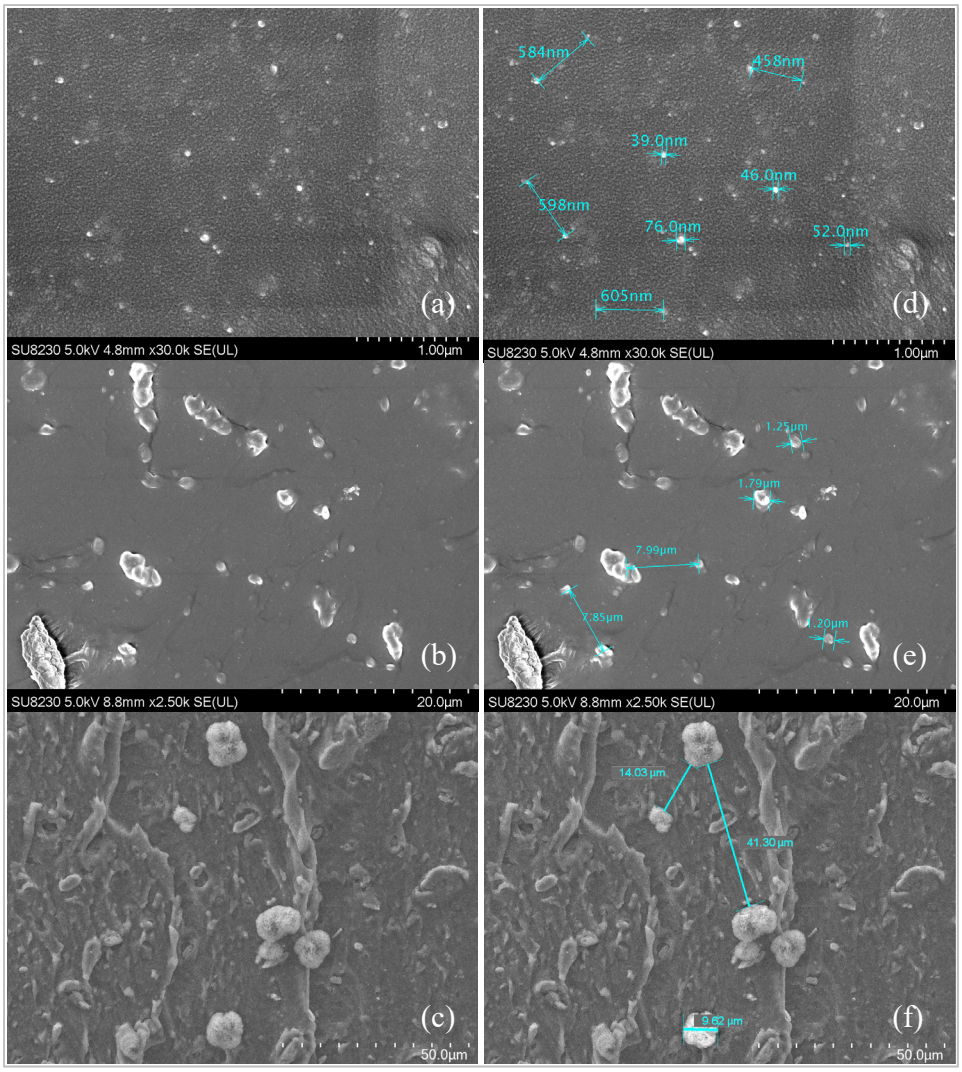

Figure 3.1 SEM images for samples of (a) SiR+5wt% NS07, (b) SiR+5wt% NA10, and (c) SiR+5wt% BN137 composites with their corresponding particle size measurements shown in images (d), (e) and (f) respectively
The average filler average particle sizes shown in images (d), (e) and (f) are approximately of 50 nm, 2 µm and 10µm respectively

3.2.2 The IPT

Figure 3.2 shows the circuit diagram and test setup for the IPT which conforms to the IEC 60587 test standards in assessing the erosion performance of outdoor insulation materials (IEC 2007). The composites were electrically tested under the positive voltage polarity which reportedly produces intense DBA that lead to deep erosion. Following the procedures in relevant research work (Cherney, Gorur et al. 2015), the test voltage was set to +3.5kV for a

test run of 6 hours with the contaminant flow rate being set at 0.3 ml/min and conductivity of 2.5 mS/cm. Once the testing is complete, erosion depth measurements are done using a digital Mitutoyo 571-200 micrometer with an accuracy of 0.1 mm.

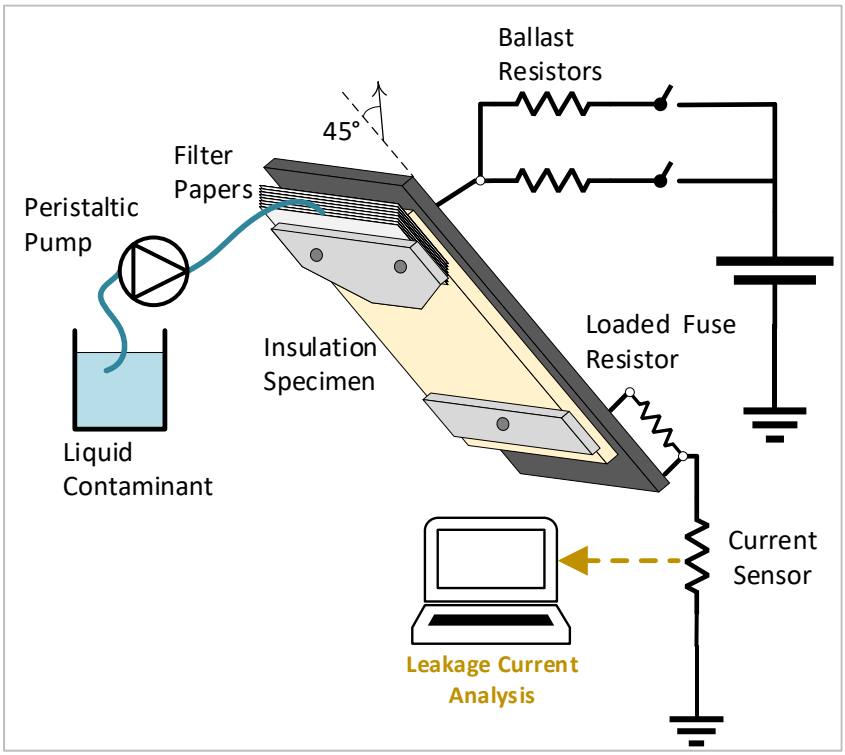

Figure 3.2 Overall HVDC Inclined plane tracking and erosion test setup

3.2.3 Material Analysis

The thermal decomposition characteristics of the SiR composites were analyzed using simultaneous thermogravimetric-differential thermal (TGA-DTA). A SDT Q600 TGA-DTA analyzer from TA instruments was used to test the composites in air and nitrogen (N_2) atmospheres at a heating rate of 25 °C/min and temperature span between 80-800°C. The tested samples weighed between 10-20 mg. A Trident Thermal Conductivity Analyzer was used to measure the composites' thermal conductivity as per ASTM D7984 test standard (ASTM 2021). Examining the thermal conductivity measurements with the IPT outcomes could

support finding a correlation between the composite's thermal conductivity and erosion performance.

3.2.4 Leakage Current Analysis

A data acquisition system is integrated with the IPT setup to capture the LC waveforms of the composite samples during the test run. Figure 3.3 shows the circuit schematic for the LC acquisition setup prepared in the laboratory. For a given test run, five SiR sample specimen are tested simultaneously with the LC through each specimen being acquired through the integrated current sensor shown in Figure 3.3. A National Instruments NI USB-6356 data acquisition device is used to acquire the current waveform at a sampling rate of 7 kHz with the aid of MATLAB. Similar to the procedure followed in (Ghunem, Jayaram et al. 2012), a sample window of 468 samples is stored for data analysis at each second. The root-mean-square value of the LC is computed for each sample window to represent the LC value at any given second.

Statistical analysis of LC waveforms could primarily indicate the nature of the current in terms of the magnitude, intermittency and stability which in turn could be correlate with outcomes of the other tests in this study. A statistical box plot analysis technique is introduced to visually illustrate the data distribution of the LC at different time intervals for the entire test run. For a given time interval, the boxplot shows the median, 25^{th} and 75^{th} percentile for the LC data which allows the representation of the change in LC randomness and distribution with time. This representation indicates the pace at which the DBA goes from the intermittent state to the stable severe state. In the intermittent arcing state, the LC waveform is characterized of being randomly distributed taking a wide range values within a given time interval. In the stable severe arcing state, however, the LC waveform tends to deviate from randomness with the variance of distribution of current values being very low. The DBA characteristics and inception of the stable DBA state could vary for different composites which could indicate the role of fillers in suppressing erosion with these composites.

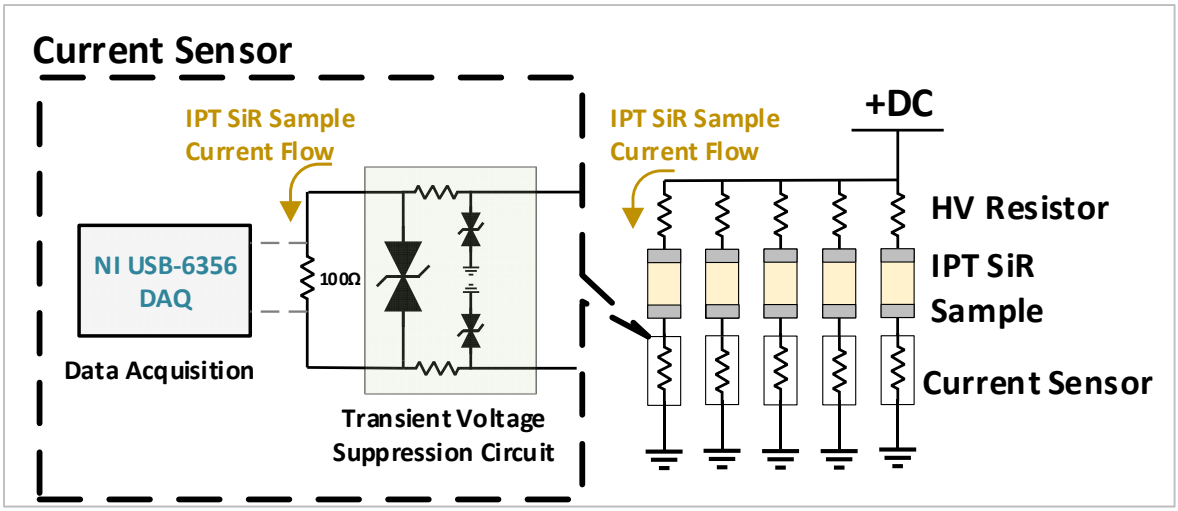

Figure 3.3 Leakage current acquisition circuit for the current flowing in one of five parallel testing specimens in the DC IPT

3.3 Results and Discussion

3.3.1 Thermal Analysis

Table 2 tabulates the thermal conductivity measurements of the prepared SiR composites. The BN137 filler is known to be thermally conductive with values up-to 550 W/m.K at room temperature (Yuan, Li et al. 2019). NS07 and NA10 fillers have reported thermal conductivities of approximately 1.5 W/m. K and 21.34 W/m. K (Meyer, Grishko et al. 2002). However, the reported measurements in Table 3.2 show a slight difference in the thermal conductivity between the BN137 filled composites and the NS07 and NA10 filled composites. This was similar to the finding of Meyer et al. (Meyer, Cherney et al. 2004) where they reported slightly higher thermal conductivities with silica filled samples compared to ATH-filled composites despite the 15 times higher intrinsic thermal conductivity of the ATH filler compared to silica. Table 3.2 shows a slight improvement in the composite thermal conductivity with increasing the loading level of BN137 from 5 to 10wt%. These findings are similar with the observations noted by Kemaloglu et al. in (Kemaloglu, Ozkoc et al. 2010), where they noted insignificant improvements in the thermal conductivity values with the

increased nano boron nitride filler loading in their SiR composites. The slight increase in thermal conductivity at 10 wt% of the BN137 filled composite is possibly a result of the higher volume of the thermally conductive filler available in the composite.

Table 3.2 SiR composites thermal conductivity measurements (k)

Composite Code	**Measurement Statistics of k**			
	No. of Measurements	**Min.**	**Max.**	**Average**
	-	W/m.K		
SiR+5wt% NS07	15	0.169	0.205	0.188
SiR+5wt% NA10	15	0.155	0.188	0.170
SiR+5wt% BN137	15	0.184	0.215	0.194
SiR+10wt% BN137	15	0.246	0.341	0.287

Figure 3.4 shows the TGA performed on the SiR composites in N_2 atmosphere, while Figure 3.5 shows the corresponding differential TGA. As can be observed, Figures 3.4 and 3.5 clearly indicate that all the composites begin their weight loss at approximately 400 °C. According to Camino (Camino, Lomakin et al. 2002), this initial weight loss stage represents the beginning of SiR depolymerization in which the Si-O bonds undergo bond scission to yield volatile cyclic oligomers. Similar results were also reported for the ATH filled SiR by Kumagai et al. in (Kumagai, Yoshimura 2001). Between 200 and 300 °C, Figure 3.4 shows a slightly higher decomposition rate for the NA10 filled SiR than the other composites which matches with the findings of Ghunem el al. in (Ghunem, Koné et al. 2020) indicating the dehydration of the ATH filler prior SiR depolymerization. If the ATH filler loading was higher than 5 wt%, a much higher decomposition rate after 200 °C could have been observed with respect to the other composites as a result of the increased amount of water of hydration.

Beyond 400 °C, Figure 3.5 indicates the presence of two distinct decomposition peaks for the NS07 and NA10 filled composites which are similar to those observed in (Ghunem, Koné et al. 2020; Koné, Ghunem et al. 2019). Camino indicated the presence of two competing mechanisms during the decomposition of SiR which are depolymerization and radical-based crosslinking

(Camino, Lomakin et al. 2002). Radical-based crosslinking is explained to be initiated through the homolytic scission of Si-CH_3 bonds at elevated temperatures. Similar DTGA results indicating the presence of these two decomposition peaks can be found in (Ghunem, Koné et al. 2020; Koné, Ghunem et al. 2019) where the SiR composites have been prepared with micro-sized silica and ATH fillers. Figure 3.4 indicates a faster weight loss rate for the SiR filled with NA10 as compared to NS07, with a higher remnant residue obtained at the end of the TGA for the NS07 filled composite. Hamadani reported that the rate at which depolymerization of SiR occurs is governed by the mobility and flexibility of the siloxane chains (Hamdani, Longuet et al. 2009). Fumed silica fillers were shown to favorably interact with the siloxane chains of SiR due to the silanol groups on the filler surface (Vondráček, Schätz et al. 1977). This favorable interaction tethers the polymer chains which in turn suppresses the Si-O bond scission and thus the depolymerization of SiR (Hamdani, Longuet et al. 2009). Therefore, the interaction between the fumed silica and the SiR tethering the siloxane chains would be expected to suppress the Si-O bond scission, thus the depolymerization and volatilization of SiR. This accordingly could explain the higher decomposition rate and remnant residue obtained for the NS07 filled composite.

Figures 3.4 and 3.5 indicate that the BN137 composites at both loading levels show a single decomposition peak with the highest decomposition rate for the 5wt% loaded BN137 filled composite amongst all composites. The BN137 5wt% filled composite decomposes at an elevated rate compared to the other composites. Kemaloglu et al. in (Kemaloglu, Ozkoc et al. 2010) illustrated that both the nano and micro sized-boron nitride used in their study lowered the tensile strength of their SiR composites compared to unfilled SiR. Kemaloglu attributed this effect to the poor interfacial interaction between the silicone and boron nitride which could similarly be the case in this study. Figures 3.4 and 3.5 show that increasing the filler loading of BN137 to 10 wt% improved the decomposition rate and increased the final remnant residue with respect to the NA10 filled composite, but did not surpass those of the NS07 filled composite which further emphasizes the role of fumed silica's interface on suppressing the depolymerization of SiR and promoting the radical based crosslinking mechanism. However, increasing the BN137 filler loading level to 10wt% did lower decomposition rate obtained compared to 5wt% BN137 composite. This

improvement could be attributed to the higher volume content of the filler replacing SiR, which results in reducing the amount of depolymerizable content in the composite.

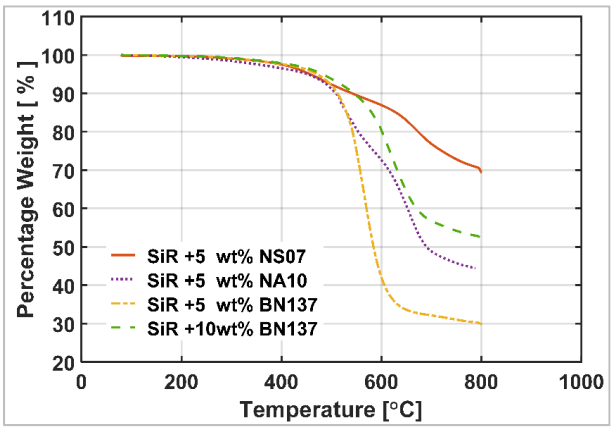

Figure 3.4 TGA for the prepared composites in N_2 atmosphere

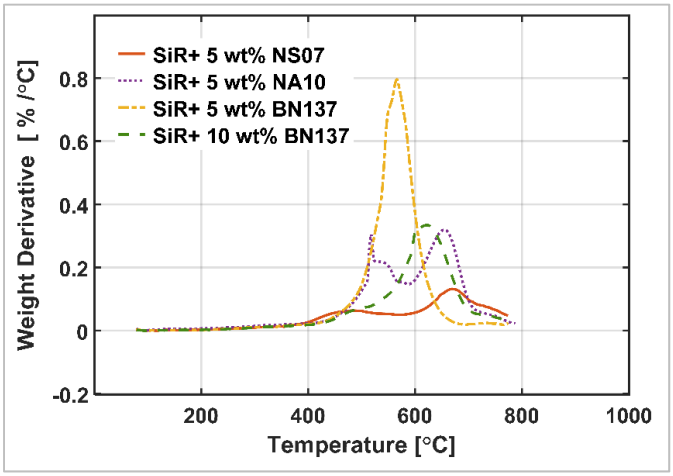

Figure 3.5 DTGA for the prepared composites in N_2 atmosphere

Figure 3.6 shows the DTA performed for the prepared SiR composites. Under air, or O_2, atmosphere, an exothermic hump occurs for all composites which indicates the combustion of volatile SiR oligomers produced in depolymerization. The smallest exothermic peak was obtained for NS07 filled composite which implies a more suppressing effect on depolymerization and volatilization of SiR with the fumed silica composite. Figure 3.6 also shows the DTA performed for the NS07 filled composite under nitrogen, N_2, atmosphere. In comparison, the exothermic humps observed for the NS07 filled composite in air atmosphere

are seemingly suppressed under the nitrogen atmosphere at the same temperature points. This comparison indicates the exothermic effect of oxygen in combusting the volatile cyclic oligomers produced during depolymerization which is absent in an inert atmosphere. Kone in (Koné, Ghunem et al. 2019) suggested the formation of silica residue in air atmosphere as a possible by-product of thermo-oxidation of the volatile silicone oligomers during depolymerization which could suppress the depolymerization of SiR.

At the filler loading of 5 wt%, it appears that the endothermic dehydration associated with nano ATH was not evident in Figure 3.6 with the NA10 filled composite. Literature reports that the endothermic dehydration mechanism of ATH enhances the heat capacity of the SiR composite, with the released water of hydration diluting the DC DBA plasma of the depolymerized SiR (Ghunem, Koné et al. 2020). Kumagai et al. in (Kumagai, Yoshimura 2001), observed that critical micro ATH filler loading above 40 wt% is needed in SiR for an evident effect of suppressing erosion under the AC IPT. Therefore, it appears that a critical ATH level above 5 wt% is needed to have a comparable erosion suppression effect on SiR such as that influenced by the filler interface of NS07 at 5 wt% filler loading.

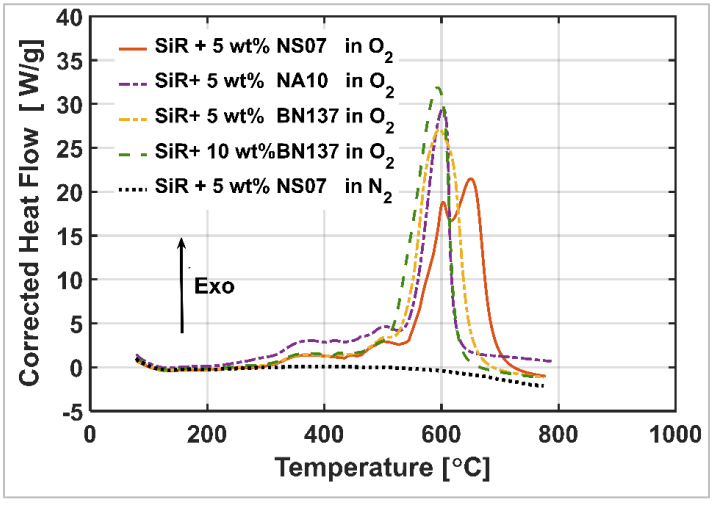

Figure 3.6 DTA for the prepared composites in air, O_2, atmosphere. The plot also shows the DTA performed in N_2 atmosphere for the NS07 filled composite

These findings suggest a predominant role for the filler interface in deterring the decomposition, thus erosion, of the SiR composites. Moreover, the effective dispersion of the

filler particles with minimal filler agglomeration could significantly impact the thermal decomposition characteristics shown for all the composites in this study. In their prepared SiR composites, Kemaloglu et al. in (Kemaloglu, Ozkoc et al. 2010) reported an agglomeration of the nano boron nitride in the silicone base polymer as a result of the weak filler-polymer interfacial interactions. Additionally, Khanum et al. in (Khanum, Sharma et al. 2020) illustrated the impact of filler surface treatment on improving the erosion resistance of alumina filled SiR nanocomposites. Khanum attributed this improvement to the enhanced filler-polymer interaction at the interface which aided in dispersing and distributing filler particles in the silicone base polymer. The conclusions drawn from (Khanum, Sharma et al. 2020) and (Kemaloglu, Ozkoc et al. 2010) indicate the role of the particle dispersion on the properties of the SiR composites. Compared to the NS07 filled composite SEM image shown in Figure 3.1a, NA10 and BN137 particles are poorly dispersed with agglomerates visibly evident in SEM images of Figure 3.1b and Figure 3.1c respectively. Furthermore, the agglomeration of filler particles in a given volume fraction of the filler can significantly undermine the effect of the small particle size in terms of the available interactive layer area to bond with the host polymer. To further clarify the impact of the agglomeration on the available interactive surface area of the filler, a simple calculation of the total surface area available can be done for unit volume of the filler in the composite. The SEM images shown in Figure 3.1 indicate an approximate average filler particle radius sizes, r_{fp}, of 25 nm, 1 µm and 5 µm for the NS07, NA10 and BN137 filler particles respectively. Assuming a spherical geometry for the filler particles, the surface area per filler particle, sa_{fp}, and volume per filler particle, v_{fp} can be geometrically calculated using

$$sa_{fp} = 4\pi {r_{fp}}^2 \tag{3.1}$$

$$v_{fp} = \frac{4}{3}\pi {r_{fp}}^3 \tag{3.2}$$

The number of filler particles per unit volume of the filler, N_{fp}, is found by reciprocating the value of v_{fp}. N_{fp} can be of a non-integer value when computing the calculations in µm^3 volume units. Accordingly, the total surface area of the filler interfacial layer available, SA_f, for a given unit volume of the filler in the composite can be calculated using

$$SA_f = N_{fp} \times sa_{fp} \quad (3.3)$$

Table 3 tabulates the calculations obtained using Equations (3.1) to (3.3) to calculate SA_f for a unit volume of the filler. The results indicate that fumed silica's total filler surface area for a given unit volume of the filler is 40 times greater than that of the other fillers. The much higher interfacial surface area provided in the smaller particle size could significantly reduce the depolymerization and promote the crosslinking of SiR as a result of the increased interaction with the SiR polymer. Kone et al. in (Koné, Ghunem et al. 2019) observed similar effects in the reduction of the silica particle filler size in the micro-range which was attributed to the improved filler interface.

Table 3.3 *SAf* parameters calculations for unit volume of the fillers

Inorganic Filler Code	NS07	NA10	BN137
r_{fp} **[µm/ particle]**	2.50×10^{-2}	1.00	5.00
v_{fp} **[µm³/particle]**	6.54×10^{-5}	4.19	523.60
sa_{fp} **[µm²/particle]**	7.90×10^{-3}	12.57	314.16
N_{fp} **[particles/ µm³]**	1.53×10^{4}	2.39×10^{-1}	1.90×10^{-3}
SA_f **[µm²]**	120	3	0.6

3.3.1 Erosion Resistance

Figure 3.7 shows a subset of the SiR composite specimen samples obtained after IPT testing. As can be noticed, a difference exists in the extent of damage on the surfaces of SiR composites containing NS07 with respect to the other composites in terms of the eroded depth and damaged area. Erosion depths exceeding 2 mm were noted for all the tested composites with the combustion of material being evidently visible during the IPT test run. Figure 3.8 shows the corresponding average erosion depth as a percentage of the 7 mm sample thickness for five tested specimen samples for each composite formulation. A superior erosion performance was

obtained with the NS07 filled composite compared with the other composites. An insignificant difference, however, was shown in the erosion performance amongst the BN137 and NA10 filled composites.

The fumed silica filled composite had an improved erosion performance as indicated in Figure 3.8, despite the higher and comparable thermal conductivity measurements shown in Table 3.2 for the other composites. This suggests a predominant influence of the filler interface over the improvement in the composite thermal conductivity on suppressing the erosion of SiR. The influential effect of the filler interface could be attributed to a number of factors. The DTGA curve obtained in Figure 3.5 suggests a crosslinking mechanism being promoted at elevated temperatures for the fumed silica filled composite as explained in (Camino, Lomakin et al. 2002). Delebecq et al. in (Delebecq, Hamdani-Devarennes et al. 2011) explained that the thermal decomposition characteristics of SiR are predominantly impacted by the extent of siloxane chain immobility as a result of crosslinking. The experimental observations in (Delebecq, Hamdani-Devarennes et al. 2011) suggest an essential role for the vinyl groups on the silica surface to promote crosslinking linking between the siloxane chains and silica at high temperatures in the presence of a platinum catalyst. Moreover, Ramirez in (Ramirez, Jayaram et al. 2009) indicated a superior erosion performance with hybrid composites containing fumed silica as compared to only micro silica which was attributed to the increase in twice the number of silanol groups available on the silica surface which goes in accordance with the interfacial surface area values computed in Table 3.3 of this study. Furthermore, natural silica filled SiR composites could form a coherent residue which shields the material against the influx of heat from the eroding DBA as reported in (Koné, Ghunem et al. 2019).

Another observation to be noted in the IPT results would be the superior performance of the NS07 over the NA10 filler on suppressing erosion at the same filler loading, despite the heat capacity enhancement and arc plasma dilution mechanisms that are reportedly associated with ATH. Higher filler loading of the ATH could properly enrich such erosion suppression mechanisms. However, increasing the filler loading would be on the expense of possible agglomerate formation which will weaken the effects associated with the nano particle size in terms of the available interfacial area.

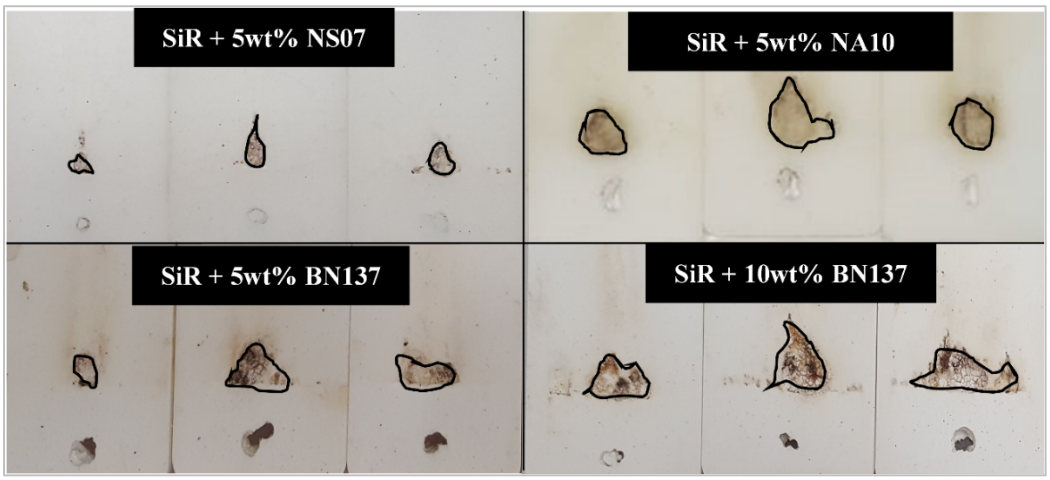

Figure 3.7 Selected NS07, NA10, BN137 SiR composite samples from the DC IPT

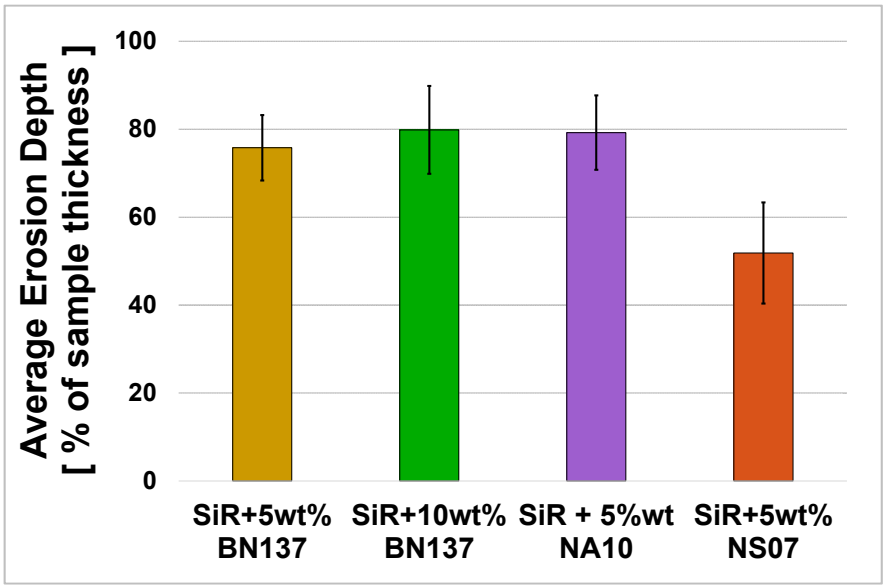

Figure 3.8 DC IPT average erosion depth outcomes for five sample specimens for each of the prepared SiR composites as % of the original sample thickness

3.3.2 Leakage Current Analysis

LC waveforms for the samples tested in the DC IPT have been acquired through the data acquisition system integrated in the test setup. Figure 3.9 depicts the LC waveforms for tested

specimens for each of the NS07 and BN137 composite formulations. The interest in this particular comparative analysis was to observe the LC characteristics associated with the fumed silica and boron nitride filled composites, given the higher composite thermal conductivity measured for the composites of the later filler as indicated in Table 3.2. A moving average window of 300 samples was used to produce the average LC which shows the average trend/ trendline of the LC with time during the 6 hour running time of the IPT.

Figure 3.9 shows a variation in the current waveforms amongst the composites in terms of the current randomness which in turn indicates the intermittency and stability of the DC DBA. Based on the LC randomness, the NS07 filled composite transitions into a stable LC region of reduced nonconducting periods at a slower pace compared to the BN137 filled SiR composites. A correlation between the induction of hotspots and the development of stable DBA was reported in (Ghunem, Jayaram at al. 2015). The study in (Ghunem, Jayaram at al. 2015) indicates that the incorporation of inorganic fillers suppresses the effect of the eroding DBA by delaying the significant increase in temperature and thus the inception of the stable DBA. The inception of the stable DBA stage was suggested to be attributed to the rate at which the silica residue forms to effectively slow the rate of evaporation of the liquid contaminant making contact with the anode. Thermal analyses outcomes of this study imply a relatively lower depolymerization rate for the NS07 filled composite compared to BN137 filled composites, which indicates higher SiR volatilization for the BN137 filled composites. Timpe explained the Andrinov mechanism involving the formation of SiO_2 residue as a result of thermal oxidation of SiR in the presence of volatile oxidation products at a low temperature 200°C (Timpe 2007). With the higher volatilization rate observed with the BN137 filled composite, it is plausible to assume that at lower temperatures the silica residue could be forming at a faster rate with the BN137 filled SiR composite compared with that of NS07. This could possibly explain the shorter time required to reach the stable DBA stage with the BN137 SiR filled composites.

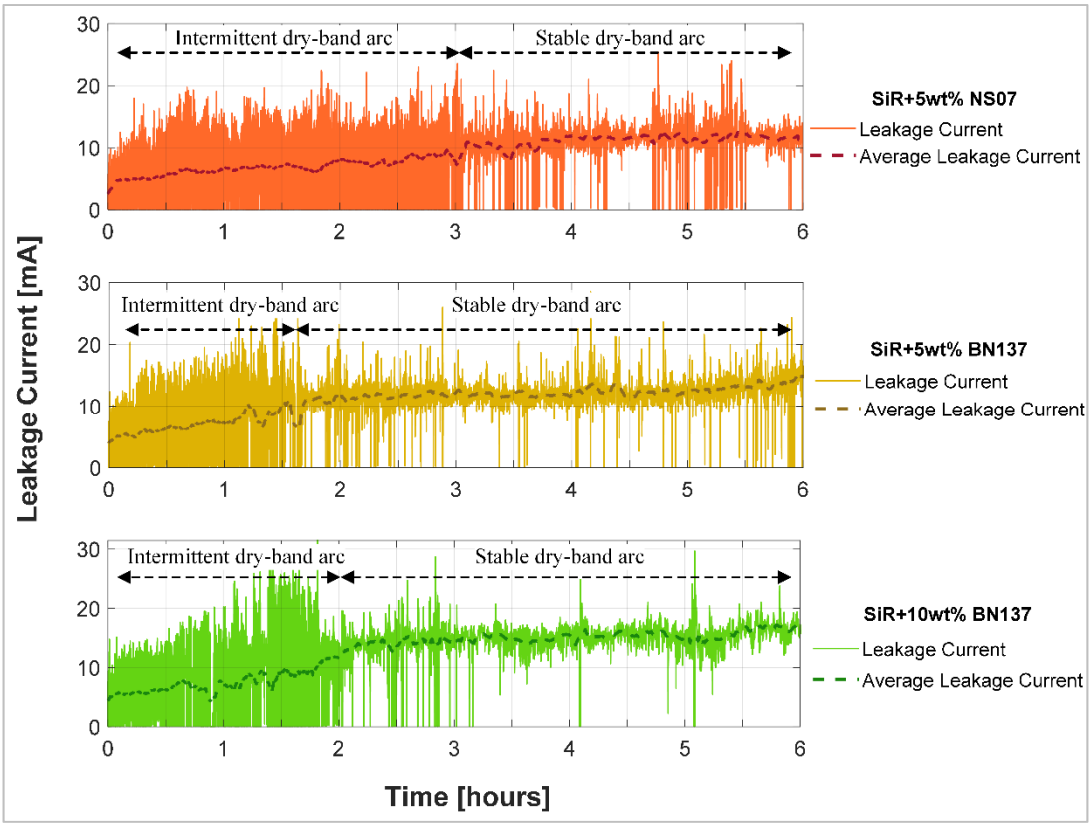

Figure 3.9 Samples of the LC waveform acquired for the tested composites showing both the LC and average current obtained

Figure 3.10 shows a novel approach using statistical boxplot analysis to represent the LC waveform during the entire test run of the DC IPT. This visual representation allows a fair comparison between the different composites in terms of the DC DBA characteristics and distribution of the LC values, or the LC randomness. The statistical boxplots shown in Figure 3.10 illustrates the LC for four specimen samples from each of the composite formulations prepared in this study during 12 time intervals of the 6 hour test run.

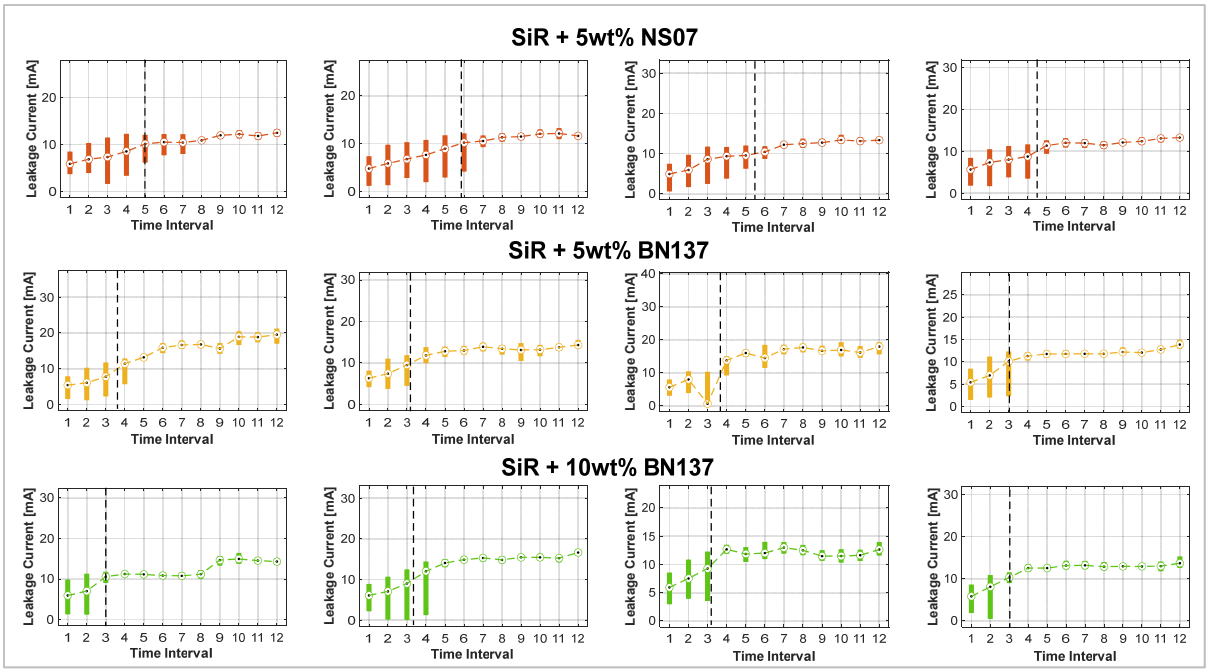

Figure 3.10 Statistical boxplots showing the distribution of the LC values for the tested composites at 12 time intervals with the dashed line indicating the time at which a 10mA LC was reached

A number of general trends can be noticed in Figure 3.10 for the illustrated boxplots of the tested composites. First, the distribution of LC values between the bars' top and bottom edges, corresponding to the 25th and 75th percentile LC measurement, reduces with the progress of test which indicates a change in the DC DBA characteristics in terms of the reduced arc randomness and the transition from the intermittent DBA stage into the stable severe DBA. As depicted in Figure 3.10, the time required to transition into the stable dry-arc stage, or shorter bar width, is longer with the NS07 filled composite compared to the BN137 filled composites. Secondly, the median value of the LC increases as the test progresses which represents the increasing severity of the DBA and its consequent eroding effects on the composites. The dashed lines shown in Figure 3.10 indicate the time at which the median LC values of the bars reach or surpass an arbitrary chosen reference of 10mA which is reached at a slower pace with the NS07 filled composite compared with that of BN137. These observations collectively indicate an evident erosion suppression effect associated with the fumed silica filler during the DC DBA exhibited by the composite.

Comparatively analyzing these observations with the erosion resistance outcomes of Figure 3.8, could suggest a correlation between time to reach the stable eroding DBA and the amount of eroded mass in the tested composite. That is, the longer the time it takes to reach the stable eroding dry-band stage, the lower is likelihood that the DBA would severely erode the material. Moreover, the presence of a coherent residue could prevent progressive erosion of the SiR composite by shielding the material from the diffused heat (Koné, Ghunem et al. 2019). The TGA results of Figure 3.4 show higher residue for the fumed silica filled composite which could have been attributed to the crosslinking mechanism suggested in (Camino, Lomakin et al. 2002). This mechanism in turn, was explained to be predominantly governed by the filler interface properties which would tether the siloxane chains. Therefore, the LC waveform representation could show the role of the filler in improving the DBA transient characteristics during the IPT.

3.4 Conclusion

This paper investigated the role of the filler interface on suppressing the erosion of RTV SiR composites under DC DBA. Fumed silica, nano ATH and sub-micron hexagonal boron nitride fillers were used to prepare the SiR composites in the study. Simultaneous TGA-DTA outcomes indicate an evident role for fumed silica's interface in suppressing SiR depolymerization and promoting radical based crosslinking in SiR. This could be attributed to the role of the filler interface in tethering the siloxane chains of SiR. Contrarily, ATH and boron nitride fillers had insignificant effects on suppressing depolymerization of SiR. These results match with the calculated filler interfacial area which are the highest for the fumed silica filler. Moreover, the thermal analyses outcomes correlate with the DC IPT outcomes indicating an improved erosion performance with the fumed silica filled composite despite the comparable and slightly higher thermal conductivity measurements for the other composites at the equal and higher filler loading respectively. LC measurements acquired during the DC IPT were analyzed in a novel statistical boxplot approach to examine the DC DBA mechanism throughout the test. The boxplots indicate a faster rate for reaching the stable eroding DBA

stage with the boron nitride filled composites. This translates into a prolonged exposure to the stable DC DBA energy which severely degrades the boron nitride composites compared to those filled with fumed silica. Accordingly the results presented in this study could indicate a more influential role for the filler interface in improving the erosion resistance of SiR composites tested under the +DC voltage.

Acknowledgment

The authors gratefully acknowledge the Natural Sciences and Engineering Research of Canada (NSERC) for their support and funding to develop this paper. The authors would like to thank Dr. Yazid Hadjadj, National Research Council Canada, for his continuous support and valuable discussions in the subject of this paper. Moreover, the authors acknowledge Mr. Yuksum Tam, National Research Council Canada, for his remarkable efforts in designing the electronic circuitry for the data acquisition system along with other integral parts of DC IPT test setup.

CHAPTER 4

A NOVEL FRAMEWORK TO STUDY THE ROLE OF GROUND AND FUMED SILICA FILLERS IN SUPPRESSING DC EROSION OF SILICONE RUBBER OUTDOOR INSULATION

Alhaytham Y. Alqudsi[a], Refat A. Ghunem[b] and Éric David[a]

[1]Department of Mechanical Engineering, École de technologie supérieure,
1100 Notre-Dame West, Montreal, Quebec, Canada H3C 1K3
[2]Metrology Research Center, National Research Council Canada,
1200 Montreal Road, Ontario, Ottawa, Canada K1A 0R6

Paper published in *Energies,* June 2021

Abstract

This paper investigates the effect of ground and fumed silica fillers on suppressing DC erosion in silicone rubber. Fumed silica and ground silica fillers are incorporated in silicone rubber at different loading levels and comparatively analyzed in this study. Outcomes of the +DC inclined plane tracking erosion test indicate a better erosion performance for the fumed silica filled composite despite having a lower thermal conductivity compared to the ground silica composite. Results of the simultaneous thermogravimetric and thermal differential analyses are correlated with inclined plane tracking erosion test outcomes suggesting that fumed silica suppresses depolymerization and promotes radical based crosslinking in silicone rubber. This finding is evident as higher residue is obtained with the fumed silica filler despite being filled at a significantly lower loading level compared to ground silica. The surface residue morphology obtained, and the roughness determined for the tested samples of the composites in the dry-arc resistance test indicate the formation of a coherent residue with the fumed silica filled composite. Such coherent residue could act as a barrier to shield the unaffected material underneath the damaged surface during dry-band arcing, thereby preventing progressive erosion. The outcomes of this study suggest a significant role for fumed silica promoting more interactions with silicone rubber to suppress DC erosion compared to ground silica fillers.

Keywords: HVDC outdoor insulators; silicone rubber; fumed silica; ground silica; dry-band arcing; erosion performance

4.1 Introduction

With the rising awareness of the impacts of fossil fuel-based electricity generation on climate change, solutions for integrating renewable energy sources into the existing electric grid infrastructure have been investigated. Utilizing a high voltage direct current (HVDC) transmission system would facilitate such integration by enabling an efficient transmission of electric power over long distances from remote renewable energy sources such as hydro, wind and solar farms to load centers (Sun, Li at al. 2017; Fleeman, Gutman et al. 2009). Accordingly, HVDC outdoor insulators should be designed to ensure the reliability of the power transmission system. Silicone rubber's (SiR) characteristic hydrophobicity makes it highly desirable for use as a housing material in polymeric outdoor insulators. SiR, however, is susceptible to erosion caused by DBA sustained under heavily polluted conditions. Incorporating silica fillers in composite formulations of SiR was considered for enhancing the thermal conductivity and, in turn, the erosion performance of SiR.

Meyer et al., in (Meyer, Jayaram et al. 2004), highlighted the correlation between the thermal conductivity and the erosion resistance of their silica filled SiR composites. It was concluded that the increase in silica filler loading from 10 to 50 wt% (percent by weight) caused a significant increase in the thermal conductivity, which resulted in lower eroded masses in the inclined plane-tracking and erosion test (IPT). El-Hag et al., in (El-Hag, Simon et al. 2006), illustrated that adding fumed silica by 10 wt% to SiR would result in a comparable erosion performance with 50 wt% micro silica filled SiR. This observation was attributed to the role of fumed silica in favorably bonding with the silicone rubber matrix. Nazir et al., in (Nazir, Phung et al. 2018), reported an improvement in the IPT erosion performance of their hybrid SiR composites containing nano silica and aluminum nitride fillers with an increase in the nano silica loading level. An increase in the composite thermal conductivity was observed with an increased loading of nano silica fillers. Ramirez et al., in (Ramirez, Jarayam et al. 2010), explained that the high specific surface area of the fumed silica filler facilitates a better

interaction with SiR as a result of the increased concentration of the silanol groups interacting with the siloxane chains of the polymer. Ansorge et al., in (Ansorge, Schmuck et al. 2012), highlighted the effect of an additional factor influencing the erosion performance of silica filled SiR that is related to the material curing temperature. It was reported in (Ansorge, Schmuck et al. 2012) that the erosion performance of micro silica filled room temperature vulcanized (RTV) SiR showed higher erosion depths under the IPT compared to high consistency silicone rubber. This outcome was attributed to the improved filler-polymer bonding at high temperature curing. Similar findings were reported in (Meyer, Jayaram et al. 2004), highlighting the effect of high temperature curing on the erosion performance of silica filled SiR composites.

Several research studies conclude that the erosion performance of SiR worsens under DC voltage, particularly +DC, compared to AC (Bruce, Rowland et al. 2010; Cherney, Gorur et al. 2015). The dry-band arcing (DBA) exhibited by the insulators under DC voltage is of higher relative severity compared to that of AC in terms of arc discharge duration and (LC) magnitude (Cherney, Gorur et al. 2015). Ghunem et al., in (Ghunem, Jayaram et al. 2015), illustrated the effect of increasing silica filler loading and, subsequently, the composite thermal conductivity on delaying the inception of stable eroding DC DBA in SiR. Comparable magnitudes of the third detail wavelet component of LC were obtained between the SiR composites filled with silica and alumina trihydrate (ATH) at 30 wt%, despite the additional effect of the water of hydration of ATH in suppressing erosion (Ghunem, Jayaram et al. 2015). These findings suggest the presence of erosion suppression mechanisms associated with silica's interaction with the silicone matrix. Kone et al., in (Koné, Ghunem et al. 2019), demonstrated the effect of the silica filler size and loading level on the integrity of the silica residue produced under the IPT. The coherency and porosity of such residue could shield the SiR material against progressive erosion under DC DBA (Koné, Ghunem et al. 2019). In an earlier study (Alqudsi, Ghunem et al. 2021), fumed silica was found to have a significant effect in suppressing DC erosion as compared to nano ATH and sub-micron boron nitride (BN) in SiR composites, despite the comparable thermal conductivities reported for all of the composites. Accordingly,

the literature suggests that the role of silica fillers in suppressing the DC erosion in SiR is more than simply improving the composite thermal conductivity.

The literature indicates that the use of silica fillers in SiR composites, with their different particle sizes and loading levels, would improve the erosion performance of the composites as a result of an increase in the thermal conductivity of the composite. Merely using the +DC IPT as a means to rank the erosion performance of such composites without considering any additional analytical tools would overshadow the true role of the silica size in suppressing the DC erosion of SiR. Moreover, this would limit the role of the silica filler in merely improving the composite thermal conductivity. This paper introduces a framework to thoroughly investigate the role of fumed silica and ground silica fillers on suppressing the DC erosion of SiR. The study would enable using a number of analytical tools with outcomes that could be correlated with the IPT outcomes. This study, in turn, could ultimately support the developments in SiR outdoor insulators for their reliable use in the HVDC electric grid.

4.2 Materials and Methods

Fumed silica and ground silica, whose properties are shown in Table 4.1, are used as the fillers for this study. Based on the literature, fumed silica was selected due to its high specific surface area facilitating a favorable interaction with silicone at small weight fractions in the composite. Ground silica, on the other hand, can be filled at much higher loading levels to replace a significant portion of the SiR material and, subsequently, reduce the cost of the composite. A two-part RTV SiR is used in the study, where Part A is the main potting compound and Part B is the crosslinking agent. Part A and Part B are maintained at a weight ratio of 10:1, respectively. Weighed portions of the filler are added to Part A and mixed using a ROSS high shear mixer until all of the filler is added to the mixture. Part B is then added and mixed for one minute to be later poured into IPT specimen molds and degassed under a vacuum. The mixture is cured at room temperature for a 24 h time period, followed by thermal treatment at 85 °C for 3 h. An unfilled SiR was also prepared for selected tests in this study.

Table 4.1 Filler properties and prepared composites.

Filler Type	Supplier	Filler Code	Particle Size [µm]	Specific Surface Area [m^2/g]	Specific Gravity	Composite Formulation
Fumed silica	Sigma Aldrich	FS07	7×10^{-3}	390	2.3	SiR + 5 wt% FS07
Ground silica	US Silica	GS10	10.5 [1]	NA [2]	2.65	SiR + 30 wt% GS10

[1] Median particle size. [2] Not applicable for micro-sized fillers.

The +DC IPT is used in this study as part of the electrical analysis to assess the erosion performance of the prepared composites. The test setup is set as per the IEC 60587 standard (IEC 2007) and modified for +DC testing as per the recommendations in (Cherney, Gorur et al. 2015). The test voltage was set at +3.5 kV for a 6 h run time with a contaminant flow rate of 0.3 mL/min and a contaminant conductivity value of 2.5 mS/cm. A digital Mitutoyo 571-200 micrometer with an accuracy of 0.1 mm was used to measure the erosion depth of 10 specimen samples for each composite.

LC for the tested specimens during the IPT are acquired using a National Instruments NI USB-6356 data acquisition device at a sampling rate of 7 kHz. A sample window is then applied to capture the first 468 samples from each second. The root-mean-square value (RMS) of the LC is computed and stored as a single value for the 468 acquired samples at every second. Computing the RMS value for every second of the test run would suffice for representing the change in the LC values during the test and would provide a practical approach for acquiring the data with smaller storage requirements instead of saving the entire current waveform of 468 samples per second. Following the analytical approach presented in an earlier study (Alqudsi, Ghunem et al. 2021), a statistical boxplot method is used to observe the distribution of the RMS LC values acquired during the IPT in 20 min time intervals. This statistical analysis allows one to observe the evolution of the DBA from the intermittent state to the stable severe state, which is reflected in the changing distribution of the RMS LC values between consecutive time intervals in the boxplot. An increase in the DBA stability and severity is reflected in a reduction in the non-conducting periods of the LC. This corresponds to a

transition from the initial intermittent state of the DBA, which is characterized by a large number of nonconducting periods and frequent RMS LC values below 1 mA. Figure 4.1 shows the +DC IPT test setup used in the study.

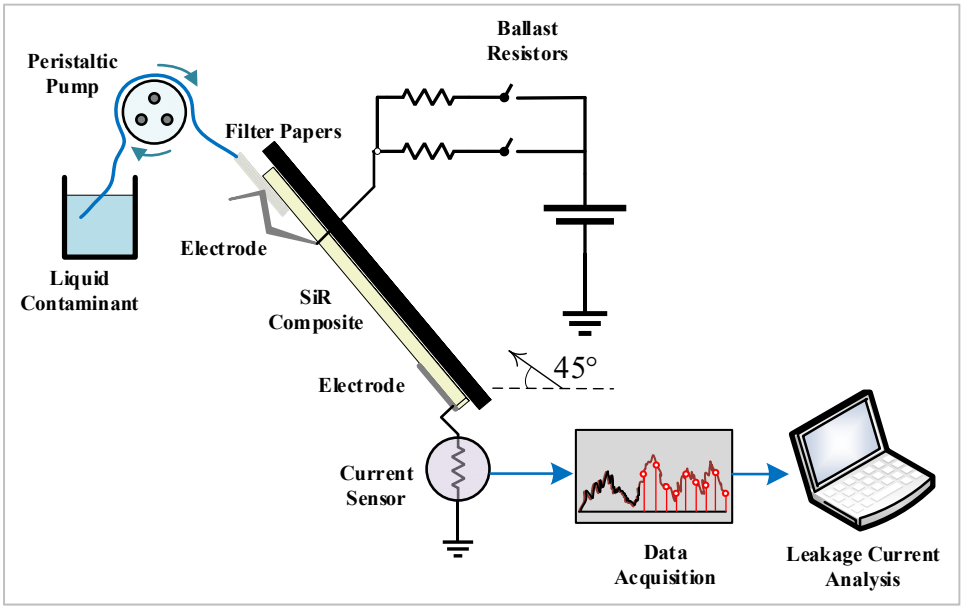

Figure 4.1 +DC IPT setup with the LC acquisition system

The dry-arc resistance test is used in this study as a method to produce a controlled and quick heat ablation through the sample thickness rather than progressive erosion on the surface, as is the case with the IPT. The test will enable the fast production of tested composites whose surface residue could be analyzed for drawing preliminary conclusions regarding the role of the filler on defining the surface residue characteristics that could be observed using microscopy. The test setup is set as per the ASTM D 495 (ASTM 2014) standard, which utilizes tungsten electrodes to generate low current arcs under high voltages on the tested composites. The arc is generated in current steps that define the current magnitude and the duty cycles of the rms AC voltage applied, as per the schedule set in (ASTM 2014) and with each current step lasting for one minute. For this study, only the first 4 current steps of the 7 steps in (ASTM 2014) are used in the dry-arc resistance test; i.e. total test run of 4 min. Detailed description of the on and off duration of the current in these 4 current steps are described in details in (ASTM 2014). The first 3 current steps of the test (denoted here as cycles 1 to 3) are analogous to an intermittent state of the DBA. The degree of intermittency decreases as test goes from the first

current step (cycle 1) to the third (cycle 3). The fourth current step (cycle 4), on the other hand, is analogous to the stable eroding state of the DBA without intermittency. All the current steps used have a constant current magnitude of 10mA. Modifying the existing test setup to generate a DC DBA could impair the proper functionality of the power electronics of the setup controlling the duty cycles. Figure 4.2 shows the dry-arc resistance test setup.

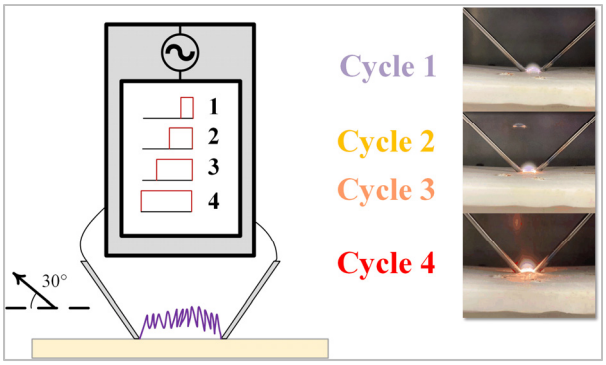

Figure 4.2 Dry-arc resistance test with images of the test during the 4 cycles of operation

Simultaneous thermogravimetric–differential thermal analysis (TGA–DTA) was performed on the prepared composites under nitrogen (N_2) and air atmospheres to understand the thermal decomposition characteristics of the composites. The heating rate was set at 25 °C/min for a temperature span from 80 to 800 °C. Thermal conductivity measurements for the prepared composites were acquired using a thermal conductivity analyzer instrument as per the ASTM D7984 standards (ASTM 2021), which enables the acquisition of measurements in short test times without the use of a vacuum chamber. These measurements are necessary to understand the relationship between the composite thermal conductivity and the erosion performance of the composites.

Surface residue on post tested specimens of the +DC IPT, dry-arc resistance test and TGA are analyzed using two various methods. The surface morphology of the samples is observed using scanning electron microscopy (SEM) on 20 nm gold sputter coated surfaces and a laser confocal microscope. Surface roughness analysis on the samples is performed using a Keyence VR-5000 optical microscope. Quantitative representation of the surface roughness is performed by means of the average roughness parameter, R_a, whose computation details can

be found in (ASME 2019). All of the aforementioned tools serve to observe the effect of the filler on the residue characteristics of the composite in terms of coherency and roughness.

4.3 Results and Discussion

4.3.1 Erosion Performance

Figure 4.3 shows the +DC IPT outcomes of the study. The results preliminarily indicate a better erosion performance of the FS07 filled composite compared to that of GS10. Figure 4.3a shows a higher average erosion depth obtained for the GS10 filled samples compared to the FS07 filled samples. Figure 4.3b further illustrates the inferior erosion performance of the GS10 filled composite through images of the post tested specimen, indicating larger eroded areas with the composite compared to those filled with FS07. It is important to note that the better erosion performance of the FS07 filled SiR does not necessarily conclude a superior erosion performance for the composite as compared to the GS10 filled SiR. The outcomes simply show that the FS07 filled SiR had a better or comparable erosion performance to the GS10 filled SiR, despite being filled at one sixth of the filler loading level of the GS10 filled SiR. This highlights a significant role for fumed silica in suppressing erosion and potentially facilitates its use as a co-filler with ground silica in practical formulations of SiR composites of high filler loadings that could be used in industry.

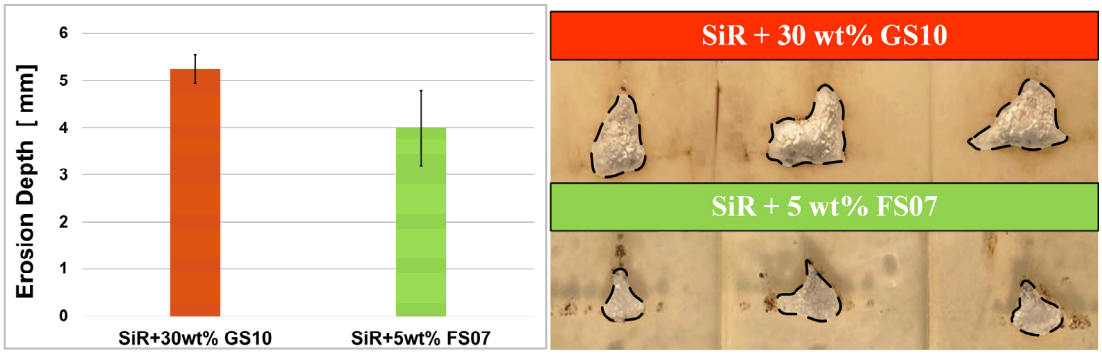

(a) (b)

Figure 4.3 (a) +DC IPT erosion depth outcomes for the tested composites
(b) Images of the post tested +DC IPT composite specimens

Table 4.2 shows the measured thermal conductivity of the prepared composites. The thermal conductivity values acquired were consistent with those found in (Meyer, Jayaram et al. 2004;

El-Hag, Simon et al. 2006). The increase in the weight fraction of the GS10 and FS07 fillers in the composite leads to a significant increase in the composite thermal conductivity (Meyer, Jayaram et al. 2004). It is important to note that despite having twice the thermal conductivity of the FS07 filled SiR, the GS10 filled SiR showed inferior erosion performance, which suggests that that the thermal conductivity is not the main governing factor in suppressing the erosion of SiR under DC voltage. In an earlier study (Alqudsi, Ghunem et al. 2021), it was found that the favorable interaction of fumed silica with the SiR matrix was more decisive in determining the erosion performance of SiR under the +DC IPT than the improvement of the composite thermal conductivity using BN fillers. The difference in DC and AC erosion in silica filled SiR was thoroughly investigated and discussed in studies such as (Koné, Ghunem et al. 2019) and is not the subject of this work. Rather, this study presents a practical framework for highlighting the prominent role of the fumed silica-silicone interactions on suppressing the DC erosion of SiR. According to Hshieh in (Hshieh 1998), the silica-ash layer formed during the combustion of silicones produces a barrier effect that shields the silicone material against the influx of heat, preventing further combustion of the material. Accordingly, the presented framework aims to highlight the role of the silica filler size and its interaction with SiR in promoting the formation of a coherent residue with a barrier shielding effect that enhances the erosion performance of SiR, as shown in the outcomes of Figure 4.3.

Table 4.2 Thermal conductivity measurements (k) of the composites based on the 15 acquired measurements of each composite with a precision of ±1%

Composite	**Minimum k [W/m·K]**	**Maximum k [W/m·K]**	**Average k [W/m·K]**
SiR + 5 wt% FS07	0.169	0.205	0.188
SiR + 30 wt% GS10	0.400	0.430	0.409

A statistical boxplot representation of the RMS LC of the composites during the +DC IPT is illustrated. Figure 4.4 shows the RMS LC waveform obtained for one of the GS10 filled SiR composites and its corresponding boxplot analysis. The boxplot shows the LC distribution for

the first 3 h of the test, which was comprised of twelve 20-min time intervals. Each bar shown in the boxplot represents the value distribution of the RMS LC values acquired during that time interval of the test. For example, the bar in the third time interval represents the RMS LC values acquired from minute 60 to minute 80 of the IPT. The bar width in the boxplot represents the distribution of the LC values during any given time interval. The top and bottom of the bar and the circled marker represent the 75th and 25th percentile and the median value of the RMS LC during that time interval, respectively. In Figure 4.4, the DC DBA is shown to develop through two distinct stages in terms of arc stability and severity. The reduction in the bar width is an indication of the changing nature of the DBA, from intermittent to stable with less nonconducting periods. As illustrated in (Ghunem, Jayaram et al. 2015; Alqudsi, Ghunem et al. 2021), the initial stage of the DBA is intermittent with inconsiderable erosion noted on the composite surface. The subsequent stage, however, is stable with reduced nonarcing periods leading to severe erosion of the composite. The inception of the stable DBA stage was suggested to be dependent on the rate of formation of surface residue promoted with thermo-oxidation at temperatures just below 200 °C by Si-C bond scission, as illustrated in the Andrinov mechanism (Timpe 2007). This residue would reduce the rate of evaporation of the liquid contaminant in the IPT, leading to the development of a stable DBA (Ghunem, Jayaram et al. 2015).

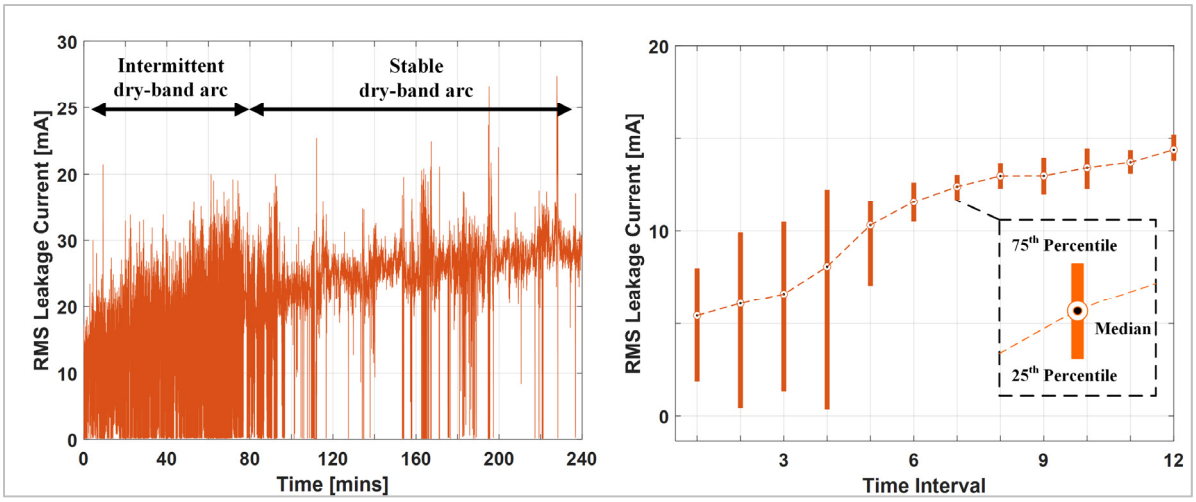

(a) (b)

Figure 4.4 (a) RMS LC for a GS10 filled SiR sample during the +DC IPT and (b) corresponding statistical boxplot representation for the first 12 20-minute time intervals, first 240 min, of the test

Figure 4.5 shows the statistical boxplots for a number of tested composites. The results indicate a faster inception of a stable eroding DBA for the GS10 filled SiR compared to that of FS07 by 40–60 min (about 20% of the total testing duration). Similar outcomes were found in (Alqudsi, Ghunem et al. 2021) for fumed silica filled composites against BN filled composites, which were attributed to the favorable interaction of fumed silica with SiR and a possible delay in the formation of the early surface residue by thermo-oxidation of the silicone volatiles.

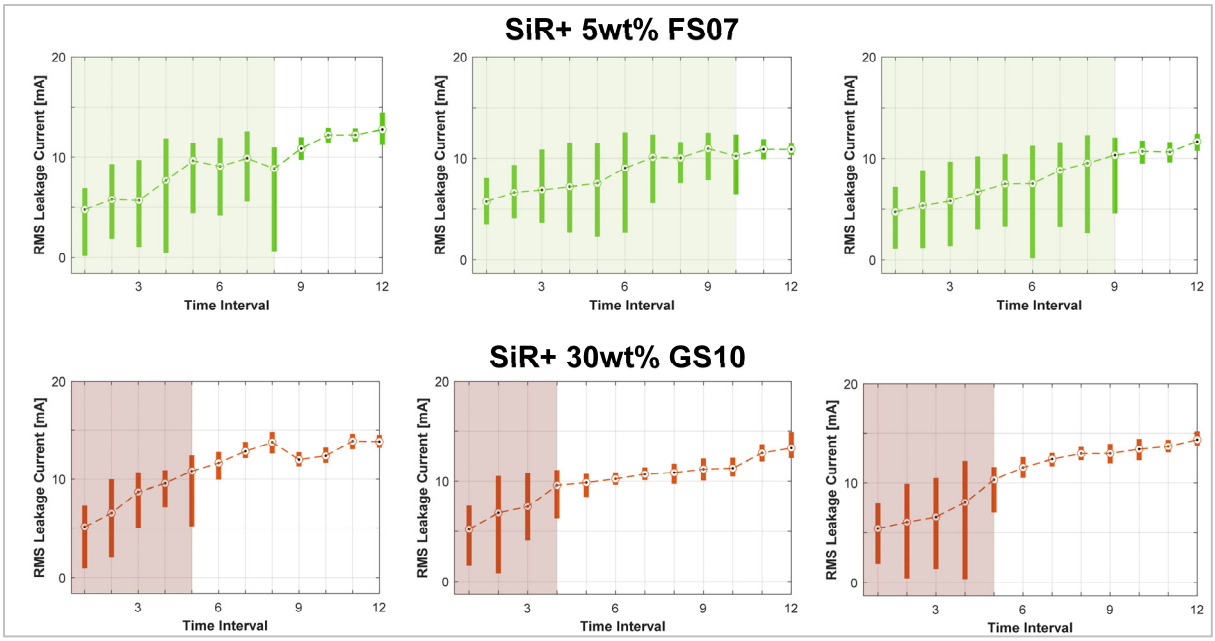

Figure 4.5 Statistical boxplot outcomes for selected samples of the +DC IPT tested composites during the first twelve 20-minute time intervals of the test

4.3.2 Thermogravimetric–Differential Thermal Analysis

Figure 4.6 shows the TGA–DTA outcomes of the study. The TGA plot shown in Figure 4.6a is conducted for the prepared silica composites and the unfilled SiR. All of the composites and the unfilled SiR begin depolymerization at 400 °C, which, according to Camino et al. in (Camino, Lomakin et al. 2002), represents the scission of the Si-O bonds in SiR to produce cyclic oligomer volatiles. The rapid depolymerization of the unfilled SiR eventually leaves a low remnant residue of about 14.5 wt%. The TGA plot illustrated in (El-Hag, Simon et al. 2006) showed similar low remnant residues, while other studies (Camino, Lomakin et al. 2001; Hermansson, Hjertberg et al. 2003) have shown the complete depolymerization of an unfilled SiR at the end of a TGA test. This variation could be attributed to a number of issues, such as the difference in suppliers and material preparation methods. For this study, 14.5 wt% was considered as the additional residue, possibly fused or crosslinked residue, produced for an unfilled SiR under TGA in an N_2 atmosphere. Beyond 400 °C, the FS07 composite decomposes

at a slightly higher rate than that of GS10, which is still considered comparable despite having a much lower filler loading.

Figure 4.6b shows the DTGA plot for both of the composites under an N_2 atmosphere. The DTGA plot suggests the presence of multiple decomposition peaks, with the second one starting at temperatures higher than 500 °C. Camino et al., in (Camino, Lomakin et al. 2002), reported a radical-based crosslinking mechanism involving the homolytic scission of Si-CH_3 bonds in SiR, which competes with depolymerization during the second decomposition stage at elevated temperatures. At the onset of the 500 °C temperature, the decomposition rate of the FS07 filled composite becomes lower than that of the GS10 filled composite, as observed in the shaded region of the DTGA plot in Figure 4.6b. This observation may suggest the influence of FS07 on suppressing depolymerization and promoting radical based crosslinking, despite being filled in SiR at one sixth of the filler loading level of the GS10 composite. In other words, the DTGA peaks appearing more distinctively with FS07 as compared to the GS10 filled SiR suggest interactions between fumed silica and the SiR matrix to promote radical-based crosslinking to a greater extent as compared to the interactions between ground silica and SiR. The rate of SiR depolymerization was found to be subject to the mobility and flexibility of the SiR siloxane chains, as indicated by Delebecq et al. in (Delebecq, Hamdani-Devarennes et al. 2011) and Hamadani et al. in (Hamdani, Longuet et al. 2009). It was reported in (Ramirez, Jarayam et al. 2010) that the high silanol group concentration on the fumed silica's surface favorably interacts with the siloxane chains of SiR. Accordingly, this interaction could suppress the depolymerization and volatilization of SiR, as explained in (Hamdani, Longuet et al. 2009). To further support this conclusion, the DTA of both composites was conducted in an air atmosphere.

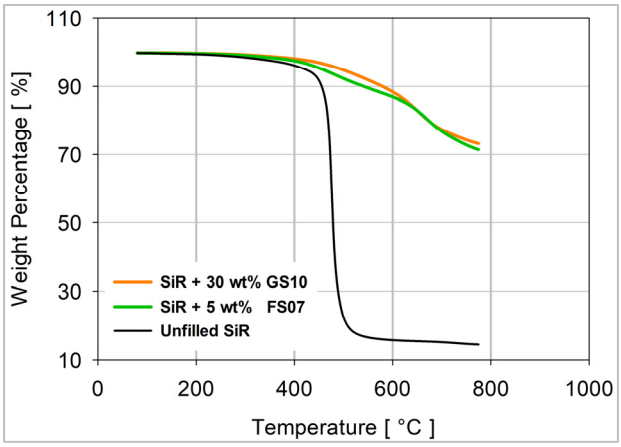

(a)

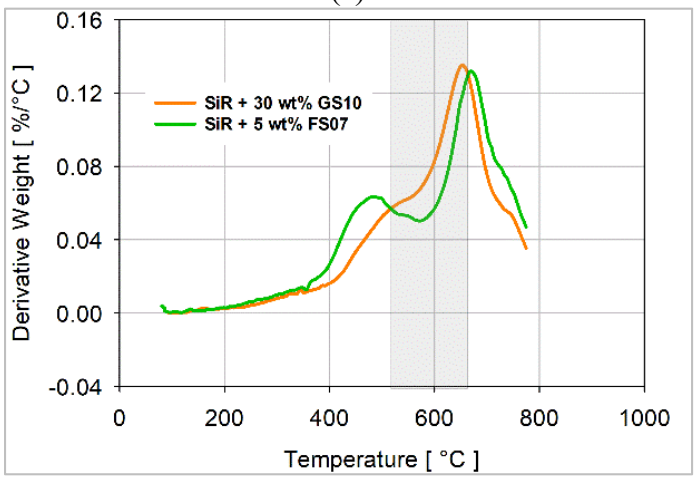

(b)

Figure 4.6 (a) Thermogravimetric analysis (TGA) for the prepared composites and the unfilled SiR in an N_2 atmosphere (b) Corresponding differential thermogravimetric analysis (DTGA) plot for the silica filled composites

The DTA plot shown in Figure 4.7 indicates the exothermic peaks obtained for both composites, which represent the combustion of the volatile SiR oligomers produced in depolymerization. Clearly, the suppressed depolymerization of the FS07 filled SiR leads to a lower exothermic peak compared to that of GS10.

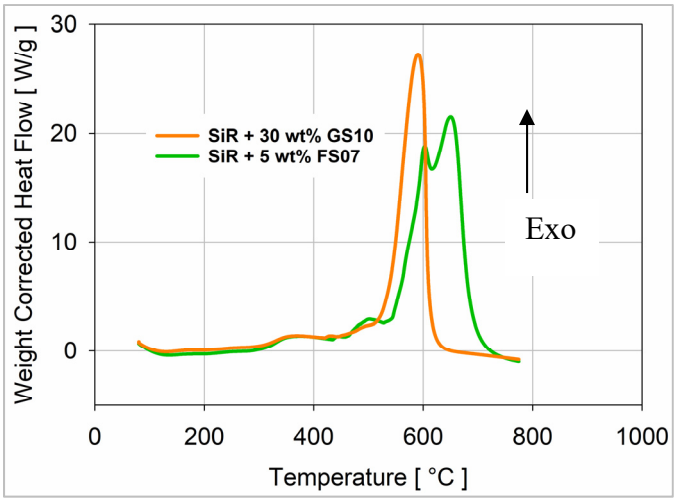

Figure 4.7 DTA for the prepared composites in air atmosphere

The final wt% of TGA remnant residues (R_{TGA}) obtained for both composites was found to be comparable, with the GS10 filled SiR having a slightly higher remnant residue by a difference of only 1.8%, despite being loaded at six times the filler loading of the FS07 filled SiR. This further indicates the role of FS07 in suppressing SiR depolymerization and promoting radical-based crosslinking. To clarify this quantitively, based on the computation illustrated in (El-Hag, Simon et al. 2006; Koné, Ghunem et al. 2019), the final assumed residue R_{asm} if the composite polymer and filler components independently decompose without interaction is calculated as follows:

$$R_{asm} = (14.5\% \times W_{SiR}) + W_{filler} \tag{4.1}$$

where W_{SiR} and W_{filler} are the weight fractions of the SiR and the filler in the composite, respectively. As mentioned earlier, the 14.5% represents the undecomposed portion of SiR that was found in the TGA plot of Figure 4.6a. The additional residue R_{add} obtained, which accounts for the role of the filler interaction with the SiR polymer, is calculated as follows:

$$R_{add} = R_{TGA} - R_{asm} \tag{4.2}$$

Table 4.3 shows the calculated additional residue for each composite. Clearly, the additional residue obtained for the FS07 filled SiR, 52.6%, is much higher than that of GS10, 33%, by a

factor of 1.6. This difference in the additional residue differentiates between the effect of each filler and its interaction with SiR on suppressing depolymerization and promoting crosslinking. The higher additional residue for the FS07 filled SiR could indicate a better suppression of depolymerization and a higher degree of crosslinking exhibited by the composite during TGA.

Table 4.3 Calculation of the additional residue R_{add} of the composites

Composite	W_{SiR}**[%]**	W_{filler}**[%]**	R_{TGA}**[%]**	R_{asm} **[%]**	R_{add}**[%]**
SiR + 5 wt% FS07	95	5	71.4	18.8	52.6
SiR + 30 wt% GS10	70	30	73.2	40.2	33

Figure 4.8 shows an SEM image of the obtained TGA residues for both of the composites. The GS10 filled SiR TGA residue surface was observed to be of a coarser nature in comparison to the FS07 filled SiR TGA residue. This could in part be a result of the higher particle size of GS10, as shown in the image, or a result of the lower crosslinking and higher volatilization leading to a more porous residue compared to that of the FS07 filled SiR. The FS07 filled SiR, on the other hand, appears to promote a coherent residue with radical-based crosslinking. The weakness of the GS10 filled SiR residue can be certainly observed in terms of the propagating surface fractures shown in Figure 4.8, which are not present in the FS07 filled SiR residue, indicating coherency in the residue characteristics of the latter. The coherency of the residue was proposed to have a barrier shielding effect on the SiR material against the progressive erosion of silica filled SiR composites under DC voltage (Koné, Ghunem et al. 2019). These observations shown in the TGA plots and residues could be correlated with the erosion performance of the composites illustrated earlier, indicating the role of the FS07 filler and its interaction with SiR in promoting a more coherent residue, which, in turn, suppresses the progressive erosion of SiR and enhances the erosion performance of SiR.

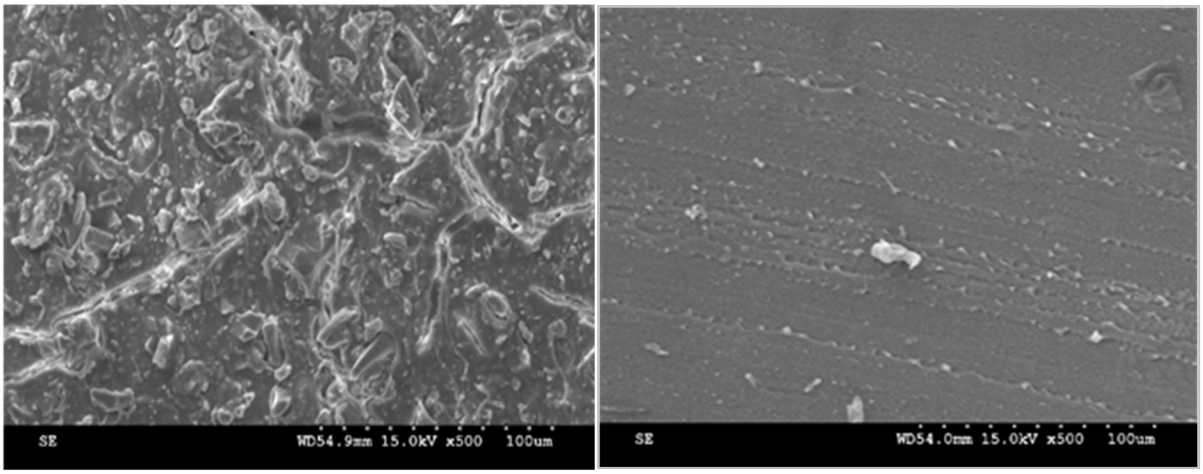

(a) (b)

Figure 4.8 (a) SEM images for the TGA residue for the SiR + 30 wt% GS10 and (b) TGA residue for the SiR + 5 wt% FS07 under an N_2 atmosphere

4.3.3 Residue Morphology Using the Dry-Arc Resistance Test

The formation of high additional residue with SiR composites could improve the erosion performance of SiR composites as a result of the formation of a coherent residue that shields the composite against an influx of heat from DBA. To better investigate this possible correlation, the dry-arc resistance test is utilized as a fast and controllable test for preparing eroded samples of the composites whose residues can be observed. Figure 4.9 shows the microscopic images obtained for the eroded pits of the post-tested silica composites of the dry-arc resistance test. Figure 4.9a,b clearly shows that the residue obtained from the FS07 filled SiR is more coherent, with less cracks and surface splitting compared to the GS10 filled SiR residue, which is seemingly rougher with porous surfaces. This observation is also confirmed by the SEM images shown in Figure 4.9c,d. Through SEM, Nazir et al., in (Nazir, Phung et al. 2016), reported similar observations with corona-aged SiR composites showing less cracks with nano silica filled SiR compared to micro silica. The integrity of the residue could be attributed to the role of the radical-based crosslinking promoted by FS07 interacting with SiR, leading to a more stable residue with coherency characteristics similar to that shown in the

TGA residue of Figure 4.8. These observations could explain the better erosion performance obtained for the FS07 filled SiR, as shown in Figure 4.3.

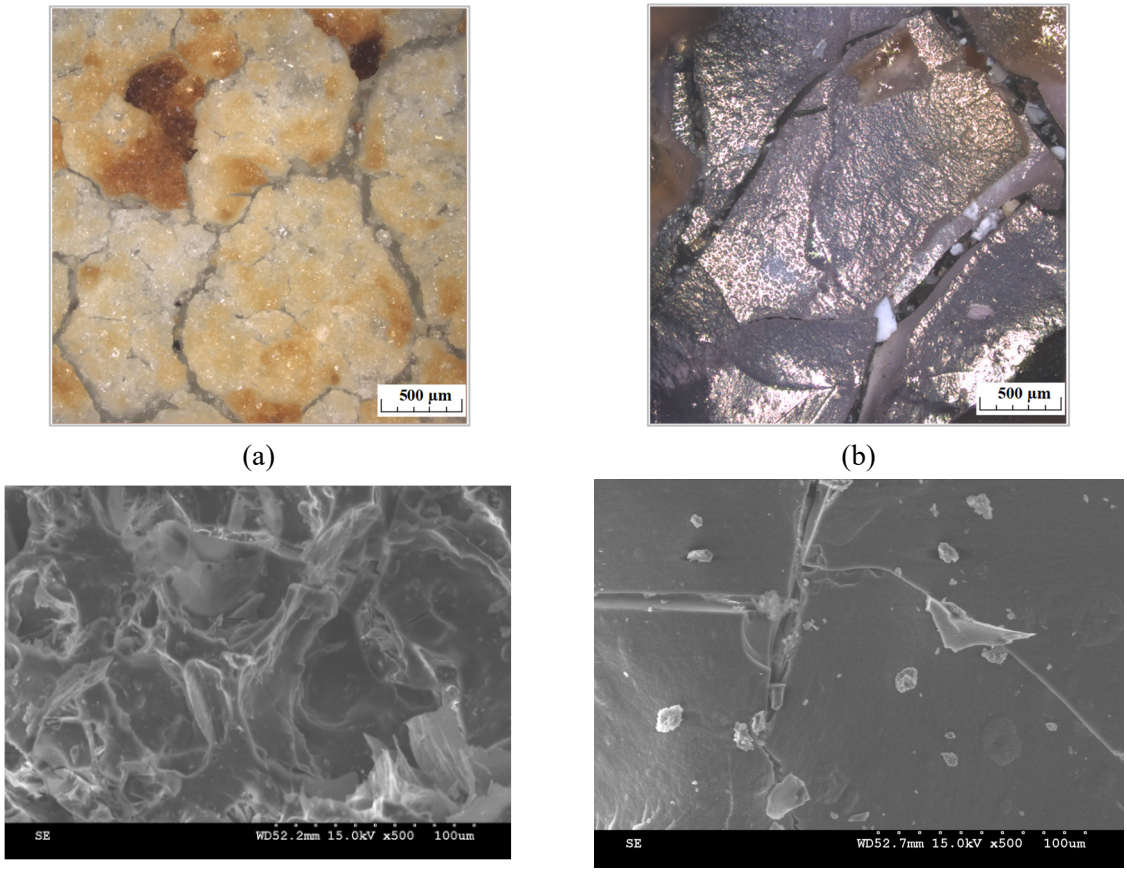

(a) (b)

(c) (d)

Figure 4.9 Microscopic images of dry-arc resistance post-tested samples at a magnification of 50 for (a) SiR + 10 wt% GS10 and (b) SiR + 5 wt% FS07 composites, and SEM imaging at a magnification of 15 k for (c) the SiR + 30 wt% GS10 and (d) SiR + 5 wt% FS07 composites

To further validate the applicability of using the dry-arc test for observing the residue morphology of eroded composites, SEM was used to observe the eroded residue of the post IPT tested composites for comparison against those obtained under the dry-arc resistance test. Figure 4.10 shows the images obtained using SEM for the IPT tested composites. As can be seen in Figure 4.10, the surface morphology of both of the composites under the IPT are similar to their counterparts in the dry-arc resistance test in terms of roughness and coherency. This similarity further justifies the use of the dry-arc test as part of this mechanistic study. Though the experimental conditions involved in both of the tests are completely different, such as the absence of a wet contaminant in the dry-arc resistance test, the interest of this study is to

observe the heat ablation effect of the arc on the composites and analyze the eroded residue characteristics accordingly. Creating this joule heating effect using either test does not necessarily dictate that similar testing methods or experimental conditions are to be followed. With this understanding, the dry-arc resistance test is advantageous in terms of the higher degree of controllability obtained with stimulating fast SiR erosion as a result of sustaining the arc at one fixed location above the sample during the test. The difference between the testing conditions of the tests has no effect on changing the residue characteristics of the composites, as can be seen in Figure 4.10, which further justifies the use of the dry-arc resistance test.

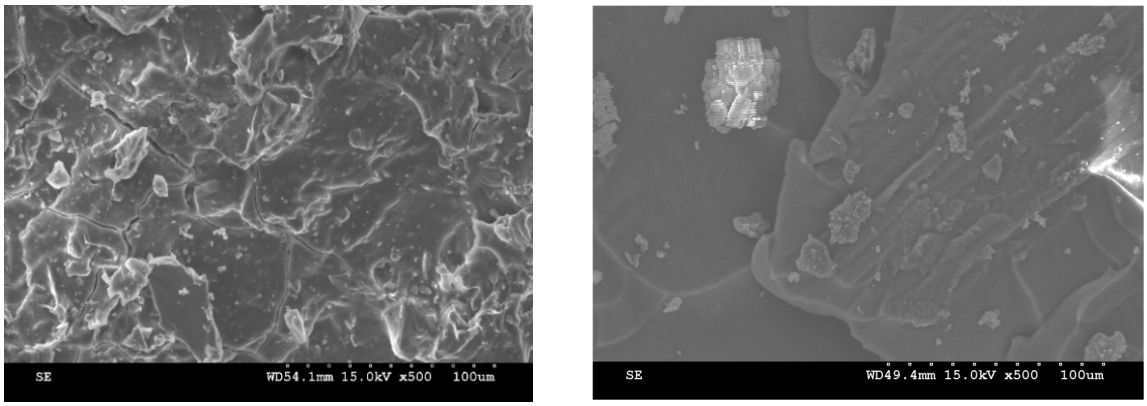

(a) (b)

Figure 4.10 SEM imaging at a magnification of 15 k for (a) the SiR + 30 wt% GS10 and (b) SiR + 5 wt% FS07 composites tested using the +DC IPT

Though the formation of coherent residue could enhance the erosion performance of the silica filled SiR composites, Delebecq et al., in (Delebecq, Hamdani-Devarennes et al. 2011), did explain that the carbon content of the residue could increase with increased SiR crosslinking. This increase in carbon content, however, would not significantly impact the composite during the IPT to cause a tracking failure, as explained in (Koné, Ghunem et al. 2019). According to Kumagai et al., in (Kumagai, Wang et al. 1998), the analysis of the residue formed as a result of DBA in RTV SiR was found to contain 1 wt% of elemental carbon, which was considered insignificant for tracking. A simple demonstration of this would be achieved by testing the composites using the dry-arc resistance test for 10 s during the 1st current step of the test in cycle 1. Figure 4.11 shows the surface residue obtained for both composites after 10 s of the

test in cycle 1 with equal electrode spacing. The FS07 filled composite shows a tendency to form a slightly higher burnt residue, possibly containing carbon, during the test compared to the GS10 filled composite. Still, however, the difference is insignificant, which is in line with (Kumagai, Wang et al. 1998; Koné, Ghunem et al. 2019).

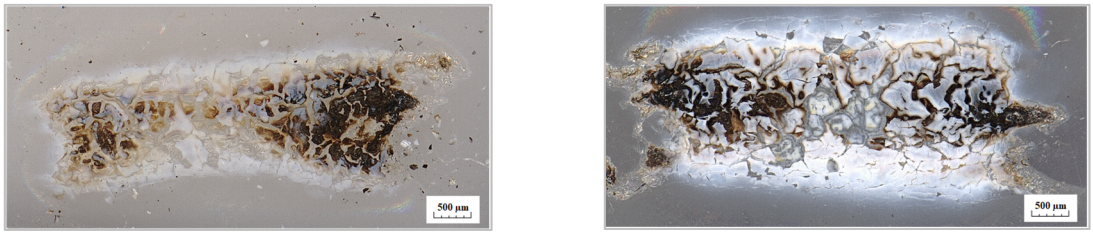

(a) (b)

Figure 4.11 Surface residue of (a) the SiR + 30 wt% GS10 and (b) SiR + 5 wt%FS07 composites tested using the dry-arc resistance test for the first 10 s of cycle 1

4.3.4 Surface Roughness of Eroded Composites

Analyzing the surface roughness of eroded silica filled SiR composites could further elaborate on the role of silica fillers in the DC erosion performance of SiR composites. The two elements that are associated with the roughness analysis are waviness and average roughness. Waviness describes the texture of the overall surface profile along a defined displacement axis, while average roughness describes the short-wavelength (high frequency) variations superimposed on the waviness along the same displacement axis (ASME 2019). Figure 4.12 shows the 3D topography and corresponding waviness profiles for the silica filled samples eroded using a dry-arc test. Clearly, the waviness of the FS07 filled SiR composite indicates a smoother surface with lower variations in the peak heights and valley depths within different segments of the profile. It is important to highlight that the erosion depth of the fumed silica filled SiR composite was found to be of higher value compared to that of the ground silica filled composite in the dry-arc resistance test, as shown in Figure 4.12c,d. This contrasts the +DC IPT outcomes of this study, which have been highlighted in Figure 4.3a. This implies that the use of the dry-arc resistance test in its standard testing conditions to assess the erosion performance of the composites in terms of erosion depth would not suffice. Rather, further

modification of the testing conditions of the dry-arc resistance test are required to produce erosion depth ranking outcomes similar to those of the IPT for these specific composites. As mentioned earlier, the dry-arc resistance test is only used for the purpose of producing controlled arcing for post-testing residue analysis and not as means to rank the erosion performance of the composites in terms of the erosion depths. Using the dry-arc test in its standard form as a means to compare the erosion performance of the composites could work if both of the composites had equivalent filler loadings. An example of this would be in using the dry-arc resistance setup to test the erosion performance of a 30 wt% GS10 filled SiR against a 5 wt% FS07 + a 25 wt% GS10 filled SiR or a 10 wt% FS07 + a 20 wt% GS10 filled SiR composites.

Figure 4.13 shows the statistical boxplot for the average roughness value distribution, R_a, of the sampled areas shown in the plot. A total of 10 profile lines were taken for each sampled area. Accordingly, each boxplot shows the median, 25th and 75th percentile and the minimum and maximum values for R_a within the 10 profiles. The wider variation and higher median value of R_a for the GS10 filled composite indicates a rough profile within small segments of the composites, which could indicate a higher degree of surface porosity compared to the FS07 filled SiR composite.

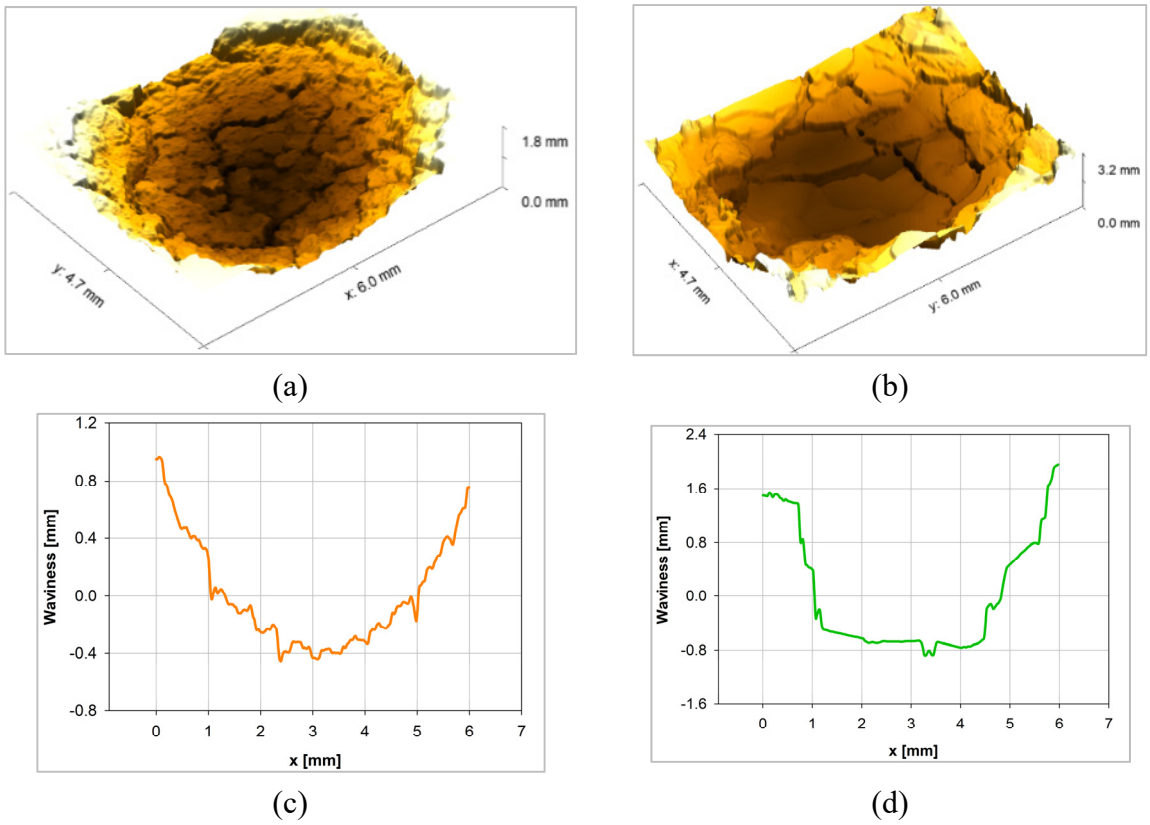

Figure 4.12 Three-dimensional topography of the (a) the SiR + 30 wt% GS10 and (b) SiR + 5 wt% FS07 composites tested using the dry-arc resistance test
Corresponding waviness profiles for (c) SiR + 30 wt% GS10 and (d) SiR + 5 wt% FS07 composites

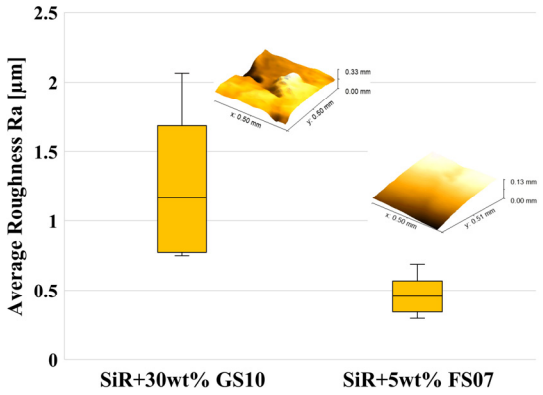

Figure 4.13 Statistical boxplot representation of 10 values of R_a for the sampled areas shown for each composite
The center bar represents the median value, the top and bottom box edges represent the 25th and 75th percentile values, respectively, while the top and markers represent the minimum and maximum values of R_a, respectively.

Based on Figures 4.12 and 4.13, the GS10 filled composite surface residue is of higher roughness with the overall surface waviness and within the smaller segments of the surface. Surface roughness could significantly impact the erosion performance of the composite due to a number of reasons. Under the salt-fog test, Deng et al., in (Deng, Hackam et al. 1995), explained that rough SiR surfaces with large filler particle sizes tend to cause a higher impairment of the hydrophobicity retention properties of SiR. In their study, LC developed at higher magnitudes with SiR composites having small filler particle sizes and less surface roughness. On the other hand, Kozako et al., in (Kozako, Higashikoji et al. 2012), illustrated that the addition of nano silica to their SiR composites did not have much of an influence on changing the hydrophobic properties of SiR, despite a slight increase in the surface roughness with respect to the unfilled SiR. Moreover, it is possible that the rough surface texture of the residue at early stages of the IPT could interrupt the smooth flow of liquid contaminant during the test, leading to more localized DBA being formed on the insulator surface as a result of liquid contaminant being trapped within small, eroded pits.

4.4 Conclusion

The presented paper illustrated the role of fumed silica and ground silica fillers in suppressing the DC erosion of SiR through a novel framework. The erosion performance outcomes suggest that fumed silica and its interaction with SiR were effective in promoting the formation of a coherent shielding residue, which resulted in suppressing the DC erosion of SiR. This was found despite the higher composite thermal conductivity of the ground silica filled composite, which further supports the influence of the filler's interface interactions over enhancements in the thermal conductivity on suppressing DC erosion. Simultaneous TGA–DTA analysis shows the significant influence of fumed silica in suppressing depolymerization and promoting radical-based crosslinking at high temperatures in SiR as a result of its favorable interaction with the siloxane chains of the polymer tethering their flexibility and mobility during depolymerization. This results in the formation of a much higher additional residue with the fumed silica filled composite, despite being filled at one sixth of the loading level of the ground silica filled composite. The formation of a higher additional residue could result in a higher

carbon content, which still would not be enough to promote a tracking failure during the IPT. The microscopy conducted on the eroded composites from the dry-arc resistance test shows coherency and low surface fracture in the residue of the fumed silica filled composite. This could also explain the better erosion performance of the composite as a result of the shielding effect of the coherent residue preventing progressive erosion. Moreover, the surface morphology outcomes of the dry-arc tested composites are consistent with those of the IPT, which validates the use of the dry-arc test as part of this framework. The surface roughness outcomes show a rougher surface waviness and higher values of Ra for the ground silica filled composite, which could further indicate the weakness and porosity of the residue, leading to an inferior performance under the IPT. The overall conclusion of the study suggests a significant role for the silica filler size in suppressing the erosion of SiR under DC voltage as a result of its influence on the eroded residue characteristics.

Acknowledgments

The authors would like to thank Prof. Souheil-Antoine Tahan, Mr. Simon Laflamme, Dr. Mohammad Saadati and Mr. Joel Grignon for providing the permission, technical help and advice needed to complete the microscopic part of this study.

CHAPTER 5

THE VIABILITY OF THE FILLER BARRIER EFFECT DURING THE DC DRY-BAND ARCING ON SILICONE RUBBER

Alhaytham Y. Alqudsi[a], Refat A. Ghunem[b] and Éric David[a]

[1]Department of Mechanical Engineering, École de technologie supérieure,
1100 Notre-Dame West, Montreal, Quebec, Canada H3C 1K3
[2]Metrology Research Center, National Research Council Canada,
1200 Montreal Road, Ontario, Ottawa, Canada K1A 0R6

Paper submitted for publication, August 2021

Abstract

This paper investigates the filler barrier effect on suppressing the erosion of silicone rubber composites during the DC dry-band arcing, by supplementing main micro fillers in silicon rubber, i.e. ground silica and micro-sized alumina tri-hydrate, with fumed silica and nano-sized alumina tri-hydrate fillers. A study framework employing simultaneous thermogravimetric-differential thermal analyses, the inclined plane tracking and erosion test and the dry-arc test is employed. Fumed silica in silicone rubber increases the amount of the crosslinked residue and suppresses silicone rubber depolymerization; whereas nano-sized alumina tri-hydrate releasing water of hydration may adversely impact the residue coherence and promote combustion. The viability of the filler barrier effect is synergistically achieved by adding fumed silica to the main ground silica filler, thereby maintaining the residue integrity. The inclined plane-tracking erosion test confirms the importance of the filler barrier effect of fumed silica in supplementing the volume effect of ground silica in the suppression of the DC dry-band arcing. These filler effects appear to mainly govern the erosion resistance, with insignificant effect shown for thermal conductivity under DC. The dry-arc resistance test is shown as a useful method to simulate a stable dry-band arcing and obtain reproducible surface

erosion patterns that correlates with the outcomes of the DC inclined plane tracking and erosion test.

Keywords: Silicone rubber, DC erosion resistance, DC inclined-plane test, dry-arc resistance test, fumed silica barrier effect.

5.1 Introduction

Silicone elastomers are commonly utilized as housing materials for outdoor polymeric insulators in electric power distribution and transmission systems. When used in areas of severe pollution, SiR insulators are prone to erosion from dry-band arcing (DBA) which worsens under the DC as compared to AC voltages (Liang, Shaohua et al. 2020; Vas, Venkatesulu et al. 2012; Cherney, Gorur et al. 2015). Indeed, the stability of the DBA increases under DC as compared to AC voltages, resulting into a higher amount of heat flux impinging the SiR insulator surface.

Inorganic fillers are incorporated in SiR composites, and the filler's action to enhance the composite thermal conductivity has been highlighted as the main filler action suppressing erosion under AC voltages (Meyer, Cherney et al. 2004). The DC erosion resistance of SiR, however, was found to be governed by different actions from thermal conductivity, that rather retard the progress of erosion through the thickness of the composite under the DC DBA (Ghunem, Koné et al. 2020). These actions include the filler volume fraction primarily replacing the depolymerizable SiR content, and an additional action for the filler in creating a barrier shielding the underlying silicone from the DBA heat (Ghunem, Koné et al. 2020; Koné, Ghunem et al. 2019). Simply loading the composite with more fillers replaces more of the polymeric fuel for erosion, but achieving filler loading at more than 60wt% becomes a difficult and costly task with conventional fabrication methods. Improving the DC erosion resistance of the composite could therefore be approached by adding nano-sized fillers in order to enhance the filler barrier effect. Limited number of studies have reported a role for the barrier effect of the filler during the DBA on SiR. Kone et al. in (Koné, Ghunem et al. 2019) examined the role of ground silica residue on SiR erosion during the DC inclined plane tracking and erosion test (DC IPT), and explained how the integrity of the residue shield could be enhanced with larger

ground silica filler size. Hosier et al. in (Hosier, Abd Rahman at al. 2013) indicated the impact of the mechanical integrity of the residue structure in SiR on its heat ablation and performance in the IPT. It was found that heavily loaded SiR composites with 50wt% (percent by weight) silica passed the IPT under 4.5 kVrms and the laser ablation test as a result of producing a dense ash layer with coherent mechanical integrity.

The barrier effect of fillers in SiR could be obtained by promoting crosslinking reactions within the silicone polymeric matrix. Guo et al. in (Guo, Zeng et al. 2018) suggested modulating the crosslinking density of SiR, which enhanced the residue formed during the IPT. In their work, highly crosslinked SiR was found to produce a non-porous silicone oxycarbide ceramic residue at local erosion spots on the SiR surface. Xie et al. in (Xie, Zeng et al. 2021) incorporated treated silica in addition-curing liquid SiR, concluding that the compact ceramic layer formed during erosion was effective in suppressing the thermal degradation of SiR. Delebecq et al. in (Delebecq, Hamdani-Devarennes et al. 2011) illustrated that siloxane chain immobilization in SiR is key for ceramizing the SiR residue by producing silicone oxycarbide ceramics in high yield. The incorporation of a platinum catalyst was found to have a significant influence promoting residue ceramization on SiR (Guo, Zeng et al. 2018; Delebecq, Hamdani-Devarennes et al. 2011).

An earlier study in (Alqudsi, Ghunem et al. 2021) revealed a significant influence for the fumed silica's interface in tethering the siloxane chains of SiR, thereby suppressing DC erosion in SiR nanocomposites by suppressing depolymerization and promoting a radical-based crosslinking. This interaction was revealed to be more influential in suppressing erosion as compared to the enhancements in the composite thermal conductivity (Alqudsi, Ghunem et al. 2021). Investigating the barrier effect of fumed silica on the erosion resistance of SiR has been limited to studying nanocomposites (El-Hag, Simon et al. 2006), without a clear elucidation being presented on the effect adding other constituent elements that could influence erosion like micro-fillers. Reinforcing micro silica filled SiR with fumed silica to enhance the AC erosion resistance of SiR was investigated in many works such as that in (Ramirez, Jarayam et al. 2010). However, no clear elucidation was presented to highlight the combined volume

effect and residue structure characteristics on suppressing erosion, especially under DC. Emphasizing the filler barrier effect associated with fumed silica could only be utilized as a supplementary filler action to the volume of micro-sized fillers replacing the polymeric content fueling erosion.

The addition of commonly used micro-fillers, like ground silica and alumina trihydrate (ATH), in sufficient amounts is an essential requirement for reducing the cost of the outdoor insulators by reducing the silicone content used. In other words, adding fumed silica to micro-filled composites could promote the barrier effect given that the micro-filler is adequately added to enhance the erosion resistance of SiR. In addition, specific sizes of ground silica and the water of hydration released from ATH were shown to promote the formation of harmful residue that could further fuel silicone combustion under the DC IPT (Ghunem, Koné et al. 2020; Koné, Ghunem et al. 2019). Thus, investigating the viability of the barrier effect associated with supplementing fumed silica and other potential nano fillers, such as nano ATH, to micro-fillers is constrained with ensuring the residue barrier is not adversely impacted by the micro-filler constituents in the SiR composite. As such, this paper investigates the integrity of the barrier effect under the DC DBA as a result of supplementing fumed silica or nano ATH in SiR composites in the presence of ground silica and ATH as main micro-sized fillers added to the composite.

5.2 Materials and Methods

5.2.1 Material Specimen

Table 5.1 describes the fillers and SiR composites used in the study. Both fumed silica and micro ATH fillers were obtained from Sigma-Aldrich. Ground silica and nano ATH were respectively obtained from US Silica and Nanostructured&Amorphous Materials, Inc. The silicone used was a two-part room temperature vulcanized (RTV) SiR from Momentive, RTV 615, in which fillers were added and mixed using a ROSS high shear mixer. The mixer disperses the filler into the base silicone, and later with the crosslinking agent added into the mixture. The procedure followed in preparing the composites can be found in (Alqudsi, Ghunem et al. 2021).

Five composites were prepared which comprised of micro ATH filled SiR, ground silica filled SiR, and three other hybrid composites combining a micro filler and a nano filler as indicated in Table 5.1. Practical formulations of SiR should typically contain high silica and ATH micro filler loadings, at least about 40 wt%, in order to pass the critical test voltage of IPT (Ansorge, Schmuck et al. 2012; Kumagai, Yoshimura 2001) and to which fumed silica could be added to promote a barrier effect (El-Hag, Simon et al. 2006). Since only the viability of the filler barrier effect is rather explored here in principle and given the limitation in the laboratory to achieve high loading levels in the composite with nano-sized fillers using the high shear mixer, the total weight fraction of the filler in all composites was maintained at 30wt%. Therefore, this study investigates hybrid composites with micro filler as the main filler replacing the silicone, and a nano filler as the supplementary filler promoting barrier effect respectively in a 25:5 ratio between the micro and nano fillers.

Table 5.1 Fillers and composites used in the study

Filler Name	**Particle Size (µm)**	**Specific Gravity**
Ground silica	10.5[(1)]	2.65
Micro ATH	<45	2.42
Fumed silica	7×10^{-3}	2.3
Nano ATH	5×10^{-2} [(2)]	2.42

Composite Sample Code	**Filler Level**				**Total Filler (wt%)**
	Base Filler	Level (wt%)	Supplementary Filler	Level (wt%)	
A30	Micro ATH	30	NA[(3)]	0	30
S30	Ground silica	30	NA[(3)]	0	
A25a5	Micro ATH	25	Nano ATH	5	
A25s5	Micro ATH	25	Fumed silica	5	
S25s5	Ground silica	25	Fumed silica	5	

[1]Median particle size. [2]Average particle size. [3]Not applicable.

5.2.2 The IPT and Dry-Arc Resistance Test

Figure 5.1 shows the test setup for the IPT and dry-arc resistance test, which conforms to the IEC 60587 and ASTM D495 standards (IEC 2007; ASTM 2014). The test voltage in the IPT, was set to the positive polarity at 3.5 kV level, which produces a severe DBA that leads to deep erosion on SiR composites (Cherney, Gorur et al. 2015). Detailed experimental procedure of the test can be found in (Alqudsi, Ghunem et al. 2021), which were based on previously recommended procedures for conducting the IPT under +DC voltages, or +DC IPT (Cherney, Gorur et al. 2015). Ten samples from each of the composites in Table 5.1 were tested. After testing was complete, the erosion depth was recorded using a digital Mitutoyo 571-200 micrometer with an accuracy of 0.1 mm. The eroded volume was determined using the weight measured and the known density for a clay material filling the eroded pit.

The dry-arc resistance test was employed in this study as an accelerated testing method for producing a reproducible eroded surface and residue morphology on the tested SiR composites. A low current arc was generated during the test which was utilized as a controlled heat source for controlled heat ablation of SiR. As shown in Figure 5.1b, the test uses tungsten electrodes placed at a 30° inclination angle on the sample under test and separated by a distance of 6.35mm. The followed protocol in the test was to generate the low-current arc (scintillation) in seven 1-minute current steps (CS), with specified current magnitude and scintillation duration (ASTM 2014). Figure 5.1b describes the nature of the current generated during the first four CSs, CS1 to CS4, of the original seven outlined in (ASTM 2014). As can be seen in Figure 5.1b, the scintillation duration increases with the progress of the test which indicates an increase in the degree of stability for the scintillation. The transition from CS3 to CS4 leads to a sustained scintillation. This is analogous to the behavior of the DC DBA evolving into the stable state and imposing more severe heat on the testing surface as compared to intermittent scintillation at early stages of the test (Alqudsi, Ghunem et al. 2021; Ghunem, Jayaram et al. 2014). The governing difference between AC and DC DBA comes down to the increased stability of the arc under DC as compared to AC voltages and, thus, there was no need for modifying the existing setup for DC testing. The current magnitude, 10mA, is constant during these four steps and are generated at a 6.1kV AC voltage. The stable arc was obtained by CS4

and thus there was no need to use the entire seven steps outlined in (ASTM 2014). The coherency and integrity of the damaged surfaces obtained using this test are observed using microscopic tools.

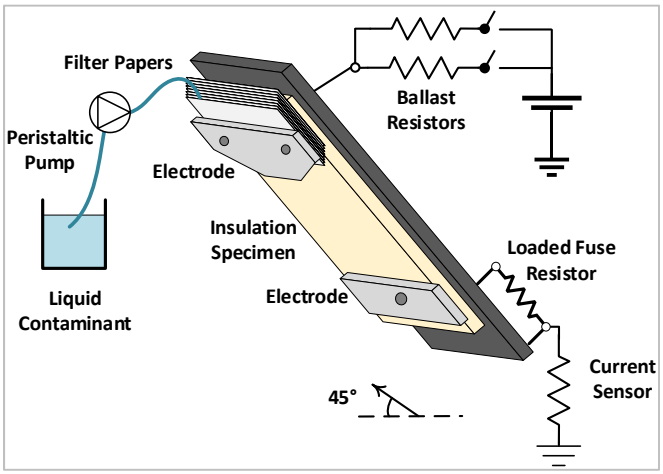

(a)

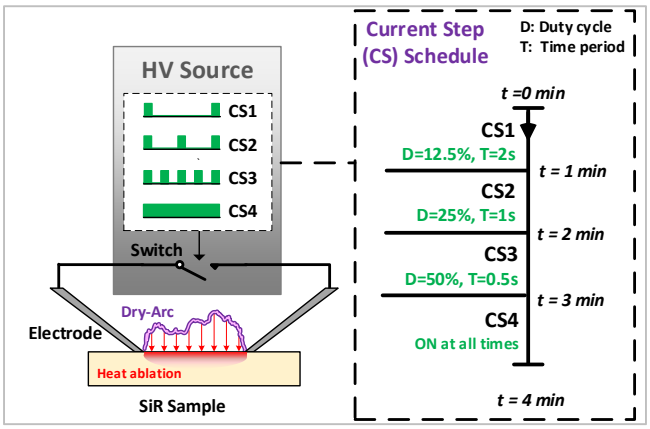

(b)

Figure 5.1 Overall (a) DC Inclined plane tracking and erosion test and (b) dry-arc resistance test setups used in the study

5.2.3 Thermal Analysis

Thermogravimetric-differential thermal analyses (TGA-DTA) were employed in this study to investigate the thermal degradation behavior of the prepared composites. Conducting such analyses is essential for observing the incremental role of the nano filler on suppressing depolymerization and promoting the formation of additional residue promoted by the filler-polymer interactions in the composite. TA instrument's SDT Q600 was used to conduct TGA-DTA under nitrogen (N_2) and air (O_2) atmospheres with an applied heating rate of 25 °C/min and a temperature span between 80-800°C. The tested samples weighed between 10-20 mg. Thermal conductivity measurements were acquired for the composites using a Trident Thermal Conductivity Analyzer which utilizes the Modified Transient Plane Source (MTPS) method as per the ASTM D7984 standard (ASTM 2021).

5.2.4 Residue Morphology

Observing the surface morphology of eroded SiR surfaces is essential in understanding the effect of the fillers in general and nano fillers in particular on altering the SiR residue characteristics in terms of coherency and integrity. Microscopy can characterize the morphology of eroded surfaces based on surface fracture, roughness and porosity. The eroded surfaces of the composites analyzed were obtained through the +DC IPT and the dry-arc resistance test. Scanning electron microscopy (SEM), S3600-N Hitachi, was used in this study to observe the surface morphology of eroded composites under both tests. The samples were prepared by blade cutting, followed by sputter coating with gold. A Keyence VR-5000 optical microscope was also used to scan the surface profiles of the composites in this study. The scanned profiles provide a clear three-dimensional (3D) surface topography that could be used to observe the surface profile in a manner that would facilitate a comparison between the characteristics of the residue structure. This would allow a preliminary observation on whether a barrier-like residue could be obtained in a given composite under erosion.

5.3 Results and Discussion

5.3.1 Thermal Analysis

Table 5.2 tabulates the thermal conductivity measurements for the composites of the study. The thermal conductivity measurements obtained for the A30 and S30 are consistent with those obtained in (Meyer, Cherney et al. 2004). The addition of 5wt% fumed silica to 25 wt% micro ATH and silica respectively in the A25s5 and S25s5 composites had a significant effect on reducing the thermal conductivity with respect to those measured in A30 and S30 respectively. This, however, was not observed with the addition of nano ATH in A25a5. Khanum et al. in (Khanum, Ghunem et al. 2020) explained that the increase in the number of filler-polymer interfaces in SiR composites could obstruct the heat flux and lower the composite thermal conductivity. It could be therefore that the better filler dispersion promoting filler-polymer interfaces with fumed silica as compared to nano ATH lead to the more remarkable decrease in the thermal conductivity with fumed silica as compared to nano ATH. In addition, an earlier study in (Alqudsi, Ghunem et al. 2021) indicated that the silanol groups on the silica surface had an influential role in promoting favorable interactions with the siloxane chains in SiR. This interaction, however, was not found to be similarly influenced by nano ATH. Rather, filling nano ATH in SiR at 5wt% resulted in the formation of agglomerates in the micron-sized range (Alqudsi, Ghunem et al. 2021). The agglomerates could be equivalent in size to the micro ATH filler particles used in A25a5 and thus resulted in no effective change in the thermal conductive pathways as compared to A30.

Table 5.2 SiR composites thermal conductivity measurements

Composite Code	**Measurement Statistics of thermal conductivity**			
	Number of Measurements	Minimum	Maximum	Average
		W/m.K		
S30	15	0.411	0.432	0.420
A30		0.473	0.523	0.495
A25a5		0.474	0.487	0.481
A25s5		0.332	0.371	0.344
S25s5		0.310	0.358	0.332

Figure 5.2 shows the TGA, DTGA (differential TGA) and DTA plots conducted for the composites of the study under N_2 atmosphere. As per the plots of Figure 5.2a, the initial decomposition temperature for the composites were dependent on the type of filler being used in the composite. Composites containing an ATH filler component, A30, A25a5 and A25s5, begin their weight loss near 200 °C, which represents the onset of endothermic dehydration of the micro ATH filler as it was similarly shown in (Ghunem, Koné et al. 2020; Koné, Ghunem et al. 2019; Kumagai, Yoshimura 2001) for micro ATH filled SiR composites. At the end of the endothermic dehydration step shown in Figure 5.2a at about 350 °C, a higher remaining weight percentage can be observed for A25s5 and A25a5 as compared to A30.

It is important to note that the amount of depolymerized SiR in the 200 °C - 350 °C temperature range was shown to be insignificant, and therefore the difference in the percentage weight loss remaining at 350 °C, as shown in Figure 5.2a, can be primarily attributed to corresponding differences in the amount of the water of hydration released amongst composites. This was similarly reflected in the DTGA plot of Figure 5.2b indicating a higher decomposition rate for A30 as compared to A25a5 and A25s5 composites during the dehydration. An increase in the depth of the corresponding endothermic dent of ATH dehydration is also evident for A30 as compared to A25s5 and A25a5 composites in Figure 5.2c. For A25s5, the higher remaining weight percentage at 350 °C was as expected, as a result of the lower weight fraction of the ATH filler releasing water of hydration which is lower in A25s5 as compared to A30 (by 5wt%).

For A25a5, higher remaining weight percentage at 350 °C was also obtained indicating less water of hydration amount released as compared to A30, despite the same total loading level of ATH filler (30 wt%) in A25a5 and A30. It should be noted however that A30 included higher amount of micro ATH as compared to A25a5 (by 5wt%). Therefore, the nano ATH component in A25a5 does not seem to undergo endothermic decomposition in the same manner as compared to the micro ATH during the TGA-DTA. The equal amounts of final residue obtained near 800 °C for the A25a5 and A30 composites suggest the possibility that, with similar total amount of ATH at 30 wt% loaded, similar amount of water of hydration can be released, but the dehydration of the

nano ATH component is more distributed during the entire temperature span of the test than micro ATH.

The decomposition stage starting at 400 °C in Figure 5.2 for the composites represents the beginning of SiR depolymerization as a result of the bond scission of Si-O bonds in the siloxane chains of SiR as reported by Camino et al. in (Camino, Lomakin et al. 2002). Depolymerization of SiR entails the formation of cyclic oligomers that depart the composite in the form of gaseous volatiles. Hamadani explained that the depolymerization and volatilization of SiR is governed by the mobility and flexibility of the siloxane chains (Hamdani, Longuet et al. 2009). Delebecq et al. in (Delebecq, Hamdani-Devarennes et al. 2011) illustrated that the weakly retained portions of the siloxanes chains are prone to depolymerization and volatilization between 400 °C and 640 °C. The constrained mobility of SiR during this decomposition step is highly influenced by the physical interactions between the filler surface and the polymer through hydrogen bonds.

Figure 5.2b indicates the presence of additional decomposition peaks for all the composites beyond 600 °C. This suggests the presence of a competing mechanism with depolymerization during the decomposition of SiR, which is radical-based crosslinking (Ghunem, Koné et al. 2020; Koné, Ghunem et al. 2019; Camino, Lomakin et al. 2002). Radical-based crosslinking is explained to be initiated through the homolytic scission of Si-CH_3 bonds at elevated temperatures. During this crosslinking step, the siloxane chains become further restrained and depolymerization is inhibited to finally produce a ceramized residue (Hamdani, Longuet et al. 2009). Kumagai et al. described the nature of this ceramized residue to be composed of a semiconductive silicon oxycarbide material (Kumagai, Wang et al. 1998).

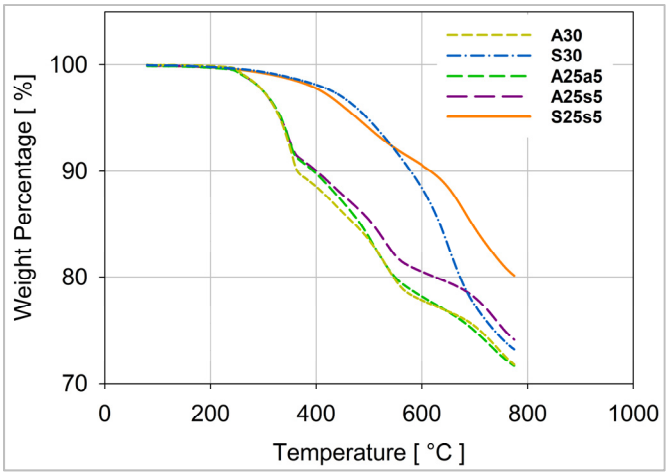

(a)

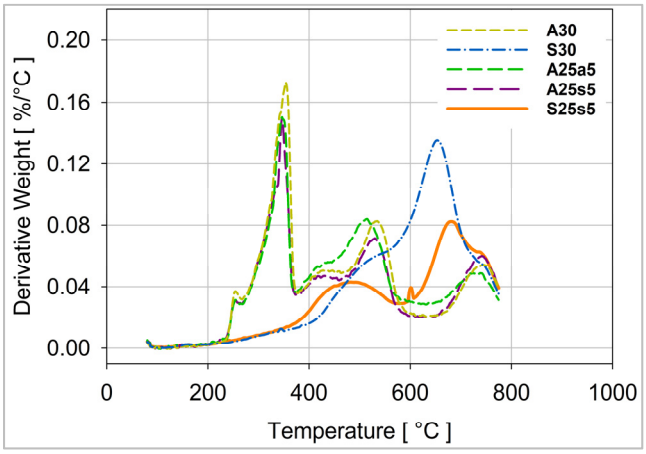

(b)

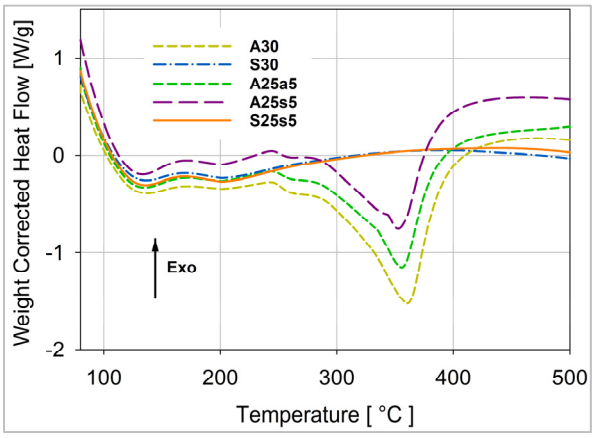

(c)

Figure 5.2 (a) TGA, (b) DTGA and (c) DTA for the prepared composites of the study under N_2 atmosphere

Comparatively analyzing the thermal decomposition characteristics amongst the composites under TGA is essential for understanding the filler effect during the depolymerization and crosslinking steps exhibited by the composites. Merely using the actual final TGA residue weight (W_{TGA}) from Figure 5.2a as a parameter for such analysis would be impractical, especially in the case of hybrid composites. Accordingly a different approach is adapted in this study which calculates the amount additional residue (W_{add}) formed in the composite during TGA; this approach was also adapted in (Koné, Ghunem et al. 2019; El-Hag, Simon et al. 2006; Alqudsi, Ghunem et al. 2021). The W_{add} estimates the amount of additional crosslinked residue formed as a result of the filler-polymer interactions, by subtracting the assumed TGA residue weight (W_{TGAasu}) from the actual W_{TGA} measured in Figure 5.2a. The W_{TGAasu} accounts for the total sum of alumina and silica filler residue and the undepolymerizable (crosslinked) SiR residue (W_{SiR}). The W_{SiR} has already been found to be around 14.5wt%, which is the final remnant TGA residue found in unfilled RTV SiR under N_2 atmosphere. The alumina residue is determined by multiplying the ATH weight fraction (W_{ATH}) with a factor of 0.65 which accounts for the 35wt% water content released from the hydrated filler during the TGA (Ghunem, Koné et al. 2020). The silica filler does not decompose during the TGA and therefore the silica residue amount is the same as the silica weight fraction (W_{silica}) in the composite. Thus W_{TGAasu} is calculated using (5.1), and then is used for the calculation of W_{add} in (5.2).

$$W_{TGAasu} = (0.65 \times W_{ATH}) + (W_{silica}) + (0.145 \times W_{SiR}) \tag{5.1}$$

$$W_{add} = W_{TGA} - W_{TGAasu} \tag{5.2}$$

To further understand the impact of the incorporated fillers on suppressing depolymerization, the depolymerized SiR content (W_{dep}) leaving the composite in the form of combustible cyclic oligomer volatiles is calculated. The W_{dep} represents the difference between the amount of SiR content that was available in the composite prior depolymerization, and the amount of additional residue formed at the end of the TGA. Accordingly W_{dep} is calculated using (5.3).

$$W_{dep} = W_{SiR} - W_{add} \tag{5.3}$$

Table 5.3 shows the calculated amounts for W_{add} and W_{dep} for each of the composites at the end of the TGA. According to Table 5.3, S30 had the least amount of additional residue produced during TGA. This finding confirms that the main filler action of micro silica in SiR is to replace the polymeric fuel of erosion and improve the composite thermal conductivity (Meyer, Cherney et al. 2004; Koné, Ghunem et al. 2019). Table 5.3 shows a significant increase in W_{add} as a result of adding fumed silica. This improvement could be attributed to the role of the fumed silica filler in restricting the mobility of the siloxane chains which was otherwise unconstrained with only ground silica added. It was emphasized in (Delebecq, Hamdani-Devarennes et al. 2011) that the physical adsorption of the siloxane chains on the fumed silica surface is a key element in promoting large crosslinking during TGA, which could further be enhanced via a radical platinum catalyst. Therefore, reinforcing the micro silica composite with supplementary amount of fumed silica could add a crosslinked residue on the surface during DBA.

The A30 and A25a5 had equivalent amounts of additional residue produced during TGA which basically indicates no significant influence for the nano ATH filler to alter the thermal degradation mechanisms when added as a supplementary filler in SiR filled with micro ATH as the main micro filler. The addition of fumed silica to micro ATH as the main micro filler in A25s5 had a slight effect on improving the additional residue, but not to a similar extent as when the main micro filler was ground silica. This finding suggests a synergistic effect for a supplementary amount of fumed silica when added with ground silica to silicone rubber in promoting the crosslinked residue during the DBA. This synergy to promote crosslinking was not observed when adding a supplementary amount of fumed silica to ATH. Therefore, promoting crosslinking is constrained with the synergistic effect of the added supplementary fumed silica filler to the main micro filler in SiR, which is dependent on the type of the base filler used.

Table 5.3 Calculation of the additional residue and depolymerized SiR amounts under thermogravimetric analysis (TGA).

Composite Code	**Filler component weights**			**Final TGA weight**		**Additional Residue (W_{add})**	**Depolymerized SiR (W_{dep})**
	W_{silica}	W_{ATH}	W_{SiR}	Assumed (W_{TGAasu})	Actual (W_{TGA})		
	[%]						
S30	30	-	70	40.2	73.2	33.1	37.0
A30	-	30		29.7	71.7	42.1	28.0
A25a5	-	30		29.7	71.6	42.0	28.1
A25s5	5	25		31.4	74.1	42.7	27.3
S25s5	30	-		40.2	80.1	40.0	30.1

The calculated amounts for W_{dep} in Table 5.3 reflect a higher amount of depolymerized SiR content leaving the S30 as combustible oligomers, when compared to the other composites. Figure 5.3 shows the DTA performed for the prepared SiR composites under air atmosphere. An exothermic hump is observed for all composites indicating the combustion of volatile oligomers produced during depolymerization. The area under the hump represents the amount of enthalpy change during the TGA run, indicating the relative amount by which each composite combusts during depolymerization. As can be evidently seen in Figure 5.3, the area under S25s5 curve is the smallest compared to the other composites indicating the lowest levels of combustion exhibited by the composite during TGA.

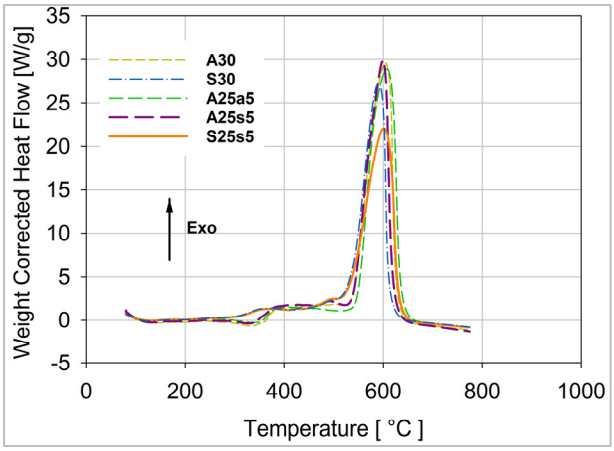

Figure 5.3 DTA for the prepared composites in air, O_2, atmosphere.

The exothermic peaks in Figure 5.3 show comparable combustion levels with S30, A30, A25a5. These comparable combustions levels were obtained, despite a much higher depolymerized content fueling combustion as determined in Table 5.3 with S30. This finding primarily indicates that the additional residue in the ATH filled composites did not inhibit combustion to a similar extent in the ATH-free composites. Rather the level of combustion seems to have been adversely effected with ATH added to the composite. Ghunem et al. in (Ghunem, Koné et al. 2020) illustrated the effect of ATH dehydration in filled SiR composites on the residue structure porosity and roughness. The porosity of the residue structure impacted oxygen diffusion and the consequent level of combustion in the composites under DTA. The weakness of such residue may diminish the possibility of creating a barrier effect for shielding the material during DBA. Thus, despite the additional residues obtained for A30, A25a5 and A25s5, the residue structure integrity would still need to be verified in order to prevent combustion failure.

5.3.2 DC IPT Test Outcomes

Figure 5.4 and Figure 5.5 show the +DC IPT outcomes for the composites of the study. As can be depicted in the post-tested sample images shown in Figure 5.4, a variation can be observed within the composites in the extent of damage caused by erosion under DC DBA. Figure 5.5 illustrates the erosion depth and eroded volume quantities measured for the composites of the study.

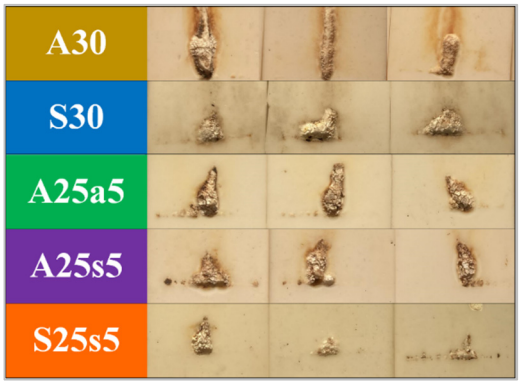

Figure 5.4 Images for the post-tested +DC IPT specimen samples

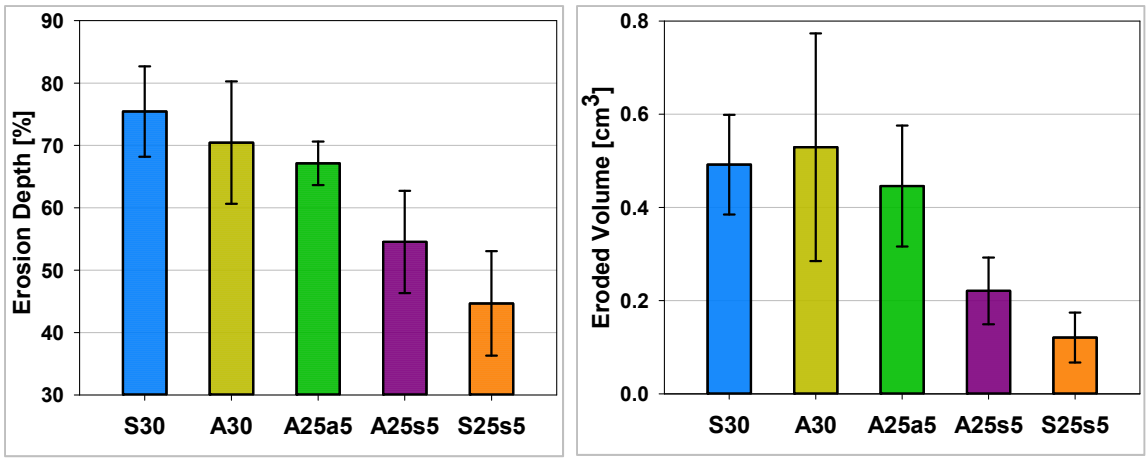

(a) (b)

Figure 5.5 (a) Erosion depth measurements for the tested composites as percentage of original sample thickness, with the average value and measured values within one standard deviation
(b) Eroded volume for the tested composites with the average value and values measured within one standard deviation

The outcomes of Figure 5.5 suggest a superior +DC erosion resistance for the S25s5 composite as compared to the others. It is also important to note that this superior DC erosion resistance was obtained despite S25s5 having the least thermal conductivity measured as shown in Table 5.2. This highlights that thermal conductivity becomes a less important factor to consider in enhancing the DC as compared to the AC erosion resistance of silicone rubber with fillers (Alqudsi, Ghunem et al. 2021). The S30 composite had a much inferior erosion resistance as

compared to S25s5 which clearly illustrates the effectiveness in supplementing ground silica with fumed silica to suppress DC erosion. These findings suggest that the synergistic role shown in TGA-DTA for the supplementary fumed silica, added to the micro silica in promoting a crosslinked residue barrier, is important to suppress the progression of erosion during the DC IPT.

The A30 and A25a5 were also among the composites with the worst erosion resistance outcomes under the +DC IPT, despite having the highest measured thermal conductivities. Figure 5.3 did indicate the highest combustion observed during depolymerization for these composites under air atmosphere. The A25s5 composite containing fumed silica seems to have a relatively better erosion resistance compared to S30, A30 and A25a5. In addition, the S25s5 surpasses all the composites in terms of the erosion resistance obtained and showed least amount of combustion in the DTA shown in Figure 5.3. These findings highlight the role of the fumed silica in constraining the mobility of the siloxane chains, which suppressed depolymerization and promoted crosslinking in the composite. These findings also emphasize on the synergistic effect in adding the fumed silica to ground silica in prompting a better shield in retarding combustion and thus improving the erosion resistance of SiR.

5.3.3 The Dry-Arc Resistance Test Outcomes

Figure 5.6 shows the 3D surface topography obtained for the tested composites under the dry-arc resistance test. The generated topography shows a variation amongst the composites in terms of the coherency and roughness of surfaces. A clear difference can be seen between the S25s5 composite surface as compared to all the other composites. The produced surface residue seems to be more intact and coherent as compared to the others. Insignificant difference in the residue morphology can be observed for eroded surfaces obtained for the A30, S30 and A25a5 with the surfaces being highly rough and incoherent. The addition of fumed silica to micro ATH in A25s5 somewhat shaped the residue towards a more coherent structure, but not as was synergistically obtained when fumed silica was added to ground silica in silicone rubber.

Ranking the order of the tested composites in terms of increasing structure coherency would result in having the S25s5 eroded surface being of superior coherency compared to all the other composites, followed by the A25s5 surface residue being somewhat more coherent as compared to the remaining composites. This ranking seems to support the correlation suggested between the +DC IPT outcomes reported in Figure 5.5 and the role of the filler barrier effect during the DBA. The coherency in the residue structure defines the filler barrier effect as an incremental mechanism to the volume effect of the filler in hindering progressive erosion in the composites.

This clarity in observing the residue structures was possible as a result of the dry-arc resistance test protocol facilitating obtaining reproducible erosion surface patterns due to a controlled scintillation activity on the surface (Alqudsi, Ghunem et al. 2021). The laser ablation method was utilized as an accelerated testing method for ranking the erosion resistance of SiR composites in (Meyer, Jayaram et al. 2005) and as means to observe the integrity of the produced residue in various insulating materials (Hosier, Abd Rahman at al. 2013). The dry-arc resistance test, however, utilizes stable scintillations during the test in a manner similar to that of the DC DBA in the IPT, which makes it more practical for the purpose of this study.

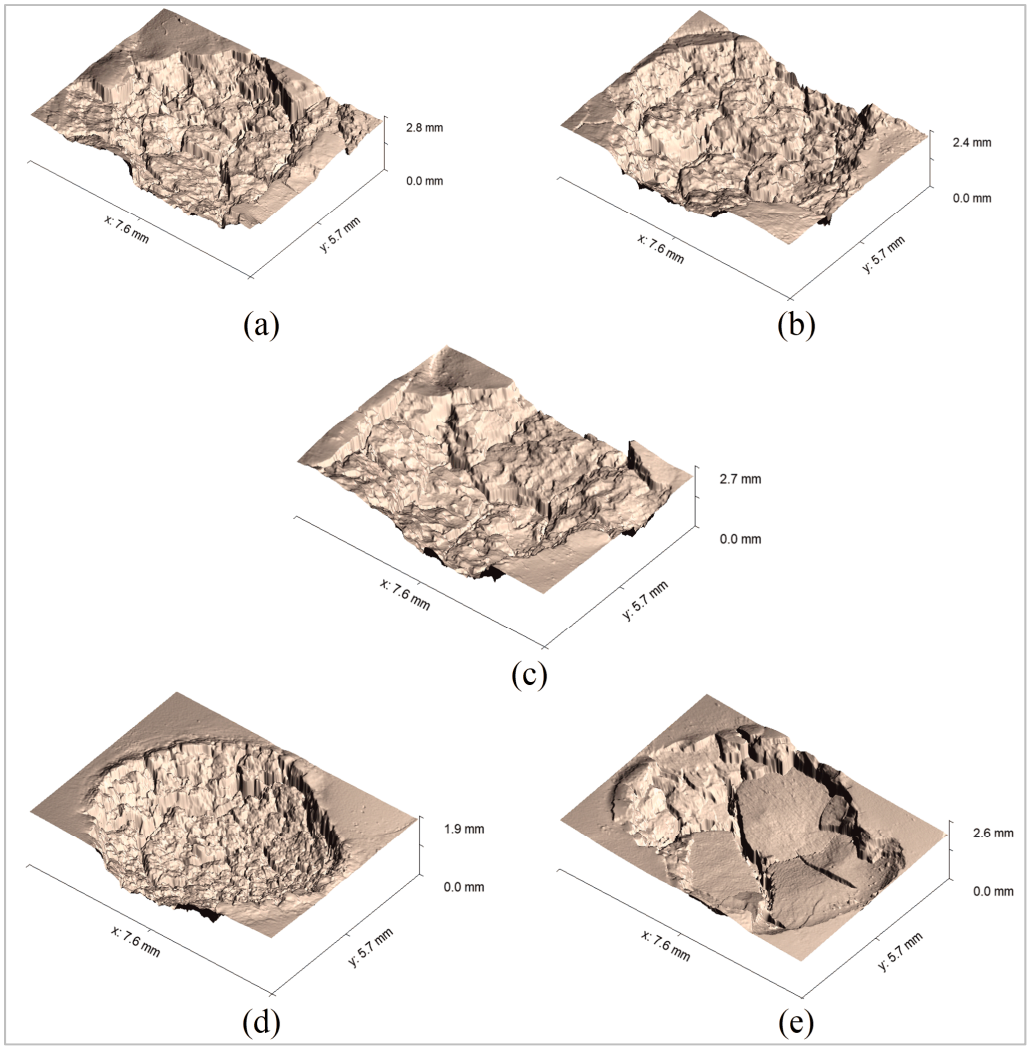

Figure 5.6 3D surface topography for the post-tested samples of (a) A30, (b) A25a5, (c) A25s5, (d) S30, and (e) S25s5 under the dry-arc resistance test

Figure 5.7 shows the SEM images obtained for the eroded surfaces of the composites under the +DC IPT and dry-arc resistance test. The images for a given composite under both tests correlate in terms of the surface roughness and coherency. This validates the approach proposed in this study in using the dry-arc resistance test as means for accelerating the erosion of the composites in a manner similar to that exhibited in the +DC IPT to observe the residue structure characteristics as was similarly done in (Alqudsi, Ghunem et al. 2021). The eroded residue obtained for S25s5 under both tests was found to be coherent and nonporous as

compared to the other composites. The eroded surfaces of S30, A30 and A25a5 were found to be much more incoherent and rougher under both tests. The surface of A25s5 was found to have slight improvements in the residue structure and integrity. The residue structure characteristics observed with SEM under both tests support explaining the impact of the residue integrity on the DC erosion resistance of the composites.

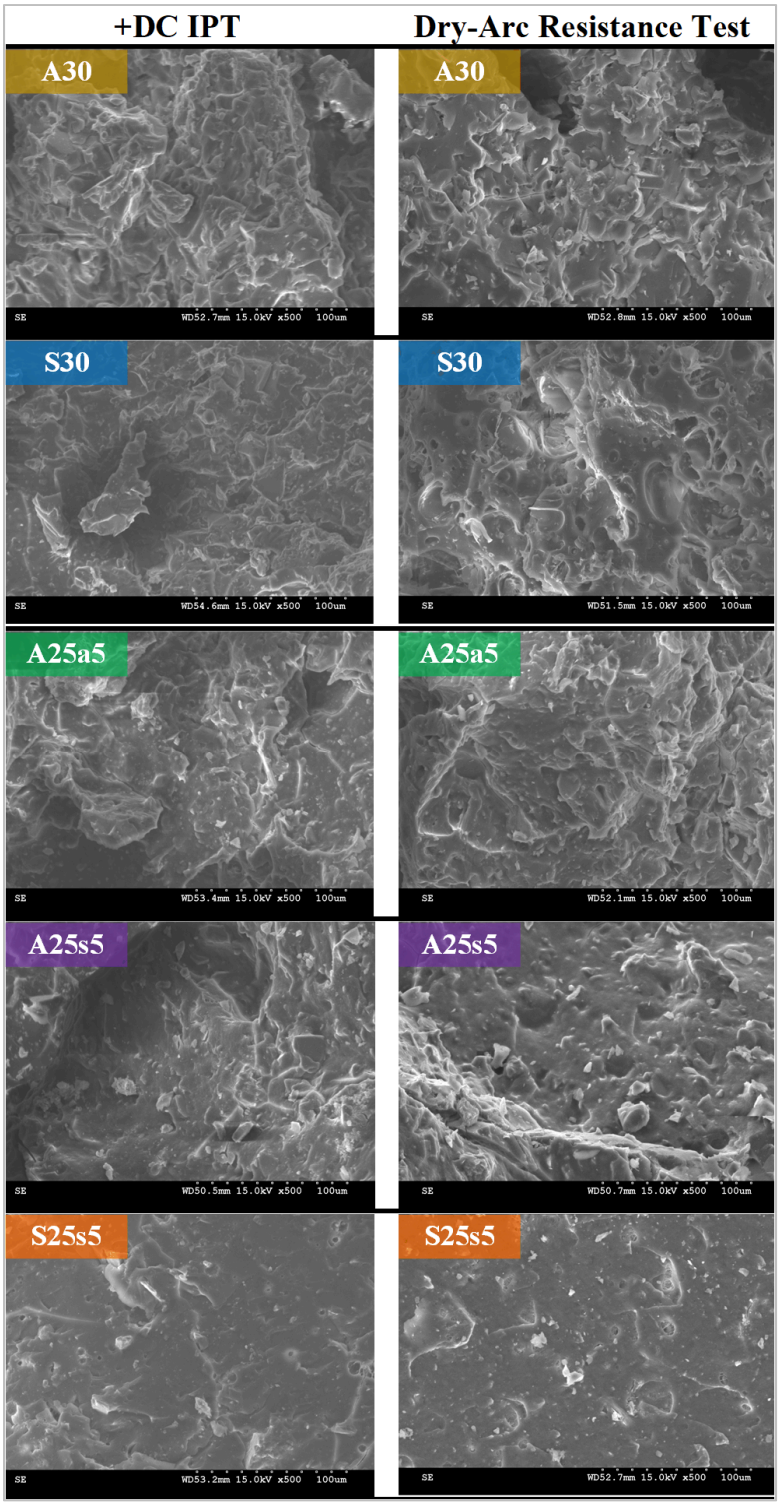

Figure 5.7 SEM imaging for the eroded surfaces under a magnification of x500 for the composites tested under the +DC IPT and dry-arc resistance test

5.4 Conclusion

This paper investigates the viability of the filler barrier effect shielding SiR composites during DC DBA. A testing framework employing the TGA-DTA, the IPT and the dry-arc test is introduced. Outcomes indicate a significant influence for fumed silica in promoting a crosslinked residue during the DBA as compared to nano ATH, which was primarily attributed to the favorable interactions between fumed silica and SiR. In addition, a synergistic effect for adding fumed silica to ground silica in SiR is shown which resulted in a remarkably coherent residue, leading to suppression of combustion and thus an enhanced erosion resistance under DC voltage. Therefore, the barrier effect which is characterized with the coherency and integrity of the residue structure should be an additional important factor to be considered with the volume effect of the filler to design silicone rubber composites for DC outdoor insulation applications. The thermal conductivity on the other hand is not shown to be a governing parameter on the DC erosion resistance of the composites. The dry-arc test is shown as a useful tool simulating the stable DBA and resulting in reproducible erosion outcomes on silicone rubber that correlate with the DC IPT outcomes.

Acknowledgments

The authors gratefully acknowledge the Natural Sciences and Engineering Research of Canada (NSERC) for the financial support. The authors would like to thank to Dr. Souheil-Antoine Tahan, Mr. Simon Laflamme, Dr. Mohammad Saadati and Mr. Joel Grignon for providing the technical help needed for the microscopic work in this paper.

CHAPTER 6

RANKING THE DC EROSION RESISTANCE OF SILICONE RUBBER COMPOSITES WITH THE DRY-ARC RESISTANCE TEST[1]

Abstract

This study investigates the use of the dry-arc resistance test for ranking the DC erosion resistance of silicone rubber composites. The study utilizes the test as a controllable testing method for accelerating the erosion of silicone rubber surfaces by creating heat ablation with a stable scintillation. Alumina trihydrate is filled in silicone rubber at different levels and tested using the dry-arc resistance test and outcomes are correlated with the outcomes of the +DC inclined plane tracking-erosion test. Comparatively ranking the erosion depth and eroded volume outcomes for both tests preliminarily indicates a direct correlation in the ranking order observed for the composites under both tests. Outcomes of thermogravimetric and differential thermal analyses suggest the ranking is correlated with the amount of depolymerized silicone rubber leaving the composite in the gaseous phase. Ranking the thermal analyses outcomes on the basis of the depolymerized silicone rubber content correlates with the DC erosion resistance outcomes under the dry-arc resistance test and the inclined plane test. The outcomes collectively signify the validity of using the dry-arc resistance test for ranking the DC erosion resistance of silicone rubber composites.

6.1 Introduction

Silicones are preferably utilized as housing materials in polymeric outdoor insulators due to their hydrophobic property. In areas of severe pollution, silicone rubber's (SiR) hydrophobicity is temporarily lost resulting in the surface being prone to erosion under dry-DBA. The arcs become increasingly severe under the DC voltage as compared to AC voltages (Heger, Vermeulen 2010). This conclusion stresses the use of a testing method that can

[1]The contents of this chapter are submitted for IEEE Conference on Electrical Insulation and Dielectric Phenomena 2021

adequately asses and rank the DC erosion resistance of SiR composites for outdoor service installation. The liquid-contaminant inclined-plane tracking and erosion test (IPT) set in the ASTM D2303 (ASTM 2013) or IEC 60585 (IEC 2007) standards ranks the tracking and erosion performance of the composites under AC voltage. The early form of the test in the 1960s primarily tested for tracking in polymeric insulating materials (Mathes, Mcgowan 1961). The importance to specify a test method for erosion was discussed later in (Mathes, Mcgowan 1961) with the constant voltage method being adapted in its current form to test for erosion in (ASTM 2013). SiR is track-resistant as it leaves a small amount of carbonaceous residue during the IPT which has been found to be less than 1wt% (percent by weight) (Kumagai, Wang et al. 1998). A widely accepted industry practice has been adapted to test for erosion resistance of SiR formulations under the constant 4.5 kV inclined plane voltage, i.e the critical voltage (Krivda, Schmidt et al. 2009). Though the test provides an erosion testing method, yet it doesn't present a clear assessment parameter for failure under erosion as it does with tracking.

Current research revolves around developing the basis for standardizing the IPT for DC voltage (Cherney, Gorur et al. 2015). The erosion resistance in the standard IPT is often determined on the basis of leakage current (LC) measurements or length of progressive erosion on the surface without presenting a clear definition of a failure criterion for the amount of erosion depth, mass, volume or any additional outcomes. Investigating the characteristics of the SiR residue, for example, and other erosion-produced outcomes could introduce a number of parameters that could be integrated into a standardized testing method for the DC erosion resistance of SiR. For instance, it was shown that the coherent residue produced in alumina-trihydrate (ATH) filled SiR in could shield the bulk SiR material from progressive erosion and improve the DC erosion resistance of SiR (Ghunem, Koné et al. 2020). A laser-based technique was developed in (Meyer, Jayaram et al. 2005) which was later used in (Ramirez, Cherney el al. 2012) to highlight the role of the residue shield in SiR. Still, however, additional investigation is needed preferably in a way that utilizes actual scintillations during the test in a standard method. Also, more work on improving the variance of measurement outcomes of the IPT as a test for erosion is needed as this test has been primarily developed and verified as a test for tracking. Increasing the number of samples to be more than five has been shown a useful strategy to improve the statistical significance of the erosion resistance determined under the

AC voltages (Ansorge, Schmuck et al. 2012). However, it could be more useful to seek the use of additional tests specifically when testing for DC, given the limited experience available about evaluating the erosion resistance under DC as compared to AC.

The dry-arc resistance test set in the ASTM D495 standard (ASTM 2014) was employed primarily in its early form as an accelerated testing method for determining the tracking resistance of polymers (Sommerman 1960). The test enables stimulating low current arcs of controllable magnitude and discharge duration under dry testing conditions. The test can be utilized as a controlled heat source for accelerating the formation of eroded residues on SiR. This paper investigates the validity of using the dry-arc resistance test as a supplementary testing method with the IPT for determining the DC erosion resistance of SiR composites. The study investigates the correlations between the testing methods in ranking the erosion resistance outcomes of ATH filled SiR composites. Validating the use of the dry-arc resistance test to assess the DC erosion resistance would enable the analysis the factors governing the erosion under DC at a more controlled and accelerated pace as compared to the standard IPT.

6.2 Materials and Methods

Table 6.1 shows the composites utilized for the study, with five specimens from composite being used in the study accordingly. The composites include room temperature vulcanized (RTV) and ATH filled SiR composites, prepared in the laboratory, and commercial high temperature vulcanized (HTV) and ATH filled SiR. A two part RTV SiR from Momentive, RTV 615, was used in preparing the ATH05, ATH30 and ATH50 composites. A high shear mixer was utilized for dispersing the filler particles into the silicone rubber base and adding the crosslinking agent at a later stage. Details on the procedure followed for preparing the composites can be found in (Alqudsi, Ghunem et al. 2021). Different ATH fillers with different filler loadings have been used in the composites to diversify all possible erosion resistance outcomes under all tests. These outcomes will be investigated in order to validate the presented approach of the study.

Table 6.1 Composite samples and associated filler properties

Inorganic Filler	Filler Type	Type of SiR	Filler Particle Size (µm)	Filler wt% in samples prepared
ATH05	Alumina Trihydrate	RTV	1×10^{-3}	5
ATH30			< 45 [a]	30
ATH50			1	50
ATH60		HTV	NP[b]	60

[a]Median particle size not specified. [b]Information not provided.

Figure 6.1 shows the +DC IPT and dry-arc resistance test setups used for this study. The positive voltage polarity, at +3.5 kV, was selected for this study as an equivalent to the critical ACrms 4.5 kV (Ghunem, Jayaram et al. 2013) and it has resulted in the formation of the most severe dry-band arcing (DBA) leading to deep erosion (Heger, Vermeulen 2010). Details of the testing procedure and parameters are explained in details in (Alqudsi, Ghunem et al. 2021). The dry-arc resistance test was set up following the ASTM D 495 standard (ASTM 2014) for testing composite materials under high voltage-low current arcs. As shown in Figure 6.1, tungsten electrodes in the dry-arc test are placed at a 30° slope on the composite sample surface whilst being spaced at 6.35 mm. The composite is subjected to a 6.1 kV AC-10mA current as per the 4 minute current steps-based schedule shown in Figure 6.1. The governing difference between AC and DC DBA comes down to a more stable DBA, i.e more energy or heat imposed on the tested surface (ASTM 2014). The dry-arc resistance test by definition employs different current steps with a stepwise protocol (ASTM 2014). The first four steps involve a stepwise increase in the scintillation duration, i.e reduction in the degree of intermittency, until eventually reaching an eroding stable arc is achieved in the fourth step. Therefore, the application of a DC source is not necessary as the AC voltage in the dry-arc resistance test protocol allows a stable DBA to be produced. The eroding stable arc was obtained within 4 current steps (CS) and therefore, for this study, only four CSs (CS1 to CS4) are used instead of the seven steps outlined in (ASTM 2014).

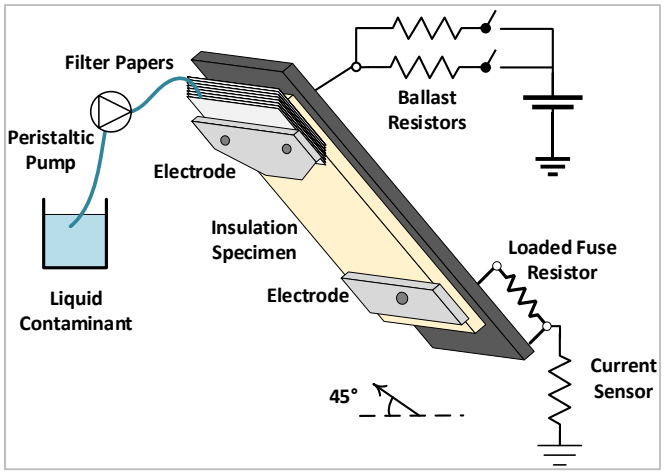

(a)

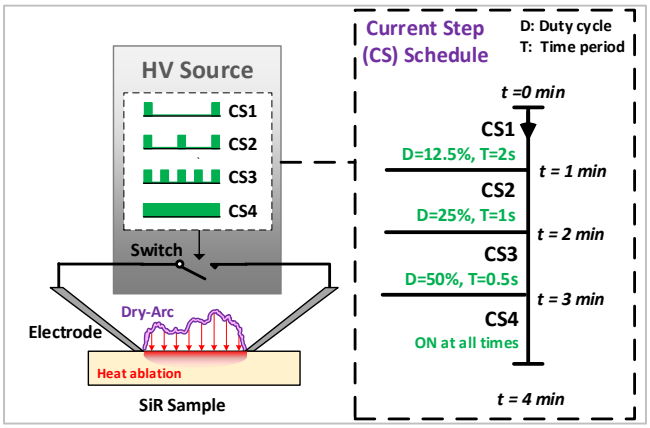

(b)

Figure 6.1 Overall (a) DC Inclined plane tracking and erosion test and (b) dry-arc resistance test setups used in the study

The erosion depth for the tested composites under all tests is determined using a digital Mitutoyo® 571-200 micrometer with a total accuracy of 0.1 mm. The eroded volume was determined by filling the eroded pit with a clay material of known density. The volume occupied by the clay was calculated using the mass of clay used and the density value.

Thermal analyses of the composites were conducted using thermogravimetric and differential thermal analyses (TGA-DTA) under air and nitrogen (N_2) atmospheres with a heating rate of 25 °C/min at a temperature span of 80-800 °C.

6.3 Results and Discussion

6.3.1 +DC IPT and Dry-Arc Resistance Test

Figure 6.2 displays images for the post-tested composites from the +DC IPT and dry-arc resistance test, while Figure 6.3 illustrates the acquired measurements for the erosion depth and eroded volume for composites of this study under both tests. The outcomes of the +DC IPT in terms of erosion depth and eroded volume suggest a superior erosion resistance for the ATH60 SiR composite followed by ATH50, ATH30 and then ATH05. Increasing the ATH loading level improves the erosion resistance of SiR as a result of increasing the filler content replacing the depolymerizable SiR material (Ghunem, Koné et al. 2020). Further increasing the ATH level in the filler to 50 and 60wt% significantly improves the outcomes of the IPT and the dry-arc resistance test. Kumagai et al explained that a filler loading of at least 40wt% of ATH is required for delaying the inception of deep erosion in SiR, as an internal oxidation between the released water of hydration and the dimethyl groups of silicone rubber dilutes the gas phase and thus the DBA plasma (Kumagai, Yoshimura 2001).

Under both tests, a variation can be observed amongst all four composites in terms of the damaged area which facilitates ranking the erosion resistance of the composites for the study. Moreover, the results obtained for the erosion depth and eroded volume under the IPT go in line with those obtained using the dry-arc resistance test for all the four composites.

Collectively, the outcomes and observations of Figure 6.2 and Figure 6.3 preliminary suggest an existing correlation between the outcomes of both tests. That is, the results correlate in terms of the ranking order of erosion depth and eroded volume for the composites under both tests. Despite the difference in the testing methods followed between the tests, the dry-arc resistance test is capable of generating a controlled heat ablation source mimicking that of DC DBA in the IPT. The erosion in SiR under both tests is initiated as a result of the heat impinged by the

ignited arc. Accordingly, the characteristics of the residue formed during this heat ablation process will be the same regardless of the test being conducted as the composite material being tested is the same. The residue formed during erosion could play a vital role in preventing progressive erosion depending on its strength and integrity as was reported in (Ghunem, Koné et al. 2020). A coherent residue could have a barrier effect on shielding the bulk SiR material against the influx of heat which could inhibit further combustion of the material. In (Ghunem, Koné et al. 2020), the effect of the residue characteristics on the SiR erosion was found to be more influential under DC testing compared to AC. This is a result of the increased severity of the DBA in DC which could be suppressed with a strong and coherent residue. These observations could collectively support the erosion resistance outcomes of the study which in turn would validate the use of the dry-arc resistance test as a method to rank the DC erosion resistance of SiR composites.

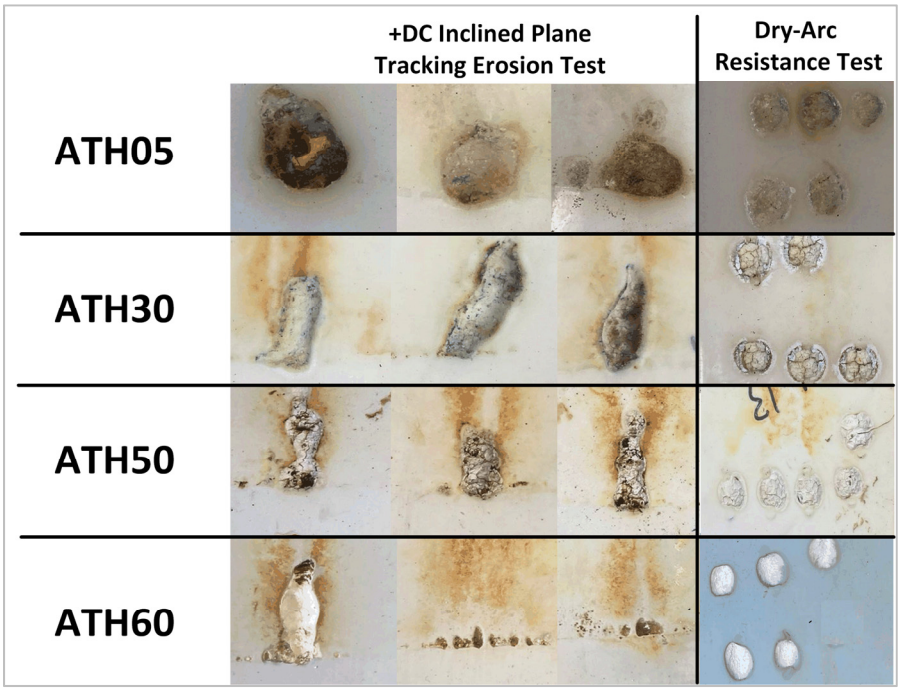

Figure 6.2 Images of the post-dry arc resistance tested composites showing the eroded pits of the samples

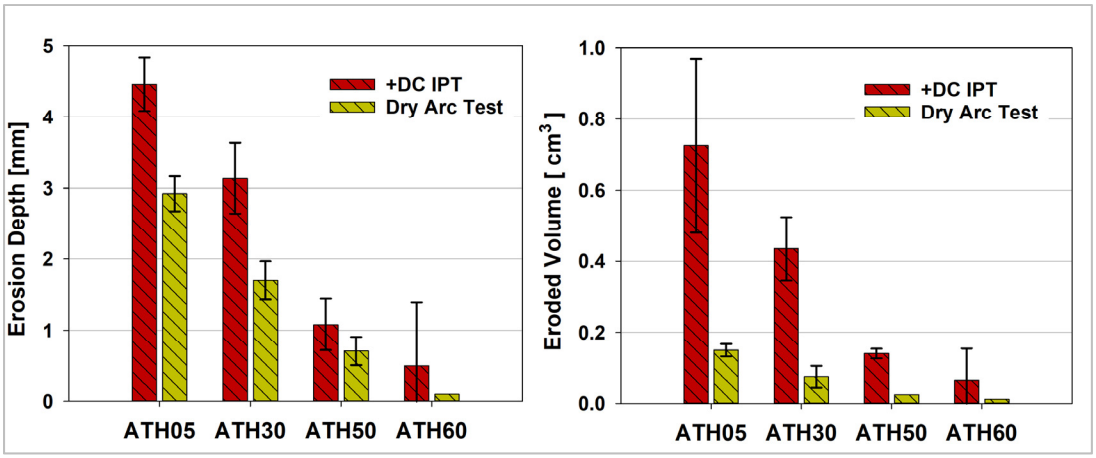

(a) (b)

Figure 6.3 Eroded (a) depth and (b) volume measurements for the composites of the study under the +DC IPT and dry-arc resistance test

6.3.2 Thermal Analysis Outcomes

Figure 6.4 shows the TGA and DTA outcomes obtained for the composites under N_2 and O_2 atmospheres respectively. With high ATH filler loadings, a two step weight decomposition could be observed in TGA with the first step representing the dehydration of the ATH filler, and the subsequent representing the depolymerization of SiR. Detailed analysis of the decomposition mechanisms in ATH filled SiR composites under TGA can be found in (Alqudsi, Ghunem et al. 2021).

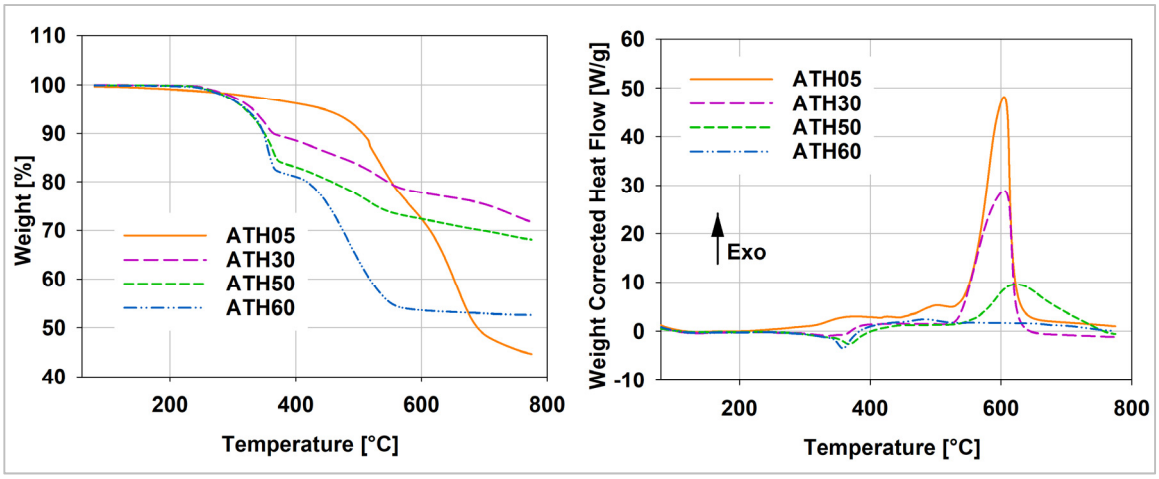

(a) (b)

Figure 6.4 Outcomes for (a) TGA under N_2 and (b) DTA under O_2 atmospheres for the composites of the study

Due to the different filler loadings between the composites, considering the final remnant TGA residue weight (W_{TGA}) as the comparison parameter for assessing the thermal performance of the composites could be misleading. Using W_{TGA} by itself would undermine the amount of depolymerized SiR content leaving the material in the gaseous phase (W_{dep}). Calculating W_{dep} and using it as the comparison parameter instead will be more meaningful as volume effect is the governing factor of erosion resistance of the composites under study with different filler levels. Obtaining the value of W_{dep} would require calculating the assumed residue, W_{assu}, which represents the theoretical remaining residue for the composite accounting for filler and polymer amount only. Accordingly, W_{assu} is calculated using (6.1)

$$(0.65\ W_{ATH}) + (\alpha W_{SiR}) = W_{assu} \tag{6.1}$$

where W_{ATH} and W_{SiR} are the weights of the ATH filler and SiR in the composite. The scale factor 0.65 is used for correcting the amount of ATH filler weight remaining in the composite as alumina after dehydrating the 35wt% water content. The scale factor α represents the fraction of undepolymerized SiR content that remains as silica residue. This is usually found by conducting the TGA test for unfilled SiR. Based on literature, unfilled HTV SiR depolymerizes completely leaving no residue, i.e. α = 0 (Delebecq, Hamdani-Devarennes et

al. 2011). For RTV SiR prepared in the laboratory, the α value was found to be 0.145 or 14.5wt% for unfilled SiR. The following step would be in calculating W_{add} which is the additional residue obtained experimentally in the TGA run. This parameter accounts for the additional residue formed as a result of the interaction between the SiR polymer and the filler which could includes the radical crosslinking mechanism explained in (Camino, Lomakin et al. 2002). W_{add} is calculated using the difference between the W_{assu} and W_{TGA} which is calculated using (2). Finally, W_{dep} is calculated as the difference between W_{add} and W_{SiR} using (6.3).

$$W_{TGA} - W_{assu} = W_{add} \tag{6.2}$$

$$W_{SiR} - W_{add} = W_{dep} \tag{6.3}$$

Table 6.2 shows the calculated values of W_{assu}, W_{add}, W_{dep} for the composites of this study. W_{TGA} for each composite is found as the final TGA weight value at 800 °C, in Figure 6.4. As per Table 6.2, ATH05 has the highest amount of depolymerized SiR with ATH30, ATH60 and ATH50 being at much lower significant levels. To further illustrate this experimentally, Figure 6.4 shows the DTA performed for the composites under air atmosphere. The exothermic humps observed for all the composites represent the combustion of the cyclic SiR oligomer volatiles released during the depolymerization of SiR. According to Figure 6.4, the highest exotherm was observed for the ATH05 composite followed by ATH30, ATH50 and ATH60. These outcomes are consistent with the Wdep calculations of Table 6.2. Table 6.3 shows the overall outcomes of the study with the ranking order of the performance of each composite with respect to the conducted test. A rank order of 4 represents the poorest performance, while a rank order of 1 represents the best performance. The thermal analyses outcomes of the study correlate with those of the +DC IPT and dry-arc resistance test. The variation in the rank order between the ATH50 and ATH60 amongst the three testing categories reflects the comparable outcomes of these composites under all three tests. This overall correlation in the ranking order of the outcomes suggests the validity of using the dry-arc resistance test as a testing method aiding the +DC IPT for ranking the DC erosion performance of the composites.

Table 6.2 Calculation of the composites' depolymerized SiR under TGA

Composite	Component weights		α	W_{assu}	W_{TGA}	W_{add}	W_{dep}
	W_{ATH}	W_{SiR}					
	[%]						
ATH05	5	95	0.145	17.0	44.5	27.5	67.5
ATH30	30	70		29.7	71.3	41.7	28.4
ATH50	50	50		39.8	68	28.3	21.8
ATH60	60	40	0	39.0	52.6	13.6	26.4

Table 6.3 Ranking the outcomes for the composites of the study

Composite	Rank for erosion resistance as per +DC IPT	Rank as per W_{dep} in the TGA outcomes	Rank for erosion resistance as per dry-arc test
ATH05	4	4	4
ATH30	3	3	3
ATH50	2	1	2
ATH60	1	2	1

6.4 Conclusion

The presented study examined the use of the dry-arc resistance test as an accelerated method for ranking the DC erosion resistance of SiR composites. The introduced approach employs the test in generating low current arcs resembling the DC DBA in terms of the heat ablation effect it imposes on SiR. The ranking order obtained under the dry-arc resistance test and the +DC IPT match in terms of the eroded depth and volume. This ranking was further supported by the outcomes of TGA-DTA in indicating the amount of depolymerized SiR leaving the composite as volatiles. Further investigation into the outcomes could validate the proposed approach in using the dry-arc resistance test in ranking the DC erosion resistance of SiR composites.

CONCLUSION

This thesis presented a mechanistic-based framework for analyzing the effect of nano-sized inorganic fillers on the erosion resistance of SiR composites for HVDC outdoor insulation applications. The studies illustrated throughout the chapters of the thesis fulfilled the objectives outlined in the introductory chapter in terms of understanding the effects of different nano filler attributes on enhancing the DC erosion resistance of SiR. The concluding remarks are summarized as follows:

The role of the nano filler interface in SiR

Different types of fillers have been filled in RTV SiR which are namely nano-sized fumed silica, nano ATH and sub-micron hexagonal BN fillers. The DC IPT outcomes show a superior erosion resistance for the fumed silica filled composite as compared to the other composites. Upon using the thermal analyses tools of the study, fumed silica was found to have a significant role in suppressing SiR depolymerization and promoting radical-based crosslinking which was not similarly observed with the other fillers. Moreover, the enhancement in the thermal conductivity as a result of incorporating inorganic fillers was not the governing factor in improving the DC erosion resistance of SiR. This was evident with the higher thermal conductivity measurements obtained for BN filled composites, at 5wt% and 10wt%, which had an inferior erosion resistance compared to the fumed silica filled composite filled at 5wt%. The dehydration mechanism associated with the use of nano ATH at 5wt% was shown to have no evident effect on improving the erosion resistance of SiR as compared fumed silica filled SiR at the same loading level. The LC measurements acquired during the DC IPT were analyzed in the presented statistical boxplot approach to examine the DC DBA mechanism throughout the test. The boxplots indicate slowest rate for the inception of the stable eroding DBA stage with fumed silica. These outcomes collectively suggest that the interactive filler interface of fumed silica with SiR was the decisive factor in suppressing the DC erosion resistance during the IPT and not the improvement in the composite's thermal conductivity. This leads to the

key conclusion that the favorability of interaction of the filler interface with SiR can be an important factor to be considered on choosing the nano filler type in SiR for HVDC insulation.

Reducing the silica filler size to the nanometric range

Based on the earlier study, it was established that the silica favorably interacts with SiR to improve its erosion resistance under DC voltage. Accordingly, micron-size ground silica and nano-sized fumed silica were filled in SiR to shed the light on the effect of reducing the size of silica to the nanometric range and investigate the impact it has on the residue shield effect during DBA. Based on the DC IPT, it was concluded that fumed silica and its interaction with SiR were effective in enhancing the DC erosion resistance of SiR to a comparable level with that of ground silica filled SiR. Thermal analyses outcomes indicate an evident role for fumed silica in suppressing SiR depolymerization and promoting radical-based crosslinking to a higher extent than ground silica. Similar to the earlier study, the role of the filler interface in tethering the siloxane chains contributed towards a more pronounced effect on suppressing DC erosion compared to silica in the micron size range. Moreover, the formation of a much higher additional residue with the fumed silica filled composite under TGA despite being filled at one sixth the loading level of ground silica filled SiR is a further indication of a better suppression of depolymerization with the former. SEM and optical microscopy highlighted a significant finding towards the role of fumed silica in the residue shield effect suppressing DC erosion. Based on observations of the residue characteristics of the eroded pits under the DC IPT and the dry-arc resistance test, fumed silica seemed to have promoted the formation of a coherent residue which introduces an effective shield against progressive erosion under sustained DBA. Thus the study highlights the impact of reducing the favorably interactive filler into the nanometric range by illustrating the effect it has on introducing the shield effect during DBA.

Supplementing base fillers with nano filler additives

Practical formulations of SiR that are utilized in industry would require high loading levels of the inorganic filler. Accordingly, the study presented in this thesis investigated nano fillers in silicone rubber outdoor insulation composites as additives to improve the DC erosion resistance. The study examined the viability of the filler barrier effect in shielding practical

formulations of SiR composites during DC DBA. The prepared SiR composites contained filler weight fractions of a total of 30wt% which would have contained either the base filler by itself or the base filler with a supplemented nano filler. The base fillers were chosen to be micron-sized ATH or ground silica, while the nano fillers where chosen to be fumed silica or nano ATH. The primary conclusion from the study was to highlight the synergistic effect for adding fumed silica to ground silica in SiR to create a coherent residue thereby introducing the barrier effect during DC DBA. This effectively leads to the suppression of combustion and enhancing the erosion resistance of SiR under DC voltage. SEM and optical microscopy were used to highlight the distinction in the residue characteristics between the fumed silica-ground silica SiR composite and the other composites in terms of the coherency and porosity levels. Therefore, the barrier effect which is characterized with the coherency and integrity of the residue structure should be an additional important factor to be considered with the volume effect of the filler to design effective SiR composites for DC outdoor insulation applications.

Dry-arc resistance test as a supplementary testing method to the DC IPT

The presented study introduced the dry-arc resistance test as a supporting test tool that could aid the DC IPT towards further investigating the role of inorganic fillers, whether nano or micrometric, in the DC erosion resistance of SiR. The dry-arc test was shown to be a very a useful tool to investigate the role of the shield effect in the suppression of stable dry-band arcing. Different ATH filled SiR composites with different filler sizes and loading levels were examined in order to versify the outcomes under the DC IPT and the dry-arc resistance test. The ranking order obtained under the dry-arc resistance test and the +DC IPT match in terms of the eroded depth and volume. This ranking was further supported by the outcomes of thermal analyses in indicating the amount of depolymerized SiR leaving the composite as volatiles.

RECOMMENDATIONS AND FUTURE WORK

The thesis established a number of findings that would require further investigation and analysis. Based on the framework presented in this research a number of potential studies could supplement the work which include:

1. Investigating the barrier effect introduced by inorganic fillers: This study only explored the use of fumed silica as being an interactive filler that favourably bonds with the siloxane chains of SiR. Future continuation of this work could be done with exploring other fillers that have similar favourability in interacting with SiR. For example, Polyhedral Oligomeric Silsesquioxanes or POSS is a hybrid material of high thermal conductivity that can be utilized for high voltage insulation materials. POSS has an inorganic silica-like core which is surrounded by side groups the react differently with different resin polymers. If the side groups are highly compatible with SiR, POSS could effectively introduce a barrier effect similar to that observed with fumed silica which would further highlight the impact of the barrier effect on the DC erosion resistance of SiR. The success of using POSS in high voltage insulation was indicated in works such as that of Heid et al. in (Heid, Fréchette et al. 2015) in which POSS was used in epoxy resin.
2. Investigating the barrier effect of supplementing nano fillers to higher filler loadings of base fillers: The practical formulations of SiR used in industry would require 60wt% of the inorganic filler. The limitations of using the high shear mixer in the laboratory would limit the weight fractions of the fillers to 30wt% in SiR. Thus, practical implementation of the findings of this research is feasible subject to further exploring the DC erosion resistance of highly filled SiR composites with supplementary nano fillers.
3. The dry-arc resistance test as a fast assessment method of the DC erosion resistance: The findings presented by the dry-arc test outcomes of this study suggest a significant potential for further investigations of its potential and feasibility. Since only ATH filled SiR were examined and ranked in order of the eroded depth and volume in comparison

with DC IPT outcomes, other SiR composites and materials could be tested and ranked using the dry-arc resistance test to be compared with their counterpart samples tested under the DC IPT. A new guideline or a standard could be structured towards using the dry-arc resistance test as a DC erosion assessment method at an accelerated pace. This could further aid in exploring the role of inorganic fillers in introducing erosion suppression mechanisms during DC DBA.

LIST OF BIBLIOGRAPHICAL REFERENCES

Akbar, M. & Basharat, M. (2020). Global experience of HVDC composite insulators in outdoor and indoor environment. *Reviews on Advanced Materials Science, 59*(1), 606-618.

Alqudsi, A. Y., Ghunem, R. A. & David, E. (2021). A Novel Framework to Study the Role of Ground and Fumed Silica Fillers in Suppressing DC Erosion of Silicone Rubber Outdoor Insulation. *Energies, 14*(12), 3449.

Alqudsi, A. Y., Ghunem, R. A. & David, E. (2021). Analyzing the Role of Filler Interface on the Erosion Performance of Filled RTV Silicone Rubber under DC Dry-band Arcing. *IEEE Transactions on Dielectrics and Electrical Insulation, 28*(3), 788-796.

Ansorge, S., Schmuck, F. & Papailiou, K. O. (2012). Improved silicone rubbers for the use as housing material in composite insulators. *IEEE Transactions on Dielectrics and Electrical Insulation, 19*(1), 209-217.

ASTM International. (2005). *Standard Practice for Rubber and Rubber Latices-Nomenclature*. ASTM D1418-05. West Conshohocken, PA: ASTM International.

ASTM International. (2013). *Standard Test Methods for Liquid-Contaminant, Inclined-Plane Tracking and Erosion of Insulating Materials*. ASTM D2303-13. West Conshohocken, PA: ASTM International.

ASTM International. (2014). *Standard Test Method for High-Voltage, Low-Current, Dry Arc Resistance of Solid Electrical Insulation*. ASTM D495-14. West Conshohocken, PA: ASTM International.

ASTM International. (2021). *Standard Test Method for Measurement of Thermal Effusivity of Fabrics Using a Modified Transient Plane Source (MTPS) Instrument*. ASTM D7984-21. West Conshohocken, PA: ASTM International.

Camino, G. , Lomakin, S.M & Lageard, M. (2002). Thermal polydimethylsiloxane degradation. Part 2. The degradation mechanisms. *Polymer, 43*(7), 2011-2015.

Camino, G., Lomakin, S.M, Lazzari, M. (2001). Polydimethylsiloxane thermal degradation Part 1. Kinetic aspects. *Polymer, 42*(6), 2395-2402.

Cherney, E. A. (2013). Nanodielectrics applications-today and tomorrow. *IEEE Electrical Insulation Magazine, 29*(6), 59-65.

Cherney, E. A. , Gorur, R. S., Krivda, A. , Jayaram, S. H. , Rowland, S. M., Li, S. , Marzinotto, M., Ghunem, R. A. & Ramirez, I. (2015). DC inclined-plane tracking and erosion test of insulating materials. *IEEE Transactions on Dielectrics and Electrical Insulation, 22*(1), 211-217.

CIGRE. (2011). *Important Material Properties of RTV Silicone Rubber Insulator Coatings* (Taskforce D1.14, Report No. 478). Retrieved from https://e-cigre.org/publication/ELT_258_6-important-material-properties-of-rtv-silicone-rubber-insulator-coatings

CIGRE. (2015). *Feasibility Study for a DC Tracking and Erosion Test* (Taskforce D1.27, Report No. 611). Retrieved from https://e-cigre.org/publication/611-feasibility-study-for-a-dc-tracking--erosion-test

David, E. & Fréchette, M. (2013). Polymer nanocomposites-major conclusions and achievements reached so far. *IEEE Electrical Insulation Magazine, 29*(6), 29-36.

Delebecq, E. , Hamdani-Devarennes, S. , Raeke, J., Cuesta, J-M. L. & Ganachaud, F. (2011). High Residue Contents Indebted by Platinum and Silica Synergistic Action During the Pyrolysis of Silicone Formulations. *ACS Appl. Mater. Interfaces,3*(3), 869–880.

Deng, H., Hackam, R. & Cherney, E. A. (1995). Role of the size of particles of alumina trihydrate filler on the life of RTV silicone rubber coating. *IEEE Transactions on Power Delivery, 10*(2), 1012-1024.

Du, B. X. & Xu, H. (2014). Effects of thermal conductivity on dc resistance to erosion of silicone rubber/BN nanocomposites. *IEEE Transactions on Dielectrics and Electrical Insulation, 21*(2), 511-518.

Dvornic, P.R. (2000), Thermal Properties of Polysiloxanes. In Jones, R.G., Ando, W., Chojnowski, J. (Eds). *Silicon-Containing Polymers.* (pp. 185-212) . Dordrecht: Springer.

El-Hag, A. H., Simon, L. C. , Jayaram, S. H. & Cherney, E. A. (2006). Erosion resistance of nano-filled silicone rubber. *IEEE Transactions on Dielectrics and Electrical Insulation, 13*(1), 122-128.

Fleeman, J. A., Gutman, R., Heyeck, M., Bahrman, M., Normark, B. (2009). EHV AC and HVDC transmission working together to integrate renewable power. *2009 CIGRE/IEEE PES Joint Symposium Integration of Wide-Scale Renewable Resources Into the Power Delivery System*, 1-1.

Frechette, M. F. & Reed, C. W. (2006). The emerging field of nanodielectrics an annotated appreciation. *Conference Record of the 2006 IEEE International Symposium on Electrical Insulation*, 458-465.

Gao, L., Yang, X., Hu, J., He, J. (2016). ZnO microvaristors doped polymer composites with electrical field dependent nonlinear conductive and dielectric characteristics. Materials Letters, 171, 1–4.

General Electric. (2016). *High Voltage Direct Current Systems* (Technical Brochure). Retrieved from https://resources.gegridsolutions.com/hvdc/hvdc-systems-brochure

Ghunem, R. A., Koné, D., Cissé, L., Hadjadj, Y., Parks, H. & Ambroise, D. (2020). Effect of hydrated fillers in silicone rubber composites during AC and DC dry-band arcing. *IEEE Transactions on Dielectrics and Electrical Insulation, 27*(1), 249-256.

Ghunem, R. A., Jayaram, S. H. & Cherney, E. A. (2012). Statistical indicators of silicone rubber erosion in the DC inclined plane test. 2012 *Annual Report Conference on Electrical Insulation and Dielectric Phenomena, Montreal, QC, 2012*, 737-740.

Ghunem, R. A., Jayaram, S. H. & Cherney, E. A. (2013). Erosion of silicone rubber composites in the AC and DC inclined plane tests. *IEEE Transactions on Dielectrics and Electrical Insulation, 20*(1), 229-236.

Ghunem, R. A., Jayaram, S. H. & Cherney, E. A. (2014). Investigation into the eroding dry-band arcing of filled silicone rubber under DC using wavelet-based multiresolution analysis. *IEEE Transactions on Dielectrics and Electrical Insulation, 21*(2), 713-720.

Ghunem, R. A., Jayaram, S. H. & Cherney, E. A. (2015). Suppression of silicone rubber erosion by alumina trihydrate and silica fillers from dry-band arcing under DC. *IEEE Transactions on Dielectrics and Electrical Insulation, 22*(1), 14-20.

Gorur, R. S., Karady, G. G., Jagota, A., Shah, M. & Yates, A. M. (1992). Aging in silicone rubber used for outdoor insulation. *IEEE Transactions on Power Delivery,7*(2), 525-538.

Gorus, R. S., Cherney, E. A. & Hackam, R. (1988). The AC and DC performance of polymeric insulating materials under accelerated aging in a fog chamber. *IEEE Transactions on Power Delivery, 3*(4), 1892-1902.

Gorus, R. S., Cherney, E. A. & Burnham, J. T. (1999). Introduction to Outdoor Insulators, In Gorus, R. S., Cherney, E. A. & Burnham, J. T. (Eds) *Outdoor Insulators.* (pp. 16-32). Ravi S Gorur Inc.

Guo, Y., Zeng, X.,Lai, X.,Li, H. (2018). Enhancement of tracking and erosion resistance of silicone rubber with platinum/amino-silane by modulation of crosslinking density. *IEEE Transactions on Dielectrics and Electrical Insulation, 25*(2), 741-748.

Gustavsson, T. G., Gubanski, S. M., Hillborg, H., Karlsson, S. & Gedde, U. W. (2001). Aging of silicone rubber under ac or dc voltages in a coastal environment. *IEEE Transactions on Dielectrics and Electrical Insulation, 8*(6), 1029-1039.

Hackam, R. (1998). Outdoor high voltage polymeric insulators. Proceedings of 1998 International Symposium on Electrical Insulating Materials. *1998 Asian International Conference on Dielectrics and Electrical Insulation. 30th Symposium on Electrical Insulating Ma*,1-16.

Hamdani, S. , Longuet, C., Perrin, D. , Lopez-cuesta, J. & Ganachaud, F. (2009). Flame retardancy of silicone-based materials. *Polymer Degradation and Stability, 94*(4), 465-495.

Heger, G. , Vermeulen, H. J., Holtzhausen, J. P. & Vosloo, W. L. (2010). A comparative study of insulator materials exposed to high voltage AC and DC surface discharges. *IEEE Transactions on Dielectrics and Electrical Insulation, 17*(2), 513-520.

Heid, T., Fréchette, M. & David, E. (2015). Epoxy/BN micro- and submicro-composites: dielectric and thermal properties of enhanced materials for high voltage insulation systems. *IEEE Transactions on Dielectrics and Electrical Insulation, 22*(2), 1176-1185.

Heid, T., Fréchette, M. & David, E. (2015). Nanostructured epoxy/POSS composites: enhanced materials for high voltage insulation applications. *IEEE Transactions on Dielectrics and* Electrical Insulation, 22(3), 1594-1604.

Hermansson, A., Hjertberg, T., Sultan, B.-A. (2003). The flame retardant mechanism of polyolefins modified with chalk and silicone elastomer. *Fire Materials, 27*(2), 51-70.

Hosier, I. L., Abd Rahman, M. S., Vaughan, A. S., Krivda, A., Kornmann, X., Schmidt, L. E. (2013). Comparison of laser ablation and inclined plane tracking tests as a means to rank materials for outdoor HV insulators. *IEEE Transactions on Dielectrics and Electrical Insulation, 20*(5), 1808-1819.

Hshieh, F.-Y. (1998). Shielding effects of silica-ash layer on the combustion of silicones and their possible applications on the fire retardancy of organic polymers. *Fire Materials, 1998*(22), 69-76.

Huang, X., Jiang, P. & Tanaka, T. (2011). A review of dielectric polymer composites with high thermal conductivity. *IEEE Electrical Insulation Magazine, 27*(4), 8-16.

Hull, T. R., Witkowski, A., Hollingbery, L. (2011). Fire retardant action of mineral fillers. *Polymer Degradation and Stability, 96*(8), 1462-1469.

International Electrotechnical Commission (IEC). (2007). *Electrical insulating materials used under severe ambient conditions - Test methods for evaluating resistance to tracking and erosion.* IEC 60587 2007-05. Geneva: International Electrotechnical Commission.

Institute of Electrical and Electronics Engineers (IEEE). (2021). *IEEE Guide for DC Inclined Plane Tracking and Erosion Test for Outdoor Insulation Applications*. IEEE Std 2652-2021. Piscataway, NJ: IEEE.

Jeon. Y., Hong, S-K., Kim M. (2019). Effect of Filler Concentration on Tracking Resistance of ATH-Filled Silicone Rubber Nanocomposites. *Energies, 12*(12), 2401.

Kemaloglu, S., Ozkoc, G., Aytac, A. (2010). Properties of thermally conductive micro and nano size boron nitride reinforced silicon rubber composites. *Thermochimica Acta 499*(1-2), 40-47.

Khanum, K. K. & Jayaram, S. (2019). Hybrid Fillers for Thermal Conductivity and Erosion Resistance Enhancements in Silicone Composites. *2019 IEEE Conference on Electrical Insulation and Dielectric Phenomena (CEIDP)*, 101-104.

Khanum, K. K., Ghunem, R. & El-Hag, A. (2020). Thermal Characteristics of Various Silicone Rubber Composites Filled with Silica. *Ann. Conf. Electr. Insul. and Dielect. Phenom. (CEIDP) 2020*, 31-34.

Khanum, K. K., Sharma, A. M., Aldawsari, F., Angammana, C. & Jayaram, S. H. (2020). Influence of Filler-Polymer Interface on Performance of Silicone Nanocomposites. *IEEE Transactions on Industry Applications, 56*(1), 686-692.

Koné, D. , Ghunem, R. A. , Cissé, L. , Hadjadj, Y. & El-Hag, A. H. (2019). Effect of residue formed during the AC and DC dry-band arcing on silicone rubber filled with natural

silica. *IEEE Transactions on Dielectrics and Electrical Insulation, 26*(5), 1620-1626.

Kozako, M., Higashikoji, M., Tominaga, T., Hikita, M., Ueta, G.,Okabe, S.,Tanaka, T.., Fabrication of silicone rubber nanocomposites and quantitative evaluation of dispersion state of nanofillers. *IEEE Transactions on Dielectrics and Electrical Insulation 19*(5), 1760-1767.

Krivda, A., Schmidt, L. E., Kornmann, X. , Ghorbani, H., Ghorbandaeipour, A., Eriksson, M., Hillborg, H., (2009, November/December). Inclined-plane tracking and erosion test according to the IEC 60587 Standard. *IEEE Electrical Insulation Magazine,25*(6), 14-22.

Kuffel, E., Zaengl, W. S. & Kuffel, J. (2000), Design and testing of external insulation, In Kuffel, E., Zaengl, W. S., Kuffel, J. (Eds) *High Voltage Engineering Fundamentals* (2nd Edition). (pp. 509-532). Newnes.

Kumagai, S. & Yoshimura, N. (2001). Tracking and erosion of HTV silicone rubber and suppression mechanism of ATH. I*EEE Transactions on Dielectrics and Electrical Insulation, 8*(2), 203-211.

Kumagai, S. & Yoshimura, N. (2003). Hydrophobic transfer of RTV silicone rubber aged in single and multiple environmental stresses and the behavior of LMW silicone fluid. *IEEE Transactions on Power Delivery, 18*(2), 506-516.

Kumagai, S., Wang, X. & Yoshimura, N. (1998). Solid residue formation of RTV silicone rubber due to dry-band arcing and thermal decomposition. *IEEE Transactions on Dielectrics and Electrical Insulation, 5*(2), 281-289.

Lewis, T. J. (2004). Interfaces are the dominant feature of dielectrics at the nanometric level. *IEEE Transactions on Dielectrics and Electrical Insulation, 11*(5), 739-753.

Liang, X., Li, S., Gao, Y., Su, Z., Zhou, J. (2020, July-August). Improving the outdoor insulation performance of Chinese EHV and UHV AC and DC overhead transmission lines. *IEEE. Electr. Insul. Mag., 36*(4), 7-25.

Loganathan, N., Muniraj , C. & Chandrasekar, S. (2014). Tracking and erosion resistance performance investigation on nano-sized SiO2 filled silicone rubber for outdoor insulation applications. *IEEE Transactions on Dielectrics and Electrical Insulation, 21*(5), 2172-2180.

Mathes, K. N. & McGowan, E.G. (1962). Electrical insulation tracking – a design engineering problem. *Eletrotechnology*, 146-151.

Mathes, K. N. & McGowan, E.J. (1961). Erosion — Inclined plane, liquid contaminant tracking test. *Annual Report 1961 Conference on Electrical Insulation*, 121-124.

Mathes, K. N. & McGowan, E.J. (1961). Surface electrical failure in the presence of contaminants: The inclined-plane liquid-contaminant test. *Trans. of the Amer. Inst. of Electr. Eng., Part I: Comm. and Electron., 80*(3), 281-289.

Mathes, K. N., Sieffert, L. E., Walker, H. P. & Lindsey, R. H. (1949). Methods for Determining the Effect of Contaminants on Electrical Insulation. *Transactions of the American Institute of Electrical Engineers, 68*(1), 113-119.

Meyer L. H., Cherney E. A. & Jayaram S. H. (2004). The role of inorganic fillers in silicone rubber for outdoor insulation alumina tri-hydrate or silica. *IEEE Electrical Insulation Magazine, 20*(4), 13-21.

Meyer, L. H., Jayaram, S. H. & Cherney, E. A. (2005). A novel technique to evaluate the erosion resistance of silicone rubber composites for high voltage outdoor insulation using infrared laser erosion. *IEEE Transactions on Dielectrics and Electrical Insulation, 12*(6), 1201-1208.

Meyer, L., Grishko, V., Jayaram, S., Cherney, E. & Duley, W. W. (2002). Thermal characteristics of silicone rubber filled with ATH and silica under laser heating. *Annual Report Conference on Electrical Insulation and Dielectric Phenomena, Cancun, Quintana Roo, Mexico 2002*, 848-852.

Meyer, L., Jayaram, S., Cherney, E. (2004). Thermal conductivity of filled silicone rubber and its relationship to erosion resistance in the inclined plane test. *IEEE Transactions on Dielectrics and Electrical Insulation, 11*(4), 620-630.

Meyer, L., Omranipour, R., Jayaram, S. & E. Cherney, E. (2002). The effect of ATH and silica on tracking and erosion resistance of silicone rubber compounds for outdoor insulation. *Conference Record of the the 2002 IEEE International Symposium on Electrical Insulation*, 271-274.

Moreno, V. M. & Gorur, R. S. (1999). AC and DC performance of polymeric housing materials for HV outdoor insulators. *IEEE Transactions on Dielectrics and Electrical Insulation,6*(3), 342-350.

Nazir, M. T., Phung, B. T., Hoffman, M. (2016). Performance of silicone rubber composites with SiO2 micro/nano-filler under AC corona discharge. *IEEE Transactions on Dielectrics and Electrical Insulation, 23*(5), 2804-2815.

Nazir, M.T., Phung, B.T., Yu, S., Zhang, Y., Li, S. (2018). Tracking, erosion and thermal distribution of micro-AlN + nano-SiO2 co-filled silicone rubber for high-voltage outdoor insulation. *High Voltage, 2018, 3*(4), 289-294.

Nelson, J.K. (2010), Background, Principles and Promise of Nanodielectrics. In Nelson, J. (Ed.). *Dielectric Polymer Nanocomposites.* (pp. 1-30). Boston, MA: Springer.

Rajini, V. & Udayakumar, K. (2009). Degradation of Silicone Rubber under AC or DC Voltages in Radiation Environment. *IEEE Transactions on Dielectrics and Electrical Insulation, 16*(3), 834-841.

Ramirez I. , Cherney, E. A. & Jarayam, S. (2012). Comparison of the erosion resistance of silicone rubber and EPDM composites filled with micro silica and ATH. *IEEE Transactions on Dielectrics and Electrical Insulation, 19*(1), 218-224.

Ramirez I. , Jarayam, S., Cherney, E. A. , Gauthier, M. & Simon, L. (2009). Erosion resistance and mechanical properties of silicone nanocomposite insulation. *IEEE Transactions on Dielectrics and Electrical Insulation, 16*(1), 52-59.

Ramirez, I., Cherney, E. A., Jayaram, S. & Gauthier, M. (2008). Nanofilled silicone dielectrics prepared with surfactant for outdoor insulation applications. *IEEE Transactions on Dielectrics and Electrical Insulation, 15*(1). 228-235.

Ramirez, I., Jarayam, S. & Cherney, E. A. (2010). Performance of silicone rubber nanocomposites in salt-fog, inclined plane, and laser ablation tests. *IEEE Transactions on Dielectrics and Electrical Insulation, 17*(1), 206-213.

Rothon, R. (2003). Effects of particulate fillers on flame retardant properties of composites. In Rothon, R. (Ed). *Particulate Filled Polymer Composites.* (pp. 263-302). Shrewsbury: Rapra Publishing.

Sommerman, G. M. L. (1960). Electrical Tracking Resistance of Polymers. Trans. of the Amer. Inst. of Electr. Eng., Part III: Powr. *Appar. and Syst., 79*(3), 969-974.

Sun, J., Li, M., Zhang, Z., Xu, T., He, J., Wang, H., Li, G. (2017). Renewable energy transmission by HVDC across the continent: system challenges and opportunities. *CSEE Journal of Power and Energy Systems, 3*(4), 353-364.

Tanaka, T. (2005). Dielectric nanocomposites with insulating properties. *IEEE Transactions on Dielectrics and Electrical Insulation, 12*(5), 914-928.

Tanaka, T. (2010), Interface Properties and Surface Erosion Resistance. In Nelson, J. (Ed.). *Dielectric Polymer Nanocomposites.* (pp. 229-258). Boston, MA: Springer.

Tanaka, T., Montanari, G. C., & Mulhaupt, R. (2004). Polymer nanocomposites as dielectrics and electrical insulation-perspectives for processing technologies,

material characterization and future applications. *IEEE Transactions on Dielectrics and Electrical Insulation, 11*(5), 763-784.

The American Society of Mechanical Engineers (2019). *Surface Texture (Surface Roughness, Waviness, and Lay)*.ASME B46.1 – 2019. New York, NY: ASME.

Timpe, D. (2007). Silicone rubber flame resistance. *Rubber and Plastics News*.

Vas, J. V. , Venkatesulu, B. & Thomas, M. J. (2012). Tracking and erosion of silicone rubber nanocomposites under DC voltages of both polarities. *IEEE Transactions on Dielectrics and Electrical Insulation, 19*(1), 91-98.

Vaillancourt, G. H., Carignan, S. & Jean, C. (1998). Experience with the detection of faulty composite insulators on high-voltage power lines by the electric field measurement method. IEEE Transactions on Power Delivery*, 13*(2), 661-666.

Venkatesulu, B. & Thomas, M. J. (2008). Studies on the Tracking and Erosion Resistance of RTV Silicone Rubber Nanocomposite. *2008 Annual Report Conference on Electrical Insulation and Dielectric Phenomena*, 204-207.

Venkatesulu, B. & Thomas, M. J. (2010). Erosion resistance of alumina-filled silicone rubber nanocomposites. *IEEE Transactions on Dielectrics and Electrical Insulation, 17*(2), 615-624.

Verma, A. R. & Reddy, B. S. (2018). Tracking and erosion resistance of LSR and HTV silicon rubber samples under acid rain conditions. *IEEE Transactions on Dielectrics and Electrical Insulation, 25*(1), 46-52.

Vondráček, P. & Schätz, M. (1977). Bound rubber and "crepe hardening" in silicone rubber. *Journal of Applied Polymer Science, 21*(12), 3211-3222.

Wang, Z., Iizuka, T., Kozako, M., Ohki, Y. & Tanaka, T. (2011). Development of epoxy/BN composites with high thermal conductivity and sufficient dielectric breakdown strength part II-breakdown strength. *IEEE Transactions on Dielectrics and Electrical Insulation, 18*(6), 1973-1983.

Xie, C., Lai, X., Li, H., Zeng, X. (2021). Remarkable enhancement of tracking resistance of addition-cure liquid silicone rubber by alkyl-disubstituted ureido siloxane immobilized on the silica filler surface. *Polymer degradation and stability, 188*, 109565.

Yuan, C., Li, J., Lindsay, L., Cherns, D. , Pomeroy, J. W., Liu, S. , Edgar, J. H. & Kuball, M. (2019). Modulating the thermal conductivity in hexagonal boron nitride via controlled boron isotope concentration. *Commun Phys, 2*(43), 1-8.

Zha, J., Dang, Z., Li, W., Zhu, Y. & Chen, G. (2014). Effect of micro-Si3N4-nano-Al2O,sub>3 co-filled particles on thermal conductivity, dielectric and mechanical properties of silicone rubber composites. *IEEE Transactions on Dielectrics and Electrical Insulation, 21*(4), 1989-1996.

Zhang, C., Wang, L., Guan, Z., & Zhang, F. (2013). Pollution flashover performance of full-scale ±800 kV converter station post insulators at high altitude area. IEEE Transactions on Dielectrics and Electrical Insulation*, 20*(3), 717-726.